

OXYGEN ISOTOPE GEOCHEMISTRY OF PLUTONIC ROCKS FROM PUERTO RICO

by

Rafael J. Pérez

A thesis submitted in partial fulfillment of the requirements for the degree of

MASTER OF SCIENCE
in
GEOLOGY

UNIVERSITY OF PUERTO RICO
MAYAGÜEZ CAMPUS
2008

Approved by:

Hernán Santos, PhD
Member, Graduate Committee

Date

Johannes H. Schellekens, PhD
Member, Graduate Committee

Date

Aaron J. Cavosie, PhD
President, Graduate Committee

Date

Clark E. Sherman, PhD
Representative of Graduate Studies

Date

Aaron J. Cavosie, PhD
Department Director

Date

ABSTRACT

Puerto Rico is a complex island arc terrane with plutonic intrusive activity from 85 million years (Ma) to 38 Ma (Cavosie et al., 2008). Schellekens (1991) divided the island into three igneous provinces named the southwest, central and northeast igneous provinces based on stratigraphy, lithology, petrology and geochemistry. Plutonic intrusions are heterogeneously distributed among the three igneous provinces; exposed areas vary from ~1 to 500 km² (stock to batholith scale). The origin of these rocks has been studied by several authors but is still speculative since the parental magmas for the plutons are not known. Petrographic analyses, whole rock (WR) major, minor and trace elements, and oxygen isotope ratios ($\delta^{18}\text{O}$) of zircon (Zrc), quartz (Qtz) and titanite (Tnt) were used to constrain the origin of the granitoids. The data were combined with U/Pb zircon dating to place time constraints on island arc evolution. ($\delta^{18}\text{O}$) in igneous rocks record magmatic compositions if primary, and are used in this study to evaluate alteration or incorporation of sediments into Puerto Rico magmas, as proposed by Schellekens (1993). These processes will increase $\delta^{18}\text{O}$ to values higher or lower than the mantle ($\delta^{18}\text{O}=5.3\pm 0.6\text{‰}$; 2sd). Analyses for $\delta^{18}\text{O}$ were performed with laser fluorination by Isotope Ratio Mass Spectrometry (IRMS) at the University of Wisconsin, Madison. Thin sections were used to evaluate whether or not $\delta^{18}\text{O}$ values are primary (magmatic) or represent alteration. Plutonic rocks in Puerto Rico show a remarkable limited range in WR major and minor elements, suggesting a common origin. The distribution of plutonic intrusions among the three igneous provinces, $\delta^{18}\text{O}(\text{Zrc})$ values, and age of crystallization shows a continuous and complex magmatic history during the evolution of the Cretaceous island arc. Plutons with the same age of crystallization and in close proximity to each other record isotopically bimodal ratios over the entire magmatic evolution of the arc beginning in the Santonian [Coamo Arriba stock (85.6 \pm 1.3 Ma, $\delta^{18}\text{O}(\text{Zrc})=5.34\text{‰}$) and Morovis stock (85.3 \pm 1.8 Ma, $\delta^{18}\text{O}(\text{Zrc})=6.69\text{‰}$)] continuing into the Campanian/Maastrichtian [San Lorenzo granodiorite (75.1 \pm 2.1 Ma, $\delta^{18}\text{O}(\text{Zrc})=5.63\text{‰}$), San Lorenzo diorite (74.1 \pm 1.4 Ma, $\delta^{18}\text{O}(\text{Zrc})=5.51\text{‰}$), Utuado pluton (70.8 \pm 1.2 Ma, $\delta^{18}\text{O}(\text{Zrc})=5.71\text{‰}$), Caguas pluton (66.8 \pm 1.2 Ma, $\delta^{18}\text{O}(\text{Zrc})=6.32\text{‰}$) and Vieques pluton (67.1 \pm 1.6 Ma, $\delta^{18}\text{O}(\text{Zrc})=5.77\text{‰}$)] and during the Eocene [Cuyon stock (47.6 \pm 0.8 Ma, $\delta^{18}\text{O}(\text{Zrc})=5.33\text{‰}$) and Barranquitas stock (47.7 \pm 1.6 Ma, $\delta^{18}\text{O}(\text{Zrc})=6.75\text{‰}$)]. Bimodal oxygen isotope ratios during the island arc evolution (85-38 Ma) indicates the incorporation of crustal material into the magmas

The results of this study suggest that any regional tectonic changes that resulted in changes in magmatic processes in the island arc occurred prior to ~85 Ma, the age of emplacement of the oldest plutons in Puerto Rico. Smith et al. (1998) suggest that the emplacement of the batholiths, stocks and volcanism in Puerto Rico was related to subduction and magma generation in the northeastern Caribbean due to tectonic changes. This conclusion contrasts with the findings of this work, where the generation of bimodal plutons from ~85 to 48 Ma is consistent along the evolution of the arc. The generation of batholiths in Puerto Rico is therefore not interpreted to represent markers of changes in regional tectonism. Any changes in magmatism as a consequence of regional tectonism are here constrained to have occurred prior to 85 Ma.

RESUMEN

Puerto Rico es un arco de islas complejo con actividad ígnea intrusiva de 85 a 38 millones de años (Ma) (Cavosie et al., 2008). Schellekens (1991) dividió la isla de Puerto Rico en tres provincias ígneas llamadas provincias ígneas del noreste, central y suroeste basado en la estratigrafía, litología, petrología y geoquímica. Las intrusiones plutónicas están heterogéneamente distribuidas entre las tres provincias ígneas, con áreas de exposición que varían de ~1 a 500 km² (escala de “stock” a batolito). El origen de estas rocas ha sido estudiado por varios autores pero aun permanece especulativo debido a que el magma parental de estas rocas aun no se conoce. Análisis petrográfico, elementos mayores, menores y traza e isótopos de oxígeno ($\delta^{18}\text{O}$) para minerales como zircón (Zrc), cuarzo (Qtz) y titanita (Tnt) se utilizaron para conocer el origen de estas rocas graníticas. Estos datos se combinaron con edades de zircón con técnicas U/Pb se utilizaron para establecer un esquema de tiempo en la evolución de este arco de islas. Isótopos de oxígeno en rocas ígneas preservan composiciones magmáticas (si son primarias) y se utilizaron en este estudio para evaluar la alteración o incorporación de sedimentos en los magmas de Puerto Rico, según propuesto por Schellekens (1993). Estos procesos de alteración o incorporación de sedimentos en el magma aumentaría o disminuirían los valores de isótopos de oxígeno del valor del manto ($\delta^{18}\text{O}= 5.3\pm 0.6\%$; 2sd). Análisis para isótopos de oxígeno fueron realizados con el proceso de fluorización con láser en la Universidad de Wisconsin, Madison. Cortes finos de rocas fueron utilizados para evaluar si los valores de isótopos de oxígeno eran primarios (mágmatícos) o representan alteración. Rocas plutónicas en Puerto Rico tienen un rango limitado en los análisis de elementos mayores y menores, sugiriendo un origen común. La distribución de las rocas plutónicas entre las tres provincias ígneas, los valores de isótopos de oxígeno en zircón y las edades de cristalización de las rocas muestran una historia magmática continua y compleja durante la evolución de este arco de islas del Cretáceo. Plutones con la misma edad de cristalización y cercanos uno del otro, reflejan esta señal isotópica bimodal a lo largo de la completa evolución magmática del arco de islas comenzando en el Santoniano [plutón Coamo Arriba (85.6 \pm 1.3 Ma, $\delta^{18}\text{O}(\text{Zrc})= 5.34 \pm 0.10\%$) y el plutón Morovis (85.3 \pm 1.8 Ma, $\delta^{18}\text{O}(\text{Zrc})= 6.69\pm 0.04\%$)] continuando en Campaniano/Maastrichtiano [granodiorita de San Lorenzo (75.1 \pm 2.1 Ma, $\delta^{18}\text{O}(\text{Zrc})= 5.63\%$), diorite de San Lorenzo (74.1 \pm 1.4 Ma, $\delta^{18}\text{O}(\text{Zrc})= 5.51\%$), plutón de Utuado (70.8 \pm 1.2 Ma, $\delta^{18}\text{O}(\text{Zrc})= 5.71\%$), plutón de Caguas (66.8 \pm 1.2 Ma, $\delta^{18}\text{O}(\text{Zrc})= 6.32\%$) y plutón de Vieques (67.1 \pm 1.6 Ma, $\delta^{18}\text{O}(\text{Zrc})= 5.77\%$)] y finalizando durante el Eoceno [plutón Cuyón (47.6 \pm 0.8 Ma, $\delta^{18}\text{O}(\text{Zrc})= 5.33 \pm 0.04\%$) y plutón Barranquitas (47.7 \pm 1.6 Ma, $\delta^{18}\text{O}(\text{Zrc})= 6.75 \pm 0.04\%$)]. Señales bimodales para isótopos de oxígeno durante la evolución del arco de islas (85 a 38 Ma) indican la incorporación de material de la corteza en algunos magmas.

Los resultados de este estudio sugieren que cualquier cambio regional tectónico que resultara en cambios en los procesos magmáticos en el arco de islas, ocurrieron antes de ~85 Ma, la edad del emplazamiento de las rocas plutónicas mas viejas en Puerto Rico. Smith et al., (1998) sugirió que el emplazamiento de los batolitos, “stocks” y volcanismo en Puerto Rico estaba relacionado a la generación de magma y subducción en el noreste del Caribe debido a cambios tectónicos. Esta conclusión contrasta con los descubrimientos en este trabajo, donde la generación de plutones bimodales desde ~85 hasta ~48 Ma es consistente a lo largo de la evolución del arco de islas. La generación de batolitos en Puerto Rico no representa un marcador de cambios tectónicos regionales. Cambios en magmatismo como consecuencia de cambios en tectonismo regional son interpretados en este estudio a haber ocurrido antes de 85 Ma.

Dedicado a mis padres, mis suegros y especialmente a mi esposa por todo su apoyo y confianza.

ACKNOWLEDGMENTS

First I will thank Dr. Aaron Cavosie for all the help, time and effort that he gave during this project and thanks for giving me the opportunity of working on this interesting and excellent project. Thanks for all the advice and all opportunities that you gave me to grow as a professional. Also I have to thank a person who guided me and helped me develop my first steps in the field of geology from high school level to graduate school, Dr. Hernán Santos. I recognize all the help, guidance and opportunities for growth as an individual and as a professional that you gave me all these years.

Dr. Johannes Schellekens was the person that helped organize the first stages of this project, providing access to sample collections, previous rock analyses, and maps. I would like to thank the Dept. of Geology faculty members and staff that helped me during my career development. Thanks to Aaron J. Cavosie, Rob Watts, Wilson Ramirez, Alvin J. Bonilla, Jorge Velez-Juarbe, Dayanidí M. Ortiz and Edgardo Pujols for field assistance.

Special thanks to Dr. John Valley and Mike Spicuzza for their help and collaboration during the analyses at Univ. of Wisconsin- Madison; Brian Hess for zircon sample mounting; Steph Maes for housing accommodations at UW. Thanks to Mihai Ducea, George Gehrels and Victor Valencia for providing access to SEM facilities and the Arizona LaserChron Center at Univ. of Arizona.

An ExxonMobil Diversity award provided the funding for the travel expenses and chemical analyses during this research. Thanks to GUEST K-12 and Science on Wheels project, and the UPRM Department of Geology for financial support.

TABLE OF CONTENTS

ABSTRACT	2
RESUMEN	3
ACKNOWLEDGMENTS	5
TABLE OF CONTENTS	6
Chapter 1.....	8
INTRODUCTION.....	8
1.1 Igneous rocks in Puerto Rico.....	9
1.1.1 Geology of the Southwest Igneous Province.....	10
1.1.2 Geology of the Central Igneous Province.....	11
1.1.3 Geology of the Northeast Igneous Province.....	13
1.2 Paleotectonic setting of Puerto Rico.....	14
1.3 Oxygen isotope systematics of magmas.....	15
1.3.1 Zircon occurrence and systematics.....	17
1.3.2 Zircon applications.....	18
1.4 Oxygen isotopes.....	18
Chapter 2.....	20
STUDY AREA.....	20
2.1 Previous work.....	20
2.1.1 Plutons in the Southwest Igneous Province.....	20
2.1.2 Plutons in the Central Igneous Province.....	21
2.1.3 Plutons in the Northeast Igneous Province.....	25
Chapter 3.....	27
METHODOLOGY.....	27
3.1 Study sites	27
3.2 Field Work.....	27
3.3 Laboratory work.....	28
3.3.1 Thin sections.....	28
3.3.2 Mineral and whole rock sample preparation.....	28
3.3.3 Major, minor and trace elements.....	30
3.3.4 Oxygen isotope analyses.....	30
3.3.5 Zircon imaging.....	31
Chapter 4.....	33
RESULTS.....	33

4.1 Petrographic analysis of plutonic igneous rocks.....	33
4.1.1 Plutons in the Southwest Igneous Province	33
4.1.2 Plutons in the Central Igneous Province	36
4.1.3 Plutons in the Northeast Igneous Province.....	44
4.2 Mafic xenoliths.....	44
4.3 Cathodoluminescence images.....	46
4.4 Major minor and trace element analysis.....	47
4.5 Oxygen isotope analysis.....	48
Chapter 5.....	52
DISCUSSION.....	52
5.1 Oxygen isotopes of whole rock	52
5.2 Oxygen isotopes of zircon, quartz and titanite	53
5.3 Origin of plutonism in Puerto Rico	58
5.4 Tectonic model for isotopically bimodal plutons.....	59
REFERENCES.....	63
TABLES	73
FIGURE CAPTIONS.....	81
FIGURES.....	88

Chapter 1

INTRODUCTION

Puerto Rico is a complex island arc terrane that preserves a record of the geologic evolution of the northern Caribbean from Pliensbachian (196.5 – 189.6 Ma, GTS 2004) to the present (Montgomery et al., 1994; Frost et al., 1998). The arc terrane consists of volcanic, volcanoclastic, and sedimentary rocks of Jurassic to early Tertiary age which were intruded by felsic plutonic rocks during the Late Cretaceous and early Tertiary (Briggs and Akers, 1965; Schellekens, 1998a). These rock units are overlain by Oligocene and younger sedimentary rocks (Schellekens, 1998a).

Schellekens (1991, 1998a) divided the island into three igneous provinces based on differences in the stratigraphy, lithology, petrography, and geochemistry- namely the Southwest Igneous Province (SIP), Central Igneous Province (CIP) and a Northeast Igneous Province (NIP) (Fig. 1). The magma sources available during the igneous evolution of the island arc are reflected in the geochemical and isotopic compositions of the island arc rocks (Frost et al., 1998). Igneous rocks of the island arc have been extensively studied through geochemical analysis by several authors (Jolly et al., 1998a, 1998b, 2007, 2008; Schellekens, 1991, 1998a; Frost et al., 1998; Smith et al., 1998).

Oxygen isotope ratio ($\delta^{18}\text{O}$) is used to help understand the magmatic, thermal and fluid evolution of Earth's crust (Valley et al., 1994). The whole rock (WR) oxygen isotope composition of igneous rocks can be overprinted or modified by secondary processes such as high grade metamorphism, hydrothermal alteration, and retrogression (Valley et al., 1994). Chemical analyses of minerals like zircon can help to differentiate between primary magmatic processes vs. secondary (alteration) processes in magmas. Zircon is a common trace mineral in igneous, metamorphic and clastic sedimentary rocks. Chemical analyses of zircon (isotopes and trace elements) allow estimates of age, isotopic composition of coexisting minerals and melts, and constraints on the generation and protolith of the host rock (Valley, 2003). Zircon is widely used in geochemical studies based on its stability at high and low temperatures, slow diffusion rates for cations and anions, chemical inertness, and resistance to mechanical and chemical weathering (Valley et al., 2005).

Plutonic samples from the three igneous provinces of Puerto Rico collected for this study were analyzed for $\delta^{18}\text{O}$ whole rock (WR) and $\delta^{18}\text{O}$ zircon (Zrc), titanite (Tnt), and quartz (Qtz). Published geochemical data from previous studies was used to guide oxygen isotope analyses on the previously characterized samples. Existing plutonic rock samples from the studies of Smith et al. (1998) and Schellekens (1998a) in the University of Puerto Rico-Mayaguez (UPRM) Department of Geology collection were analyzed for $\delta^{18}\text{O}(\text{WR})$ and $\delta^{18}\text{O}(\text{Qtz})$.

This work is the first detailed oxygen isotope study performed on the plutonic rocks of Puerto Rico. The oxygen isotope geochemistry of plutonic rocks from Puerto Rico was studied in order to determine the magmatic processes and source composition involved during the formation of these island arc rocks. This study tested the hypothesis that some plutons had sediment incorporated in their magmas, as proposed by Schellekens (1998a). When a significant sediment component is incorporated to the melt source the $\delta^{18}\text{O}$ values of WR and co-existing minerals (Zrc, Qtz, Tnt) are usually elevated relative to values found in uncontaminated mantle-derived melts. The analyses were also used to determine whether or not the igneous rocks from the three igneous provinces described by Schellekens (1998a) have undergone low-temperature or high- temperature sub-solidus alteration.

1.1 Igneous rocks in Puerto Rico

Puerto Rico is the easternmost island of the Greater Antilles and preserves the geologic history of the northern Caribbean since the Pliensbachian (196.5 – 189.6 Ma, GTS 2004) (Schellekens, 1998a). Jolly et al. (2007) described the Antilles island arc as two sections, the volcanically inactive Late Mesozoic to Paleogene Greater Antilles (Virgin Islands, Puerto Rico, Hispaniola, Jamaica and Cuba) and the volcanically active Lesser Antilles (Fig. 2). Pindell et al. (2006) described the Greater Antilles island arc as remnants of a continuous volcanic chain formed in the Pacific region, based on volcanic geochemistry and lithological similarities between the islands of the arc. The island of Puerto Rico consists of volcanic, volcanoclastic, and sedimentary rocks of Jurassic to early Tertiary age, which were intruded by felsic plutonic rocks during the Late Cretaceous and early Tertiary, and are unconformably overlain by slightly tilted Oligocene and younger sedimentary rocks and sediments (Briggs and Akers, 1965; Schellekens,

1998a). The development of the oldest arc rocks originated in an oceanic setting in the Pacific, and younger segments were formed during migration of the arc into the Atlantic between North and South America (Frost et al., 1998; Schellekens, 1998; Jolly et al., 1998a). The limited original lateral extent of the rock units in the island of Puerto Rico and the factor that locally the rocks have undergone structural deformation and faulting makes a difficult task for island-wide lithostratigraphic correlation with the basement rock (Jolly et al., 1998a; Schellekens, 1998a). This is another reason the island was divided into three igneous provinces (Schellekens, 1998a) (Fig. 1). The NIP is separated from the CIP by a left-lateral strike-slip fault (Cerro Mula fault) of Santonian age with displacement of ~50 km (Jolly et al., 1998a). The CIP is separated from the SIP by a southeastern trending fault (Southern Puerto Rico Fault Zone) which was active from Maastrichtian to Eocene (Jolly et al., 1998b).

1.1.1 Geology of the Southwest Igneous Province

Schellekens (1998a) described the Southwest Igneous Province (SIP) as having originated in a different tectonic setting than the rest of Puerto Rico. The oldest rocks found in Puerto Rico occur in the southwestern region and consist of a serpentinite melange which contains rafts of chert and metabasalt that are collectively called the Bermeja Complex (Mattson, 1960). The Bermeja Complex contains a sequence of pre-arc basement rocks (Jolly et al., 2007a). Mattson (1960) described the Bermeja Complex and distinguished four types of rocks in the complex: serpentinitized peridotite (Mattson, 1960, 1964); altered basalt (spilite), later re-named the Las Mesas Greenstone (Schellekens et al., 1990); amphibolite, later re-named the Las Palmas hornblende schist and amphibolite (Mattson, 1973); and silicified volcanic rock and/or chert, named by Mattson (1973) the Cajul basalt and the Mariquita chert (Schellekens, 1998b). With the use of radiolarian stratigraphy and radiometric dating the Bermeja Complex was subdivided into a Jurassic (Pliensbachian, and Kimmeridgian-Tithonian) volcano-stratigraphic association (VSA) and an Early Cretaceous (Hauterivian-Aptian) VSA (Schellekens et al., 1990; Montgomery et al., 1994). Evidence of Jurassic abyssal cherts suggests that the original ocean floor on which the radiolarian cherts must have been deposited could be present as well, and may possibly be represented by the Las Palmas amphibolite (Schellekens, 1998a).

The Maguayo VSA unconformably lies on the Bermeja Complex with basaltic to dacitic volcanic and volcanoclastic rocks overlain by the Santonian age Cotui Limestone (Schellekens, 1998b; Santos, 1999). Based on K-Ar (86.1 ± 2.1 Ma, hornblende, Cox et al., 1977) and Ar-Ar (83 Ma, hornblende, Schellekens et al., 1990) dating of the Maguayo Porphyry, Rudist biostratigraphy (85.8-83.5 Ma, GTS 2004) of the overlying limestones (Mattson, 1960; Santos, 1990, 1999; Schellekens, 1990), and detrital zircon U/Pb geochronology (83.1 ± 2.3 Ma) of zircons from heavy mineral sands deposited within the Cotui Limestone (Ortiz, 2006) the volcanic sequence is well-constrained to be Santonian in age. The Cotui Limestone is overlain by the Monte Grande – El Rayo VSA (basaltic to andesitic flow rock and volcanoclastic rocks) (Volckmann, 1984a; Sampayo, 1992; Schellekens, 1998a). Shallow stocks in the remaining part of the SIP intruded stratified rocks of Late Cretaceous and early Tertiary age and are grouped into Río Blanco I and II VSAs (Schellekens, 1998). The Lower Tertiary Río Blanco II VSA is composed of volcanic formations which are intercalated with siltstone, sandstone, and conglomerates derived from the volcanic rocks, and some locally occurring limestones (McIntyre, 1971, 1974, 1975; McIntyre et al., 1970; Tobisch and Turner, 1971; Schellekens, 1998a). In the SIP the stratified rocks are intruded by a number of small and mostly shallow intrusives of Late Cretaceous and early Tertiary age (e.g., Volckmann, 1984a-c; Curet, 1986; Schellekens, 1998a).

1.1.2 Geology of the Central Igneous Province

Schellekens (1998a) described the Central Igneous Province (CIP) as those rocks that occur east of the Late Cretaceous to Eocene belt of the southwest province, and west and south of the Northern Puerto Rico Fault zone (San Francisco- Cerro Mula fault) (Fig. 1). Stratified rocks of Early Cretaceous to Eocene age are intruded by felsic plutons, such as the San Lorenzo batholith, and the Utuado, Ciales, and Morovis plutons (Weaver, 1958; Broedel, 1961; Cox et al., 1977; Rogers, 1977, 1979; M'Gonigle, 1978, 1979; Rogers et al., 1979; Schellekens, 1998a).

The CIP comprises the submarine pre-Robles (Río Majada Formation of Jolly et al., 1998a) and Robles-Río Orocovis VSA, and the subaerial Pozas Formation (Schellekens, 1993;

Schellekens, 1998a; Smith et al., 1998). The Lower pre-Robles VSA (Albian or older) is composed of flows and flow breccias ranging from basaltic to andesitic composition (Schellekens, 1998a). The Upper pre-Robles VSA also consists of flows, flow breccias, and volcanic breccias of basaltic to andesitic compositions. The Robles Formation overlies the pre-Robles VSAs in the southern part of the CIP (Pease and Briggs, 1960; Berryhill and Glover, 1960; Briggs and Gelabert, 1962) and Río Orocovis Group (Nelson, 1967) in the northern part. Both units, the Robles Formation and the Río Orocovis Group, are stratigraphically and lithologically related but are separated by the Damian Arriba fault. These formations were combined into Robles-Río Orocovis sequence (Briggs, 1971) ranging from Albian to Santonian age (Schellekens, 1993). The Vista Alegre-Tetúan VSA conformably overlies, and locally is gradational into, the underlying Robles-Orocovis VSA in the north of the CIP (Schellekens, 1998a). The Cariblanco-Pozas range in age from Santonian to Maastrichtian. The Cariblanco Formation represents a marine basin facies and Las Pozas Formation represents a subaerial environment (Schellekens, 1998a).

In general, the CIP contains the largest intrusive bodies of the island. The plutonic rocks range from Upper Cretaceous plutons to Tertiary stocks. The San Lorenzo batholith located in southeast Puerto Rico is the largest plutonic body exposed on the island with an aerial extent $>500 \text{ km}^2$. The batholith varies in composition from granodiorite, tonalite, diorite to quartz diorite, but is predominately composed of granodiorite and quartz diorite with average ages from 73 to 66 Ma in age (Cox et al., 1977; Smith et al., 1998). The second largest intrusion in the island is the Utuado pluton. This Upper Cretaceous plutonic body is located in west-central Puerto Rico with an aerial extent of $\sim 185 \text{ km}^2$. This pluton is composed of granodiorite, tonalite, quartz-monzonite, diorite and minor gabbro (Weaver, 1958; Chen, 1969). This pluton was emplaced at approximately 75 Ma (Cox et al., 1977; Smith et al., 1998). The Morovis and Ciales stocks are located in north-central Puerto Rico. These two Upper Cretaceous stocks are similar in composition, and both have been described as hornblende-bearing granodiorites (Berryhill, 1965). The Morovis stock has an aerial extent of $\sim 18 \text{ km}^2$ and the Ciales stock $\sim 2 \text{ km}^2$. The Coamo Arriba stock is an Upper Cretaceous stock located in central Puerto Rico with an aerial extent of $\sim 3 \text{ km}^2$. This stock is mainly composed of diorite (Briggs and Gelabert, 1962). Located $\sim 6 \text{ km}$ northeast of the Coamo Arriba stock is the Barranquitas stock, an Eocene quartz diorite porphyry with an aerial extent of $\sim 1 \text{ km}^2$ that intruded the Robles Formation (Jolly et al.,

1998a). Another Eocene stock located in the CIP is the Cuyon stock. The Cuyon stock has an aerial extent $\sim 0.5 \text{ km}^2$ and is mainly composed of quartz diorite.

1.1.3 Geology of the Northeast Igneous Province

Igneous activity from Early Cretaceous to the Early Tertiary has also been documented in the Northeast Igneous Province (NIP) (Schellekens, 1998a). Volcanic rocks ranging in composition from basalt to rhyolite formed during the Early Cretaceous and volcanism continued through the Late Cretaceous and early Tertiary with the extrusion of basaltic and dacitic rocks (Schellekens, 1998a). The oldest group of rocks described in the NIP is the Dagua- Figuera VSA (Lower Albian), which is composed of volcanic breccia, andesite flow rocks, and volcanic sandstones and tuffs conformably overlain by volcanoclastic rocks and rare associated flow rocks, locally with more siliceous volcanics (Schellekens, 1998a). This unit is overlain by the Hato Puerco-Toma de Agua VSA (Albian age) which consists of mudstone and volcanic sandstone. The overlying Martin Gonzalez-Tortugas VSA (Turonian – Campanian) consists of volcanic sandstones and mudstones with basaltic andesite flows. Two additional sequences that are separated by unconformities but occur as continuous sequences during the same time as the Martin Gonzalez-Tortugas are the pre-Santa Olaya and Santa Olaya Formations. The pre-Santa Olaya is composed of tuffs, flow rocks, breccias and what was interpreted as a dome by Pease (1968) representing a proximal volcanic environment. Evidence for this argument is the presence of a basaltic andesitic dome, the occurrence of flows near the base of the association, followed by andesitic flow rocks and breccias, and ending with subaerial, locally welded tuffs (Schellekens, 1998a).

The NIP is intruded by small bodies of Cretaceous-Tertiary felsic plutons and Tertiary mafic magmas (diabase dikes) (Schellekens, 1998a). The largest intrusion in the NIP is the Rio Blanco stock with an aerial extent of $\sim 40 \text{ km}^2$. This stock is located in northeast Puerto Rico and has been described as a quartz diorite (Seiders, 1971b). The Rio Blanco stock and related dikes are considered to be early Tertiary in age based on their structural relationship (Seiders, 1971a,

b; Schellekens, 1998a). The Eocene age for the Rio Blanco stock was confirmed by K-Ar and Ar-Ar dating which yield ages of about 46 Ma (Cox et al., 1977; Smith et al., 1998).

1.2 Paleotectonic setting of Puerto Rico

The location of Puerto Rico and the Greater Antilles island arc during the Cretaceous has been discussed and explored by different authors and remains controversial. Models by Malfait and Dinkelman (1972), Pindell (1985), Pindell and Dewey (1982), Burke (1988), and Pindell and Barret (1990) show the Greater Antilles island arc being swept in from the Pacific toward the east while overriding Atlantic ocean floor (Schellekens and Joyce, 1999). Draper et al. (1996) described a subduction polarity reversal and obduction of serpentized peridotite onto the early arc as a result of orogenic movements during Aptian- Albian. Burke (1978) proposed igneous activity about 80 Ma, known as the B'' event (Caribbean oceanic plateau), which emplaced enough basaltic material to thicken the Caribbean oceanic crust to ~15 to 20 km. This buoyant oceanic plateau reached the subduction zone during the Campanian (or later) causing subduction polarity to flip (Burke, 1978).

Different models showing constraints on polarity of subduction of the earliest arc have been proposed based on stratigraphic, paleogeographic and geochemical data. Mattson (1979) proposed an Albian-Cenomanian reversal (south dipping to north dipping – modern geographic location) based on the presence of a basalt plateau (Caribbean Cretaceous Basalt Province (CCBP) centered on the modern Galapagos plume that occurs within the Pacific Basin. Pindell and Barrett (1990) adopted this idea and proposed an active eastward subduction of the Pacific plate by the proto-Caribbean (Atlantic) plate from 165 to 120 Ma (Jolly et al., 1998a). Various authors, including Burke (1988), Schellekens et al. (1991), Schellekens (1993), and Pindell (1994), adopted this general model but the timing of the polarity reversal is still controversial. Pindell and Barrett (1990) and Burke (1988) suggested the polarity reversal occurred at about 88 Ma. Other authors assigned a younger polarity reversal (75 to 55 Ma) based on late arrival of the CCBP at the subduction zone, magnetic anomalies consistent with continuous eastward subduction until 75 Ma (when the hypothesized reversal occurred), emplacement of Utuado and San Lorenzo pluton in the CIP, and the presence of an unconformity along the island during this

time (Schellekens, 1993; Ghosh et al., 1994; Smith and Schellekens, 1994; Jolly et al., 1998a; Smith et al., 1998).

Most authors agree with an eastern Pacific origin of the Caribbean island arc but the controversy of timing and occurrence of the polarity reversal is still in debate. A group of authors support the idea of an Aptian time for reversal (Pindell, 1993; Draper et al., 1996; Pindell and Kennan, 2001; Pindell et al., 2006) while other authors support a Lower Cretaceous reversal (Burke, 1988; Pindell and Barrett, 1990; Smith et al., 1998; White et al., 1999). Pindell (1994) locates Puerto Rico in the Early Aptian somehow aligned with the Chortis Block and Baja California.

The largest recorded episode of magmatism in the Greater Antilles island arc occurred during the Cretaceous (Jolly et al., 1998a). Volcanism remained active during the Eocene in the Greater Antilles and lasted until the Oligocene in the Virgin Islands (Cox et al., 1977; Pindell and Barrett, 1990). In Puerto Rico, volcanism ended in late Eocene and may be related to the collision of Cuba with the Bahamas Banks (Pindell and Barrett, 1990), the subduction of the Bahamas Bank beneath the arc (Puerto Rico area) (Erikson et al., 1990), or subduction of buoyant oceanic crust (Larue et al., 1991). Thus, there is still large uncertainty regarding the precise paleogeographic location of Puerto Rico during the evolution of the Greater Antilles island arc.

1.3 Oxygen isotope systematic of magmas

Oxygen isotopes are a powerful geochemical tool for understanding magmatic processes. Oxygen isotopes can fingerprint different source reservoirs and are particularly well suited for identifying recycling of young, supracrustal rocks in convergent margin arcs (Lackey et al., 2005). Hydrothermal alteration can reset $\delta^{18}\text{O}(\text{WR})$ values in these rocks after they crystallize (Lackey et al., 2005). In young mantle-derived rocks (e.g., ocean crust) $\delta^{18}\text{O}(\text{WR})$ values can be significantly shifted by alteration away from mantle values (Lackey et al., 2005) (Fig. 3). Oxygen isotopes can thus be used as an indicator for recycling of young, mantle-derived rock

near earth's surface and can provide a quantitative estimate of such recycling (Lackey et al., 2005).

The mantle is a remarkably homogeneous oxygen isotope reservoir, with a bulk value of 5.5‰ for whole-rock peridotite (Eiler, 2001). Igneous zircons in high temperature equilibrium with uncontaminated mantle-derived magmas have average $\delta^{18}\text{O} = 5.3 \pm 0.6\text{‰}$ (2 SD, Valley et al., 1998; Valley et al., 2005). Intracrustal recycling (e.g., when magmas assimilate crustal material with elevated $\delta^{18}\text{O}$) may cause changes in $\delta^{18}\text{O}$ in zircons that crystallize in these melts away from the predicted mantle value (Valley et al., 2005). Figure 3 shows the $\delta^{18}\text{O}$ value of common geologic materials. The fractionation of oxygen isotopes between zircon and whole rock, $\Delta^{18}\text{O}$ (Zrc-WR), varies with bulk composition and can be approximated as a linear function of wt. % SiO_2 for igneous rocks at magmatic temperatures (Valley et al., 2005). The values for this fractionation vary from $\sim -0.5\text{‰}$ for mafic rocks to $\sim -2\text{‰}$ for evolved rocks according to the relation:

$$\Delta^{18}\text{O}(\text{Zrc-WR}) = \delta^{18}\text{O}(\text{Zrc}) - \delta^{18}\text{O}(\text{WR}) = -0.0612 (\text{wt.}\% \text{SiO}_2) - 2.5$$

(Valley et al., 1994; Lackey et al., 2005; Valley et al., 2005).

The $\delta^{18}\text{O}$ of whole rock can be used to distinguish magmas: (a) affected by high temperature alteration (hydrothermal alteration) that results in low $\delta^{18}\text{O}$ values; (b) in predicted high temperature equilibrium with the mantle; (c) affected by low-temperature alteration or melting of material with high $\delta^{18}\text{O}$ (e.g., sediments) that produces high $\delta^{18}\text{O}$ magmas. An example of the systematics for zircon, quartz, and whole rock in magmatic equilibrium is presented in a diagram from Lackey (2005) (Fig. 4). This diagram represents the values for WR, quartz and zircon as a function of wt. % SiO_2 . At magmatic temperatures the fractionation $\Delta^{18}\text{O}$ (Zrc – WR) remains the same regardless of the bulk WR $\delta^{18}\text{O}$ and only changes as SiO_2 changes. Low $\delta^{18}\text{O}$ (WR) values can represent alteration of magmas, and show non-equilibrium fractionation of oxygen isotopes between zircon and the whole rock. Magmatic fractionations generally record high-T equilibrium of oxygen isotopes for the zircon and whole rock values. In contrast, high $\delta^{18}\text{O}$ (WR) values can represent either low temperature alteration or magmatic equilibrium where the zircon and whole rock are in equilibrium as a result of melting high $\delta^{18}\text{O}$

materials. High values of magmatic $\delta^{18}\text{O}$, above that derived from the mantle, are most often found in granitic rocks (Valley et al., 2005). Documenting the oxygen isotope systematics of plutonic rocks in Puerto Rico will thus aid in evaluating hypotheses that sediments were incorporated in Puerto Rico magmas.

1.3.1 Zircon occurrence and systematics

Zircon (ZrSiO_4) is a remarkable mineral that is found in many geologic environments in the Earth's crust and mantle. It is found in igneous rocks (both as inherited and primary crystallization products), in metamorphic rocks (as recrystallized grains) and in sedimentary rocks (as detrital and authigenic grains) (Nesse, 2004). Their average size, e.g., in granitic rocks, is about 100-300 μm , but they can also grow to several centimeters (e.g., pegmatites and kimberlites). Since zircons have the capability to survive geologic processes like erosion, transport, and high-grade metamorphism, they can be used as protolith indicators.

Zircon is a common accessory mineral in granite, syenite, granodiorite, pegmatite, and related igneous rocks, and it is somewhat less common in more mafic rocks. Zircon is also found in metamorphic rocks such as gneiss, mica schists and quartzite, derived from clastic sediments or other zircon-bearing igneous rocks. Zircon is commonly found in clastic sediments (detrital grains) as part of the heavy mineral fraction (Nesse, 2004). It is highly resistant to weathering and does not readily alter, although it may become metamict.

Zircon has a tetragonal crystal class. It occurs as euhedral to subhedral tetragonal crystals with pyramidal terminations (Fig. 5). Euhedral overgrowths developed on rounded or subhedral cores also occur. In sedimentary rocks zircon morphology can be affected by the amount of sedimentary transportation and range from euhedral to rounded. In some igneous rocks the grains can have a rounded shape due to partial resorption in magmas. The atomic arrangement consists of isolated silicon tetrahedra bonded laterally through Zr. Zircon usually contains significant amounts of Hf^{+4} substituting for Zr^{+4} (e.g., 1-2 wt.%) and a variety of rare earth and other trace elements in minor amounts (ppm level). Metamict zircon can result when the crystal lattice of the grain is affected by the radioactive decay of elements such as U and Th.

Zircon is colorless to pale brown under plain polarized light, with very high positive relief with bright interference colors, up to third and fourth order. Zircon may produce dark halos when it occurs as an inclusion in host mineral as a product of radiation damage from Th or other radioactive elements (Nesse, 2004).

1.3.2 Zircon applications

U/Pb dating

The occurrence of zircon has become more important since the discovery of radiometric dating. Zircons contain trace amounts of radioactive uranium and thorium (from 10 ppm up to several wt. %) and can be dated using modern analytical techniques. Owing to the uranium and thorium content, some zircons may undergo metamictization (destruction of a mineral's crystal lattice leaving the crystal amorphous). This process partially disrupts the crystal structure and explains the highly variable properties of zircon. The tendency of zircon to concentrate uranium and exclude lead, its refractory nature and concentric growth patterns all allow precise geochronologic analysis of the U-Pb system to determine crystallization age (Hoskin and Schaltegger, 2003). By the imaging of zircon with high resolution techniques like cathodoluminescence (CL) or back scattered electrons (BSE) growth zoning patterns can be studied (Hoskin and Schaltegger, 2003) (Fig. 6).

U/Pb zircon geochronology is a useful geochemical tool to help provide constraints on timing of geological processes.

1.4 Oxygen isotopes

New techniques for oxygen isotope analysis have lead to studies of oxygen isotope geochemistry of zircons. Oxygen isotope ratios in igneous rocks are especially sensitive to contamination by materials that have undergone low-temperature interaction with the hydrosphere, sediments, and hydrothermally altered rocks (Peck et al., 2001). Zircon can preserve the igneous $\delta^{18}\text{O}$ even when WR samples have experienced high grade metamorphism

or hydrothermal alteration. Oxygen is a major element in zircon (ZrSiO_4) and is affected by different processes than trace elements or radiogenic isotopes that are commonly used to study crustal growth and evolution (Valley et al., 1994). $\delta^{18}\text{O}$ analyses in dated zircons can correlate the magmatic composition to known geologic events (Valley et al., 1994). Analysis of $\delta^{18}\text{O}$ zircon has been used to distinguish magmatic isotope ratios from non-magmatic ratios that can result from secondary processes including hydrothermal alteration, recrystallization and radiation damage (Cavosie et al., 2005) (Fig. 3). Several authors have used $\delta^{18}\text{O}(\text{Zrc})$ to better understand island arc evolution (Cavosie et al., 2008); mantle geochemistry (Valley et al., 1998); magmatic evolution (King et al., 1998; O'Connor and Morrison, 1999; King and Valley, 2001; Monani and Valley, 2001); Earth's crust evolution (Valley et al., 2005); crustal processes in the Precambrian (Peck et al., 2000); and the Early Earth (Wilde et al., 2001; Peck et al., 2001; Valley et al., 2002; Cavosie et al., 2004; Cavosie et al., 2005).

Chapter 2

STUDY AREA

2.1 Previous work

2.1.1 Plutons in the Southwest Igneous Province

Tibes stock: Diorite

This stock is located in the SIP and has an aerial extent of approximately 4 km². No detailed description of this stock has been published. Krushensky and Monroe (1978) described this stock as a medium-gray to light-greenish-gray diorite to quartz-diorite. The mineral composition includes twinned plagioclase, diopsidic augite, green hornblende, rare brown biotite, quartz, and accessory magnetite and titanite. Aggregates of augite, hornblende, biotite and magnetite are commonly seen. Titanite is enclosed by plagioclase, hornblende and biotite. Quartz occurs as anhedral masses or myrmekitic intergrowths with plagioclase (Krushensky and Monroe, 1978). No geochemical data for this stock have been published.

Tea Diorite: Porphyritic diorite

This quartz diorite rock occurs as sills and dikes that intrude the Lajas Formation, Cotui Limestone, and elsewhere in the Sierra Bermeja area (Mattson, 1960; Volckmann, 1984c). This rock was described as a light-gray, light-greenish-gray porphyritic rock that contains plagioclase phenocrysts (~20 mm in length), quartz phenocrysts (~5 mm in length) and sparse biotite. The groundmass is fine-grained, equigranular, and consists of plagioclase and quartz. Accessory minerals include hornblende, apatite, zircon and magnetite (Volckmann, 1984c). Alteration of primary igneous phases to sericite, chlorite, carbonate and zeolites commonly occurs in this rock. No geochemical data for these dikes have been published.

Las Tunas stock: Diorite

This stock is a small (~0.25 km²) porphyritic diorite that intruded the Lajas Formation. This rock is composed of anhedral to subhedral plagioclase grains and hornblende phenocrysts in

a fine to medium-grained aphanitic matrix composed of plagioclase and chloritized mafic minerals (Volckmann, 1984c). No geochemical data for this stock have been published.

Rincon porphyry (06RP-01)

The Rincon porphyry has not been described previously and there is no published geologic map for this area. No geochemical data for this stock have been published.

2.1.2 Plutons in the Central Igneous Province

San Lorenzo Batholith

The San Lorenzo Batholith is the largest felsic intrusion in Puerto Rico with an aerial extent of ~500 km². The batholith has been divided by field relationships (Rogers, 1977) and K-Ar ages (Cox et al., 1977) into 3 units: (1) granodiorite- quartz diorite and tonalite (~75% area of the batholith) with an average age of ~73 Ma; (2) quartz monzonite- quartz diorite with an average age of ~66 Ma; and (3) small bodies of diorite and gabbro with ages of ~78 Ma (Smith et al., 1998). A dark amphibole-rich tonalite yielded the oldest K-Ar age of 109±9 Ma (Cox et al., 1977) and a small diorite stock yielded 100±16 Ma (Cox et al., 1977; Smith et al., 1998). Ar-Ar ages of potassium feldspars and hornblende yield ages from 75 to 57 Ma, which suggest Tertiary late stage activity associated with the batholith (Smith et al., 1998). Published geochemical analyses for these rocks included major, minor, and trace elements REE; Sr, Nd, Pb, Sm isotopes (Cox et al., 1977; Kesler and Sutter, 1979; Jones and Kesler, 1980; Lidiak, 1991; Schellekens, 1998a; Jolly et al., 1998a; Smith et al., 1998; Frost et al., 1998).

The San Lorenzo granodiorite is described as a light- to medium-gray, medium- to coarse-grained rock with a late Cretaceous to early Tertiary age that is mainly composed of plagioclase, quartz and orthoclase (Broedel, 1961). Minerals described in the rock include oligoclase-andesine, potassium feldspar, quartz, hornblende and biotite; accessory minerals are magnetite, apatite, titanite, microcline and zircon (Broedel, 1961).

The San Lorenzo diorite is described as the most mafic and heterogeneous unit of the batholith and contains small subrounded autoliths(?) darker and in part more mafic than the country rock (Rogers et al., 1979). This unit contains metavolcanic xenoliths and younger more mafic diorite and hornblende filling fractures or as small intrusions (Rogers et al., 1979).

Utuaado pluton: Granodiorite

The Utuaado pluton has been well studied by several authors: Weaver (1958), Nelson (1968), Chen (1969), Lidiak (1991), Cox et al. (1977), Kesler and Sutter (1979), Barabas (1982), Smith et al. (1998) and others. This pluton is the second largest intrusion in Puerto Rico with an aerial extent of approximately 200 km². Weaver (1958) described the pluton as consisting of granodiorite, quartz diorite, quartz porphyry and gabbro. Granodiorite makes up most of the pluton. The granodiorite has been described as light in color, having a medium to coarse grained granitic texture, equigranular, and contains quartz, plagioclase, orthoclase, hornblende, biotite (locally) and altered chlorite (Weaver, 1958). The quartz diorite has been described as medium-grained, granitic texture with lath-like hornblende and is composed of plagioclase, quartz, hornblende and accessory apatite and titanite. Euhedral plagioclase with polysynthetic twinning and irregular zoning occurs and is altered to sericite along grain boundaries (Weaver, 1958). Quartz porphyrite occurs in the margin of the pluton and was described as medium gray, fine-grained, composed of plagioclase and quartz with a medium-grained granoblastic groundmass. Gabbro occurs as small bodies at one or two areas along the margin of the pluton and was described as coarse-grained, with a panidiomorphic texture composed of plagioclase and augite (Weaver, 1958). Weaver (1958) mentioned the presence of xenoliths in both the granodiorite and the quartz diorite. He described the xenoliths as dark gray, rounded or subrounded, 4 to 5 cm across (up to 30 cm), fine grained and peppered with porphyroblastic plagioclase crystals. Microscopic descriptions of the xenoliths show they consist of 40-50% plagioclase, 30% amphibole, 5% pyroxene, 15% quartz and iron oxides (Chen, 1969).

Major and minor elements have been analyzed across the pluton (Weaver, 1958; Chen, 1969; Smith et al., 1998). Average chemical composition of intrusive rocks from the pluton (excluding gabbro) is 60.59 wt.% SiO₂. The quartz diorite rock from this pluton yields an average K-Ar hornblende age of 67 Ma (Cox et al., 1977). Subsequent Ar-Ar analyses on these

rocks yield 76 Ma for hornblende and 69 Ma for K-feldspar, which is consistent with the previous analyses (Smith et al., 1998).

Morovis stock: Granite

The Morovis stock is located in the CIP with an aerial extent of approximately 20 km². The rock has been described as a monzonite with a mineral assemblage of quartz, zoned plagioclase, K-feldspar, hornblende, biotite, titanite, magnetite and zircon (Smith et al., 1998). Ages for this pluton have been determined by the Ar-Ar technique (hornblende, ~86 Ma) (Smith et al., 1998) and K-Ar techniques (88.1 ±2.1 Ma) (Cox et al., 1977). Berryhill (1965) mentioned the presence of autholiths and xenoliths in this pluton.

Ciales stock: Granodiorite

This pluton is located in the CIP and has an aerial extent of about 2 km². Chemical analyses indicate that the rock is granodiorite with 61.30 wt.% SiO₂ (Berryhill, 1965). Chemical analyses of the Ciales and Morovis stocks indicate they have the same composition and field correlation indicates that both are probably connected at shallow depth (Berryhill, 1965). Both stocks have granitic texture and hornblende crystal alignment near borders, showing flowage during emplacement. Autholiths and xenoliths occur most commonly in the border areas. Petrographic observations shows that this rock is composed of plagioclase, hornblende, orthoclase, biotite and quartz. Accessory minerals include magnetite, apatite, titanite and zircon (Berryhill, 1965). An age for the stock was previously determined using the lead-alpha decay method in zircon, yielding an age of 70±20 Ma (Berryhill, 1965).

Caguas stock: Granodiorite

The Caguas stock is located in the CIP and is exposed on the east and west sides of the town of Caguas. Rogers (1979) described this stock as medium-grained, medium-dark-gray with a hypidiomorphic granular texture. He described this rock to have a modal composition of 55% plagioclase, 12% potassium feldspar, 17% quartz, 12.5 hornblende, 2.5% biotite, 1% magnetite

and accessory minerals titanite, apatite and zircon. The Caguas and San Lorenzo plutons are hypothesized to be contemporaneous and connected at shallow depths, based on the closely related granodiorite and tonalite facies, and the presence of diorite bodies near both plutons (Rogers, 1979; Smith et al., 1998).

Vieques pluton: Granodiorite

This pluton is located on Vieques Island and has an aerial extent of ~80 km². Lidiak (1991) described this pluton as a granodiorite based on field observation and modal analyses. The granodiorite rock has been described as a medium to coarse grained and moderately porphyritic. The mineral composition of this rock is quartz, zoned plagioclase, K-feldspar, hornblende, biotite, magnetite, and accessory titanite and zircon (Lidiak et al., 1991). Secondary minerals include actinolite, chlorite, epidote, epidote and opaque minerals. No geochemical data for this stock have been published.

Cuyon stock: Quartz diorite

This stock is located in the CIP and has an aerial extent <2 km². This intrusion has been described by Berryhill and Glover (1960) as a hornblende-quartz-diorite with granitic texture. The mineral composition is plagioclase, quartz, hornblende, biotite, magnetite, orthoclase, and accessory minerals zircon and apatite. Hornblende-rich aenoliths have been reported in this stock (Berryhill and Glover, 1960). Potassium argon ages yield 47.3±1.0 Ma for hornblende and 48.2±1.3 Ma for biotite (Cox et al., 1977).

Zanja Blanca stock: Diorite

This diorite stock has not been well described. Glover and Mattson (1973) mapped this stock in the Rio Descalabrado quadrangle map and described it as an Upper Cretaceous diorite intrusion in the Coamo Formation. No geochemical data for this stock have been published.

Barranquitas stock: Diorite

This stock has been described by Briggs and Gelabert (1962) as quartz porphyry composed primarily of dipyrimal quartz phenocrysts in a light colored groundmass mainly composed of clay minerals. Most areas of this stock are covered by soil and exposures of rocks were not accessible. During May 1995, Cominco American Resources Incorporated drilled three cores in the stock trying to locate economic gold, copper and zinc mineralization. The three drill cores comprise a total of 2,035 feet. Core BA-1 reached a depth of 355 feet and shows shallow alteration and weak mineralization; core BA-2 reached a depth of 755 feet showing a thick layer of altered mudstone, siltstone, hornblende diorite and quartz diorite, and at the end of the core the quartz-porphyry and quartz-diorite fault breccia; core BA-3 reached a depth of 900 feet showing mudstone, siltstone and laharic conglomerate (Monroe and Suda, 1995). Chemical analyses made on these cores include Au, Ag, Cu, Pb and Zn. The cores are stored in UPRM storage facilities at Ramey Base in Aguadilla. Glover (1971) inferred an Eocene age for this stock based on stratigraphy.

Coamo Arriba stock: Quartz diorite

This stock is located in the CIP and is mapped in the Barranquitas Quadrangle. The stock has been described as a hornblende diorite composed of plagioclase and acicular hornblende. Associated with this diorite are some augite diorite porphyry dikes which occur within and outside the stock (Briggs and Gelabert, 1962). No geochemical data for this stock have been published.

2.1.3 Plutons in the Northeastern Igneous Province

Rio Blanco pluton: Granodiorite

The Rio Blanco pluton, located in the NIP, has an exposed area of ~20 km² and has been mapped as both quartz diorite and diorite (Seiders, 1971b). These rocks have been described as medium to coarse grained, equigranular to porphyritic, with plagioclase and hornblende

phenocrysts (Lidiak, 1991). Minerals described in this rock are quartz, zoned plagioclase, K-feldspar, hornblende, biotite, magnetite, titanite, apatite and zircon. The rock typically shows no discernable alteration and contains angular to well-rounded mafic xenoliths (Seiders, 1971b). The pluton is surrounded by a contact metamorphosed aureole.

An age of 45 Ma has been obtained by K-Ar (Cox et al., 1977; Jones and Kesler, 1980). Ages from 48 to 46 Ma have been obtained by Ar-Ar ages of hornblende, biotite and K-feldspar (Smith et al., 1998).

Chapter 3

METHODOLOGY

This chapter includes details of sample collection, description, processing and analysis. The latter includes laboratory work and the procedures for obtaining mineral separates (quartz, zircon and titanite) and whole rock samples, and the methodology for $\delta^{18}\text{O}$ and major, minor and trace element analysis.

3.1 Study sites

Samples of the major plutonic igneous rocks were collected from each of the three igneous provinces of Puerto Rico. Global positioning system (GPS) readings were used to precisely record sample locations. The plutonic rocks collected include: NIP (Rio Blanco pluton), CIP (San Lorenzo batholith, Utuado pluton, Morovis stock, Ciales stock, Caguas stock, Vieques pluton, Cuyon stock, Zanja Blanca stock, Barranquitas stock and Coamo Arriba stock), SIP (Tibes stock, Tea diorite, Rincon porphyry and Las Tunas stock). Table 1 includes quadrangle map names, GPS readings (latitude and longitude), and the name of the roads where the samples were collected.

3.2 Field Work

For this study a total of 18 plutonic rocks and 5 xenolith samples were collected from the three igneous provinces of Puerto Rico (Table 1). Usually one representative sample was collected for each pluton with the exception of the San Lorenzo batholith and the Tibes stock, where multiple samples were collected. Macroscopic observations of the samples were made in the field. In addition to the granitic rocks, mafic xenoliths were collected from the San Lorenzo, Utuado, Morovis, Vieques, and Rio Blanco plutons.

The six-digit sample labeling system used was as follows: year (2 digits); location abbreviation (2 digits); sample number (2 digits) (e.g., 06SL-01: 06=2006, SL= San Lorenzo, 01= sample #1).

3.3 Laboratory Work

3.3.1 Thin sections

In order to understand the processes involved during the formation of these rocks and to qualitatively and quantitatively analyze minerals in the rock samples, petrographic analyses were performed. Standard thin section preparation was used, as described in Nesse (2004). A total of 28 thin sections were prepared.

The rock type was determined based on mineralogical modal percentages using the quartz-alkali feldspar-plagioclase (Q-A-P) classification diagram (Streckeisen, 1973).

3.3.2 Mineral and whole rock sample preparation

Zircon separation

Zircon is an accessory mineral in igneous rocks with an average size of approximately 100 to 300 μm . When analyzing bulk samples for $\delta^{18}\text{O}$, each analysis requires 1-2 mg of zircon. To obtain enough zircons for analysis, ~5.0 kg samples were processed, with the exceptions of samples from Barranquitas (BA-2) and Tea Diorite (06TD-01) where a smaller amount of sample was processed (3.7 and 1.2 kg, respectively) (Table 2).

Zircon separation was performed at the University of Wisconsin- Madison. Samples were first crushed with a jaw crusher to <1 cm size particles and then disc milled to sand size particles. Heavy minerals (zircon, magnetite and apatite) were separated from light minerals (quartz, plagioclase, feldspar) using hydraulic sorting on a shaking table. The heavy mineral fraction was dried. Using a neodymium hand magnet, all magnetite and magnetic particles from the disc mill were removed from the sample. This is to prevent obstruction in the Frantz magnetic barrier separator. The Frantz magnetic separator was used to remove all magnetic

minerals (magnetite, hornblende, titanite, biotite) at different tilt and voltage settings. The following settings were used to concentrate zircon:

- 15° Side tilt/10 ° Forward/0.25Amps
- 15° Side tilt/10 ° Forward/0.50Amps (Separates most biotite)
- 15° Side tilt/10 ° Forward/0.75Amps (Separates most titanite)
- 15° Side tilt/10 ° Forward/2.00Amps (Zircon and apatite comprise most of the remaining non-magnetic minerals after this setting)

The heavy minerals from the last non-magnetic fraction were further separated by density with heavy liquids (acetylene tetrabromide). The minerals that sink in heavy liquids include zircon, apatite, and pyrite. Zircon in the remaining heavy mineral fraction was concentrated and purified by acid treatment. The following steps are the acid treatments applied to purify the zircon sample.

- Nitric acid (HNO₃) - This acid dissolved sulfides and phosphates in a Teflon vial after approximately half hour to an hour on a hot plate at 70°C (depending on the sulfide and phosphate concentration)
- Hydrofluoric acid (HF) - This acid treatment dissolved the minerals remaining after the nitric acid treatment and also zircons with radiation damage. Radiation damaged zircon will affect the $\delta^{18}\text{O}$ analyses.
- Hydrochloric acid (HCl) - This acid removes fluoride residues created during HF treatment, carbonates and iron-oxides.

Quartz and titanite separation

For quartz and titanite separation approximately 0.5 kg of the rock sample was crushed with the jaw crusher to sand size particles. The samples were cleaned with deionized water and dried in a furnace. Quartz and titanite fractions were hand-picked using a binocular microscope and tweezers. Each analysis for $\delta^{18}\text{O}$ requires 1-2 mg of sample. The concentrated quartz samples were immersed in HF acid for 3 to 5 minutes and then rinsed with deionized water. This creates a “frosted” appearance on clear minerals that aren’t quartz (e.g., feldspar) allowing differentiating between pure quartz under the microscope.

Whole rock preparation

Whole rock (WR) samples were prepared with careful attention to ensure that the WR sample powders represent as close as possible the uncontaminated bulk rock. All WR samples (for $\delta^{18}\text{O}$ and major, minor and trace element analysis) were carefully inspected to avoid veins, fractures, or weathered surfaces. Samples for whole rock analyses were crushed with a jaw crusher to sand size particles and powdered in a shatter box.

3.3.3 Major, minor and trace element analyses

Analyses were performed by the Washington State University Geoanalytical Laboratory. The samples were analyzed by X-ray fluorescence with a Li-tetraborate fused bead technique. Elements analyzed include: SiO_2 , TiO_2 , Al_2O_3 , FeO , MnO , MgO , CaO , Na_2O , K_2O , P_2O_5 , Ni, Cr, Sc, V, Ba, Rb, Sr, Zr, Y, Nb, Ga, Cu, Zn, Pb, La, Ce, Th and Nd. The following sample preparation is as described by Johnson et al. (1999). Each analysis required approximately 28 grams of sample. For the element concentration analyses nine USGS standard samples were used (PCC-1, BCR-1, BIR-1, DNC-1, W-2, AGV-1, GSP-1, G-2, and STM-1) with the recommended values proposed by Govindaraju (1994). The internal standard beads used for each analysis are BCR-P and GSP-1 and they were run every 28 samples. Uncertainty of the analyses is determined using the limit of determination (LOD) at 2 sigma (Table 3).

3.3.4 Oxygen isotope analysis

Oxygen isotope analyses were performed in the Stable Isotope Laboratory at the University of Wisconsin. Each analysis required 2 mg of sample and was analyzed by laser fluorination with the use of a CO_2 laser, as described by Valley et al. (1995) and Spicuzza et al. (1998). Oxygen isotope ratios were measured on a Finnigan MAT 251 mass spectrometer. Oxygen standard UWG-2 was used for every session of analyses (Valley et al., 1995). The average $\delta^{18}\text{O}$ value of a group of at least 3 standards was corrected to 5.80‰ (SMOW) as

suggested by Valley et al. (1995). All unknown samples analyzed on the same day were corrected by the same amount.

Oxygen isotope analyses for zircon, quartz, titanite and whole rock

Zircon samples were powdered with a mortar to increase the fluorination efficiency during analysis. Approximately 2 mg of powdered zircon sample is loaded for each analysis. Grains of quartz and titanite were weighed to approximately 2 mg, and loaded for analysis.

Whole rock samples were weighed, approximately 2 mg, and loaded into Ni pins. Each whole rock sample during fluorination analysis was isolated on an air lock system to prevent partial mineral reaction (e.g., feldspars) which may react with BrF_5 at room temperatures affecting the oxygen values (Valley et al., 1995; Spicuzza et al., 1998).

The average $\delta^{18}\text{O}$ for UWG-2 standard for 3 days of whole rock analyses was $5.76 \pm 0.19\%$, 2 SD. The average for $\delta^{18}\text{O}$ UWG-2 standard for 3 days of minerals analyses was $5.72 \pm 0.1\%$, 2 SD.

3.3.5 Zircon imaging

Zircon samples were mounted in 2.5 cm epoxy rounds (Fig. 7). The procedure for zircon mounting is described below: Double-sided tape approximately 1 inch in width is placed on a metal plate. A 1 inch diameter circle is drawn to mark the area where epoxy will be poured. With the help of fine tweezers, grains are picked from the sample and placed in different areas near the center of the 1 inch circle. Grains of standards for U/Pb and trace element analyses were also placed near the center of the mount. A Teflon ring was placed over the mount area and epoxy was poured into the ring to a depth of 3/8 inch. After the sample mount was left to harden for 24 hours, the mount was removed from the plate and the tape. Using 2,500 grit paper with water, the mount is sanded down until the grains are exposed. 3,000 grit paper is used to sand down until half the grains are exposed to their centers. The mount was washed with soapy water

and then alcohol to clean the polished surface. A picture of the mount surface with enough detail for navigation purposes was taken during the subsequent imaging.

Zircon grains were imaged with a scanning electron microscope (SEM) with a cathodoluminescence (CL) detector. Cathodoluminescence allowed imaging of the internal structure of the grains. Zircons with a magmatic origin usually have oscillatory zoning with no alteration in the structure. Cathodoluminescence imaging of zircon samples was conducted using SEM facilities in the Department of Geosciences at the University of Arizona.

Chapter 4

RESULTS

This chapter describes the results of different analyses and techniques used for characterization of physical and chemical properties from the plutonic igneous rocks from Puerto Rico. These techniques include macroscopic and microscopic observation of the rocks, cathodoluminescence images of mineral samples, chemical analyses for major, minor and trace elements, and $\delta^{18}\text{O}$ analyses for minerals and whole rock samples.

4.1 Petrographic analysis of plutonic igneous rocks

This section contains petrographic descriptions of 19 plutonic rocks from Puerto Rico that were analyzed for $\delta^{18}\text{O}$. Petrographic analysis in thin section is used to determine the mineralogical composition of the rock and to qualitatively evaluate the $\delta^{18}\text{O}$ values of the plutonic rocks and xenoliths based on the state of preservation of constituent minerals. In addition, polished rock slabs (5 cm to 26 cm) were prepared to describe macroscopic features of hand specimens.

4.1.1 Plutons in the Southwest Igneous Province

Tibes stock sample 06TS-01: Diorite/gabbro

This rock is medium-grained, phaneritic, holocrystalline, melanocratic with porphyroclasts of plagioclase, clinopyroxene, hornblende and quartz (Fig. 8).

In thin section the sample is pervasively altered. Mineral percentages in this rock are 45% plagioclase, 20% clinopyroxene (augite), 15% hornblende, 5% actinolite, 5% opaque oxides, 5% chlorite, 3% quartz, and 1% secondary biotite and 1% accessory minerals zircon and titanite. The modal percentage for this sample normalized to Q-A-P is 94% plagioclase and 6% quartz. The Q-A-P composition indicates the rock is diorite or gabbro. Plagioclase is subhedral to anhedral and almost completely replaced by sericite. Augite is altered in many places to

actinolite. Augite is wide spread and occurs between euhedral plagioclase grains in an ophitic texture. Hornblende shows green pleochroism and is highly altered to chlorite and or actinolite (Fig. 9).

Tibes stock sample 06TS-06: Diorite/gabbro

This rock is medium to coarse-grained, phaneritic, holocrystalline, mesocratic with porphyroclasts of plagioclase, clinopyroxene, hornblende, quartz and biotite (Fig. 10).

Mineral percentages are 55% plagioclase, 16% hornblende, 10% clinopyroxene (augite), 5% magnetite, 5% sericite, 4% chlorite, 4% biotite and 1% accessory zircon and titanite. The modal percentage for this sample normalized to Q-A-P is 100% plagioclase. The Q-A-P composition indicates the rock is diorite or gabbro. Plagioclase generally shows distinctive Carlsbad and albite twinning, and some grains showing oscillatory zoning. Plagioclase grains range from subhedral to anhedral and some grains occur in hornblende. Alteration of plagioclase to sericite is wide-spread, but alteration is also concentrated in the cores of grains (Fig. 11). Brown subhedral to anhedral hornblende contains plagioclase and augite inclusions. Anhedral augite grains occur and some have plagioclase inclusions. Secondary chlorite occurs between magnetite and plagioclase grains. Pleochroic reddish brown biotite is a minor phase that occurs both on rims around opaque oxides (ilmenite) and as interstitial anhedral grains. Biotite is commonly intergrown with chlorite.

The mineral crystallization sequence based on mineral occurrence and inclusions relation is plagioclase→ clinopyroxene→ hornblende→ biotite.

Tea Road sample 06TD-01: Porphyritic diorite

This rock is porphyritic, holocrystalline, mesocratic with porphyroclasts of plagioclase. Plagioclase phenocrysts range from 0.3 cm to 1.5 cm in length (Fig. 12). The aphanitic, melanocratic groundmass is composed of hornblende and sulfide microlites.

Mineral percentages in thin section are 32% plagioclase + quartz groundmass, 40% plagioclase, 8% quartz, 8% magnetite, 3% hornblende, 3% chlorite, 3% calcite, 3% epidote and 1% apatite and zircon. The modal percentage for this sample normalized to Q-A-P is 83%

plagioclase and 17% quartz. The Q-A-P composition indicates the rock is quartz diorite. Plagioclase phenocrysts are large, >1.0 cm in length, and are fractured and partially altered to sericite along grain margins (Fig. 13). Characteristic albite and Carlsbad twinning is present. Some plagioclase phenocrysts have hornblende inclusions. Smaller groundmass plagioclase crystals exhibit oscillatory zoning and alteration to sericite in the cores of grains. Quartz occurs as phenocrysts in a fine-grained plagioclase and quartz groundmass, filled with chlorite veins, calcite, magnetite and epidote. Matrix hornblende is almost completely replaced by chlorite and surrounded in some areas by magnetite. Magnetite occurs as veins and filling fractures. Accessory apatite occurs in the matrix and as inclusions in plagioclase grains. Calcite and chlorite occur together replacing hornblende and as veins in the groundmass. Zircon occurs in the groundmass, and a single euhedral crystal was observed as an inclusion within a hornblende lath (Fig. 14) that in turn is an inclusion mineral within one of the large plagioclase megacrysts.

The mineral crystallization sequence based on mineral occurrence and inclusion relations is hornblende → plagioclase → quartz → plagioclase (matrix)

Las Tunas stock sample 06LT-01: Diorite

This rock is pervasively altered. The rock is fine to medium-grained, phaneritic, holocrystalline, mesocratic with porphyroclasts of plagioclase and hornblende (Fig. 15). It contains aphanitic, melanocratic xenoliths that range from 1 cm to 3 cm in length.

Mineral percentages for this rock are 34% plagioclase, 30% quartz groundmass, 15% hornblende, 10% chlorite, 3% quartz, 3% zeolite, 2% K-feldspar, 2% magnetite and 1% accessory apatite and zircon. The modal percentage for this sample normalized to Q-A-P is 92% plagioclase and 8% quartz. The Q-A-P composition indicates the rock is diorite. The hand sample is phaneritic but thin section reveals a porphyritic texture. Quartz is mostly present in the fine-grained groundmass. Plagioclase occurs as subhedral to anhedral grains that are altered to sericite (Fig. 16); only a few grains preserve relict albite twinning. Hornblende shows brown-green pleochroism and occurs as euhedral phenocrysts in a fine grained crystalline groundmass and as smaller grains. Some of the grains are totally replaced by zeolite. Hornblende contains quartz and plagioclase inclusions. Zeolite, chlorite, and epidote occur as minerals replacing hornblende. K-feldspar phenocrysts are subhedral and altered to sericite. Apatite occurs in

plagioclase and some grains are present in zeolite, which is surrounded by chlorite. Zircon grains occur sporadically in the groundmass. Magnetite grains are subhedral to anhedral.

The mineral crystallization sequence based on mineral occurrence and inclusion relations is plagioclase → hornblende → quartz.

Rincon porphyry sample 06RP-01: diorite porphyry

This rock is porphyritic, holocrystalline, leucocratic with porphyroclasts of plagioclase and fine grained hornblende in an aphanitic groundmass (Fig. 17).

The sample is highly altered and weathered and the mineralogical percentages are therefore roughly estimated. The mineral percentages are 35% groundmass (quartz and chlorite), 35% plagioclase, 17% chlorite, 5% epidote, 5% opaque oxides and 3% quartz. The modal percentage for this sample normalized to Q-A-P is 92% plagioclase and 8% quartz. The Q-A-P composition indicates the rock is diorite. Plagioclase occurs as euhedral to anhedral phenocrysts. Some grains preserve albite and Carlsbad twinning. Some quartz grains show undulatory extinction while others are part of a highly altered fine-grained groundmass which is mostly intergrown with chlorite. Chlorite and epidote are the dominant alteration products together with sericite which is replacing most plagioclase grains.

4.1.2 Plutons in the Central Igneous Province

San Lorenzo Batholith

San Lorenzo sample 06SL-01: Quartz diorite

This rock is medium-grained, mesocratic, phaneritic, holocrystalline with equigranular porphyroclasts of plagioclase, quartz and hornblende (Fig. 18). The polished rock slab contains aphanitic mafic xenoliths ranging from 1 to 5 cm in length.

Calculated mineral percentages based on petrographic observation is 50% plagioclase, 30% hornblende, 10% quartz, 10% oxides and minor K-feldspar, with accessory zircon, apatite and titanite. Secondary biotite and sericite are present in small amounts. Normalized modal

abundances of quartz, alkali feldspar and plagioclase (Q-A-P) are 82% plagioclase, 16% quartz and 2% K-feldspar. The Q-A-P composition indicates the rock is quartz diorite.

Plagioclase is euhedral to subhedral in texture, shows Carlsbad and albite twinning and rare oscillatory zoning (Fig. 19). Tabular plagioclase crystals with oscillatory zoning and/or albite twinning commonly occur as inclusions in hornblende and quartz (Fig. 20). Many grains with oscillatory zoning show corroded cores, and more pronounced oscillatory zoning is preserved on rims of grains. The alteration observed in many grains is usually symmetric about the core. Plagioclase cores are inclusion rich. Some grains are partially replaced by sericite. Subhedral plagioclase grain shows albite twinning in the core surrounded by oscillatory zoning in the rim area (Fig. 21). Large hornblende crystals are subhedral to anhedral, showing both green and brown pleochroism. Sulfides occur as a minor phase in hornblende crystals. Quartz shows undulatory extinction and occurs as anhedral grains and some interstitial aggregates (Fig. 20). Large subhedral titanite grains occur interstitial with plagioclase and hornblende (Fig. 22). Zircon and apatite occur as euhedral inclusions in plagioclase and quartz (Fig. 23). Opaque oxides occur as inclusions in hornblende and interstitial with plagioclase grains.

The crystallization sequence based on mineral occurrence and inclusion relations is plagioclase → zircon + titanite → hornblende → quartz.

San Lorenzo sample 06SL-03: Granodiorite

This rock is medium-grained, phaneritic, holocrystalline, leucocratic, with porphyroclasts of plagioclase, quartz, hornblende, biotite and titanite (Fig. 24).

Mineral percentages for this sample are 55% plagioclase, 18% quartz, 10% hornblende, 10% K-feldspar, 5% magnetite and 2% secondary biotite, chlorite, and accessory minerals zircon, titanite and apatite. The normalized Q-A-P modal abundance is 66% plagioclase, 22% quartz and 12% K-feldspar. The Q-A-P composition indicates the rock is granodiorite. Plagioclase ranges from subhedral to anhedral, and shows Carlsbad and albite twinning and some grains have oscillatory zoning combined with Carlsbad twinning (Fig. 25 and 26). Small plagioclase grains are included in hornblende. Quartz is coarse grained, shows subgrains, undulatory extinction and in some areas myrmekitic texture. Hornblende is typically euhedral and some grains are partially replaced by chlorite. K-feldspar is partially altered and some show

myrmekitic texture along contacts with plagioclase. Few microcline are present and orthoclase shows perthitic texture. Magnetite grains are present, generally occurring with titanite. Biotite is a minor phase, and occurs as anhedral intergrowths with plagioclase. Zircon grains occur mostly between hornblende and magnetite crystals, but also occur as inclusions in plagioclase (Fig. 27). Accessory apatite occurs as included grains in plagioclase and quartz (Fig. 27). Large euhedral titanite (up to 1 mm) grains occur primarily along grain boundaries among all of the other minerals, and some crystals contain opaque oxide inclusions (Fig. 28 and 29). The crystallization sequence based on mineral occurrences and inclusion relations is plagioclase→ titanite→ hornblende→ K-feldspar + quartz.

Utuađo pluton sample 06UP-02: Granodiorite

This rock is coarse grained, holocrystalline, phaneritic, mesocratic, with porphyroclasts of plagioclase, hornblende, quartz, orthoclase and biotite (Fig. 30). This granodiorite outcrop also contained aphanitic, melanocratic, rounded to subrounded mafic xenoliths ranging from 1 to 35 cm in length.

The mineral percentage of this rock is 35% plagioclase, 30% quartz, 13% K-feldspar, 10% hornblende, 6% chlorite, 2% epidote, 2% magnetite, 1% apatite and 1% zircon. The modal abundance normalized to Q-A-P is 45% plagioclase, 38% quartz and 17% K-feldspar. The Q-A-P composition indicates the rock is granodiorite. Plagioclase grains are subhedral to anhedral, and commonly exhibit Carlsbad and albite twinning (Fig. 31). Many plagioclase grains are anhedral and show oscillatory zoning (Fig. 32). Some plagioclase show complete alteration to sericite, while others are better preserved. Quartz occurs as interstitial grains (some show subgrains), and some grains contain zircon and apatite inclusions. K-feldspar- microcline and orthoclase occur, some orthoclase show perthitic texture. Minor patches of myrmekite occur along K-feldspar grain boundaries. Green subhedral to anhedral hornblende is partially replaced by chlorite and epidote. Zircon occurs widely in orthoclase, hornblende, quartz and plagioclase grains. Magnetite occurs primarily where chlorite has replaced hornblende. Accessory apatite occurs in plagioclase and quartz. Subhedral titanite grains occur interstitial with quartz (Fig. 33).

The crystallization sequence, based on mineral occurrence and mineral inclusion relations, is plagioclase→ hornblende→ K-feldspar + quartz.

Morovis stock sample 06MS-01: Granite

This rock is coarse-grained, phaneritic, holocrystalline, mesocratic, with porphyroclasts of plagioclase, orthoclase, quartz, hornblende and pyrite (Fig. 34). This granite outcrop also contained aphanitic, melanocratic, subrounded mafic xenoliths of 1 to 10 cm in length (Fig. 35).

Primary igneous minerals in thin section are pervasively altered. Mineral percentages present in this rock are 29% K-feldspar, 25% plagioclase, 20% quartz, 15% hornblende, 3% magnetite and 5% epidote, chlorite and accessory minerals titanite, epidote, apatite and zircon. Normalized Q-A-P modal percentages for this sample are 34% plagioclase, 27% quartz and 39% K-feldspar. The Q-A-P composition indicates the rock is granite. Orthoclase show perthitic texture (Fig. 36). Most plagioclase grains preserve remnants of oscillatory zoning and Carlsbad and/or albite twinning but are pervasively altered to sericite (Fig. 37). K-feldspars are pervasively altered similar to plagioclase. Hornblendes are mostly subhedral to anhedral with a few euhedral grains and show green pleochroism and twinning. Hornblende crystals are altered to chlorite in some areas. Quartz occurs as large anhedral grains and shows undulatory extinction and interstitial aggregates. Chlorite is a minor secondary phase, and is present replacing hornblende grains. Epidote is a minor secondary phase, and occurs near plagioclase grains or as inclusions in hornblende grains. Large euhedral titanite grains and aggregates of subhedral grains occur primarily along grain boundaries of altered plagioclase and hornblende (Fig. 38). Accessory apatite occurs mostly in quartz and K-feldspar. Opaque oxides and magnetite occur mostly in or near hornblende grains. Zircon is present as an accessory mineral occurring mostly in hornblende but is also present in plagioclase (Fig. 39).

The crystallization sequence based on mineral occurrence and inclusion relations is plagioclase → hornblende → K-feldspar + quartz.

Ciales stock sample 06CS-01: Granodiorite

This rock is medium-grained, phaneritic, holocrystalline, mesocratic, with porphyroclast of plagioclase, quartz, orthoclase and hornblende (Fig. 40).

The abundance of minerals in this rock is 45% plagioclase, 20% quartz, 15% K-feldspar, 10% hornblende, 5% magnetite, 3% opaque oxides, 1% chlorite, epidote and sericite, and 1% accessory minerals zircon, titanite and apatite. The normalized Q-A-P modal percentages for

this sample are 58% plagioclase, 23% quartz and 19% K-feldspar. The Q-A-P composition indicates the rock is granodiorite. Plagioclase shows Carlsbad and albite twinning and is pervasively altered to sericite (Fig. 41). K-feldspars show perthitic texture and are also pervasively altered. Zircon grains occur in quartz and interstitial with quartz, opaque oxides and K-feldspars (Fig. 42). Euhedral and subhedral aggregates of titanite occur with hornblende and opaque oxides, primarily along quartz, magnetite and hornblende grain boundaries, but are also found as inclusions in quartz (Fig. 42 and 43). Apatite occurs as inclusions in quartz and plagioclase. Secondary chlorite occurs between plagioclase grains, oxides, titanite and quartz, and is commonly intergrowth with epidote.

The crystallization sequence based on mineral occurrence and inclusion relations is plagioclase → titanite → hornblende → K-feldspar → quartz.

Caguas stock sample 06CG-01: Granodiorite

This rock is medium-grained, phaneritic, holocrystalline, mesocratic, with porphyroclasts of plagioclase, hornblende, orthoclase, biotite and quartz (Fig. 44).

Mineral abundances in thin section are 37% plagioclase, 25% quartz, 15% K-feldspar, 10% hornblende, 5% biotite, 5% chlorite, 3% magnetite and accessory minerals titanite, zircon, epidote and apatite. The normalized Q-A-P modal percentages for this sample are 48% plagioclase, 33% quartz and 19% K-feldspar. The Q-A-P composition indicates the rock is granodiorite. Plagioclase grains are large and range from subhedral to anhedral in texture and show distinctive Carlsbad and albite twinning (Fig. 45) and oscillatory zoning (Fig. 46). Some grains are entirely replaced by sericite. Hornblende grains show green pleochroism and are altered to chlorite along the rims of the grains. Biotite is subhedral to anhedral, shows brown pleochroism and all grain margins are altered to chlorite. Subhedral to anhedral zircon occurs commonly in hornblende but also occurs interstitial with plagioclase. Titanite occurs as euhedral to anhedral grains, and is usually subhedral (Fig. 47). Quartz occurs as large crystals in biotite grains and along the edges of hornblende. Epidote is pleochroic yellow and occurs in hornblende grains.

The crystallization sequence based on mineral occurrence and inclusion relations is hornblende → titanite → plagioclase → K-feldspar → quartz.

Vieques pluton sample 06IV-01: Granodiorite

This rock is medium grained, phaneritic, holocrystalline, leucocratic, with porphyroclasts of plagioclase, quartz, hornblende, biotite, titanite and pyrite (Fig. 48). The outcrop sample 06IV-01 was collected from contains medium-grained, phaneritic, melanocratic mafic xenoliths ranging from 5 to 30 cm in length.

Mineral percentages in thin section are 35% plagioclase, 25% quartz, 15% biotite, 10% K-feldspar, 10% hornblende, and 5% epidote and accessory minerals zircon, titanite and apatite. The normalized Q-A-P modal percentages for this sample are 50% plagioclase, 36% quartz and 14% K-feldspar. The Q-A-P composition indicates the rock is granodiorite. Plagioclase grains are subhedral to anhedral; generally albite twinning is predominant and variably altered to sericite (Fig. 49) and few grains show oscillatory zoning. Quartz shows undulatory extinction and occurs as large anhedral grains and some interstitial aggregates. K-feldspar shows perthitic texture and is partially altered to sericite. Biotite occurs as large interstitial grains (Fig. 49), subhedral to anhedral, and shows brown pleochroism. Most biotite grains have ragged grain boundaries and are intergrown with epidote and chlorite. Hornblende grains are subhedral to anhedral, show green pleochroism, are partially altered to chlorite and epidote, and some of the grains have plagioclase inclusions. Anhedral epidote is pleochroic yellow and occurs interstitial with plagioclase. Subhedral titanite occurs between quartz and plagioclase (Fig. 50). Titanite grains are present as aggregates of subhedral grains. Anhedral zircon grains occur in quartz and between magnetite and altered biotite. Apatite occurs in quartz grains. The crystallization sequence based on mineral occurrence and inclusion relations is plagioclase → hornblende → K-feldspar → quartz + biotite

Cuyon stock sample 06CY-01: Quartz diorite

This rock is medium-grained, phaneritic, holocrystalline, mesocratic, with porphyroclasts of plagioclase, hornblende and minor quartz (Fig. 51).

Mineral percentages in this rock are 60% plagioclase, 17% hornblende, 12% quartz, 5% biotite, 4% chlorite, 3% orthoclase, 3% magnetite, and 1% accessory apatite, titanite, zircon and epidote. The modal percentages for this sample normalized to Q-A-P are 80% plagioclase, 16% quartz and 4% K-feldspar. The Q-A-P composition indicates the rock is quartz diorite.

Plagioclase grains range from subhedral to anhedral. Alteration is concentrated inside cores of grains, as evidenced by sericite replacement (Fig. 52). Most plagioclase grains contain albite and Carlsbad twinning, and oscillatory zoning commonly occurs in larger grains (Fig. 53). Subhedral hornblende grains show green pleochroism and some grains are partially replaced by chlorite. Some hornblende grains contain plagioclase inclusions. Biotite grains are typically small, subhedral to anhedral, show brown to green pleochroism, commonly contain epidote inclusions and are intergrown with chlorite. Quartz mostly occurs as small anhedral interstitial grains with undulatory extinction. Magnetite occurs mostly between plagioclase and quartz. Chlorite occurs replacing hornblende and shows characteristic anomalous (purple) birefringence. Accessory zircon occurs mostly as inclusions in plagioclase. Apatite occurs in quartz grains.

The mineral crystallization sequence based on mineral occurrence and inclusions relation is plagioclase → hornblende → K-feldspar → quartz.

Zanja Blanca stock sample 06ZB-01: Diorite

This rock is fine to medium-grained, phaneritic, holocrystalline, mesocratic with porphyroclasts of plagioclase, quartz and hornblende (Fig. 54).

In thin section the sample is pervasively altered. The mineralogical composition of this rock is 45% plagioclase, 20% plagioclase groundmass, 10% calcite, 10% epidote, 5% biotite, 5% magnetite and 5% chlorite. The modal percentage for this sample normalized to Q-A-P is 100% plagioclase, indicating the rock is a diorite. Plagioclase is highly altered and replaced by sericite (Fig. 55), calcite, and chlorite veins. Some of the plagioclase preserves relict albite and Carlsbad twinning; few grains shows oscillatory zoning. Plagioclase also occurs as a fine-grained altered groundmass. Hornblende and biotite are entirely replaced by intergrowths of chlorite, magnetite, epidote and calcite. Pleochroic yellow epidote occurs with secondary chlorite replacing hornblende, biotite and plagioclase. Calcite occurs as veins or masses surrounding chlorite. Magnetite occurs together with chlorite, calcite and epidote. All of the chlorite, epidote, magnetite and calcite is secondary and mostly produced by the alteration of hornblende.

Barranquitas stock sample BA-2: Diorite

This rock is medium-grained, phaneritic, holocrystalline, leucocratic, with porphyroclasts of plagioclase, quartz, hornblende and pyrite (Fig. 56).

The thin section is pervasively altered. Mineral percentages in this rock are 39% plagioclase, 30% groundmass (25% plagioclase and 5% quartz), 15% hornblende, 4% chlorite, 3% calcite, 3% actinolite, 3% quartz, 2% oxides and 1% accessory zircon, titanite and apatite. The modal percentage for this sample normalized to Q-A-P is 93% plagioclase and 7% quartz. The Q-A-P composition indicates the rock is diorite. The hand sample is phaneritic but thin section reveals a porphyritic texture. Euhedral to subhedral plagioclase shows oscillatory zoning; some grains preserve relict Carlsbad and albite twinning and are highly altered to sericite (Fig. 57). The rock has a crystalline plagioclase matrix. Subhedral to anhedral green hornblende is present and is mostly replaced by chlorite and actinolite. Zircon grains occur between the plagioclase grains in the groundmass. Apatite occurs in plagioclase and hornblende. A few sporadic anhedral titanite grains and pyrite are present. Opaque oxides occur interstitial with plagioclase and hornblende.

Coamo Arriba sample 06CA-01: Quartz diorite

This rock is medium-grained, phaneritic, holocrystalline, melanocratic, with porphyroclasts of plagioclase and hornblende (Fig. 58).

Alteration in this rock is pervasive. Mineral percentages in this rock are 50% plagioclase, 37% chlorite, 7% quartz, 3% magnetite, 2% calcite and 1% accessory mineral zircon. The modal percentage for this sample normalized to Q-A-P is 88% plagioclase and 12% quartz. The Q-A-P composition indicates the rock is quartz diorite. Plagioclase grains are subhedral to anhedral and are entirely sericitized (Fig. 59). Some plagioclase grains show relict albite and Carlsbad twinning. Quartz occurs as anhedral grains showing undulatory extinction and as aggregates of anhedral grains. Quartz grains appear preserved even though the rest of the rock is altered. Calcite occurs filling spaces between grains. Even though the rock doesn't appear porphyritic it has a groundmass of quartz, plagioclase and minor chlorite. Actinolite is intergrown with magnetite. Aligned elongated groups of opaque oxides associated with chlorite and calcite likely represent the alteration products of individual primary hornblende crystals.

4.1.3 Plutons in the Northeast Igneous Province

Rio Blanco pluton sample 06RB-01: Granodiorite

This rock is coarse-grained, phaneritic, holocrystalline, leucocratic, with porphyroclasts of plagioclase, hornblende, quartz, and biotite (Fig. 60). This rock contains aphanitic, melanocratic, subrounded xenoliths that range from 1.0 to 25 cm.

Mineral percentages for this sample are 43% plagioclase, 25% quartz, 10% hornblende, 10% biotite, 7% K-feldspar, 4% magnetite and 1% accessory minerals zircon, apatite, epidote and titanite. The modal percentages for this sample normalized to Q-A-P are 55% plagioclase, 32% quartz and 13% K-feldspar. The Q-A-P composition indicates the rock is granodiorite. Plagioclase grains range from subhedral to euhedral and some grains show oscillatory zoning (Fig. 61). Plagioclase is present as inclusions in biotite and hornblende. Some plagioclase has corroded cores with inclusions and oscillatory zoned rims with no inclusions. Other grains show distinctive Carlsbad and albite twinning (Fig. 62). Quartz grains are present with and without undulatory extinction. Zircon occurs between quartz and plagioclase grains. Apatite occurs in plagioclase and quartz. Titanite is euhedral and occurs between plagioclase and quartz grains.

The mineral crystallization sequence based on mineral occurrence and inclusion relations is hornblende → plagioclase → K-feldspar → biotite → quartz.

4.2 Mafic xenoliths

Mafic xenolith samples from the San Lorenzo, Utuado, Rio Blanco, Morovis and Vieques plutons are described in this section. Xenolith sizes range from 5 cm up to 35 cm in length. All xenoliths have the dominant assemblage of hornblende + plagioclase, typical of basaltic/gabbroic mafic rocks.

06SL-02 (in San Lorenzo granodiorite)

Euhedral to subhedral plagioclase grains are mostly preserved and commonly have Carlsbad and albite twinning. Some plagioclase grains have pericline twinning. Oscillatory

zoning in plagioclase is rare. Plagioclase commonly has apatite inclusions and some grain cores have hornblende inclusions while some others are partially altered to sericite. Subhedral to anhedral hornblende is pleochroic green. Biotite is pleochroic brown and most of the grains are altered to chlorite. Microcline coexists with hornblende. Interstitial opaque oxides occur between plagioclase and hornblende grains, and within the grains. Mineral percentages for this sample are 50% plagioclase, 30% hornblende, 10% biotite, 5% chlorite, 4% opaque oxides and 1% apatite.

06UP-01 (in Utuado pluton granodiorite)

This sample is pervasively altered. Subhedral to anhedral plagioclase grains with relic albite and Carlsbad twinning are mostly altered to sericite. Anhedral hornblende is pleochroic green. Anhedral biotite has been replaced by chlorite. Opaque oxides occur in hornblende and plagioclase grains. Mineral percentages for this sample are 50% plagioclase, 25% hornblende, 10% biotite, 12% chlorite and 3% oxides.

06RB-02 (in Rio Blanco pluton granodiorite)

Subhedral to anhedral plagioclase commonly has Carlsbad and albite twinning. Plagioclase with oscillatory zoning is rare. Plagioclase has apatite inclusions. Anhedral green hornblende has apatite inclusions. Anhedral biotite occurs between plagioclase grains and in some grains is replaced by chlorite. Opaque oxides occur in plagioclase and hornblende grains. Mineral percentages for this sample are 50% plagioclase, 20% hornblende, 15% biotite, 9% opaque oxides and 1% apatite.

06IV-02 (in Vieques pluton granodiorite)

This sample is pervasively altered. Subhedral to anhedral plagioclase have relic Carlsbad and albite twinning. Plagioclase grains are pervasively altered to sericite. Subhedral to anhedral hornblende is pleochroic green and is partially altered to chlorite. Anhedral biotite is altered to chlorite. Opaque oxides occur with hornblende and plagioclase. Quartz occurs between

plagioclase and hornblende grains. Mineral percentages for this sample are 50% plagioclase, 30% hornblende, 10% chlorite, 7% pyroxene and 3% opaque oxides.

06MS-01b (in Morovis stock)

This sample is pervasively altered. Subhedral to anhedral plagioclase grains have Carlsbad twinning. Plagioclase grains are mostly altered to sericite. Hornblende is green pleochroic with some grains altered to chlorite. Anhedral biotite grains are replaced by chlorite. Opaque oxides occur between plagioclase, hornblende and chlorite. Mineral percentages for this sample are 50% plagioclase, 30% hornblende, 8% pyroxene, 7% chlorite and 5% opaque oxides.

Summary

Petrographic analysis shows the variability of mineralogical composition among the plutonic rocks from the three igneous provinces. Plagioclase + hornblende is a ubiquitous assemblage. Based on the mineral composition and the percentage of quartz, alkali feldspar and plagioclase the rocks were classified on a ternary system (Fig. 63). This diagram shows the range of compositional variation among the plutonic rocks of Puerto Rico. Granodiorite and diorite are the most common rock types; granite and gabbro are rare. Variability of mineral occurrence and composition can be established among the igneous provinces. The CIP contains two samples (Morovis and Ciales stocks) that are rich in K-feldspar and are the only high-K plutonic rocks.

4.3 Cathodoluminescence images

Cathodoluminescence (CL) images of zircons from this study reveal that all zircons preserve simple igneous zoning patterns and no inherited cores. Figure 64 shows a set of representative zircon grains for 13 plutons, all showing igneous growth zoning (oscillatory and sector zoning). Zircon grains are euhedral and have similar internal structure within each pluton (Fig. 65-68)

4.4 Major, minor, and trace element analysis

Chemical analyses for major, minor and trace elements of 21 rock samples representing 13 plutons of Puerto Rico are included in this section (Table 3). Chemical analysis of 5 mafic xenolith samples from San Lorenzo batholith and Utuado, Vieques, Morovis and Rio Blanco stocks are also included in Table 3. The detection limit (DL) for each element is based on the precision of the measurements at 2 standard deviations (Table 3). Most of the samples yield analytical totals >97%, whereas 7 samples yield low analytical totals from 92-97% that may indicate alteration.

Figure 69 shows major and minor (MgO, MnO, CaO, FeO, Al₂O₃, K₂O, Na₂O, TiO₂ and P₂O₅ in wt.%) and trace element (Zr in ppm) variations against wt.% SiO₂. Samples from the NIP and CIP mimic the general trend where samples with higher wt.% SiO₂ have a lower MgO content. From the SIP, the Tea Diorite sample yields the lowest MgO (1.07 wt.%) while the Tibes stock yield the highest MgO content for the plutonic rocks (6.51 wt.%). Mafic xenolith samples yield relatively higher MgO values (4.30 to 6.85 wt.%). For MnO, CaO and FeO the plutonic and xenolith samples have a similar tendency where elevated wt.% SiO₂ samples yield lower wt.% MnO, CaO and FeO. The highest MnO (wt.%) content is 0.36 (Coamo Arriba stock) and the lowest is 0.06 (Cuyon stock). The highest CaO (wt.%) content is 12.04 (Tibes stock) and the lowest is 2.47 (Ciales stock). Values for wt.% FeO range from 3.00 (Tea Diorite) to 12.77 (Tibes stock). Both samples are from the SIP which reflects the high variability within the plutons in the SIP. Wt.% Al₂O₃ ranges from 14.36 (sample 06TS-06) to 22.01 (sample 06TS-12). For the xenolith samples the lowest wt.% Al₂O₃ value is 14.36 (Utuado pluton) and the highest wt.% Al₂O₃ value is 19.80 (Morovis stock). For the plutonic samples the K₂O content range from 4.26 (Morovis stock) to 0.39 wt.% (San Lorenzo batholith- diorite). A xenolith sample from the Utuado pluton yields the highest K₂O content (2.77 wt.%) within the other xenolith samples. Plutonic samples have a general trend where elevated wt.% SiO₂ samples have elevated wt.% Na₂O ranging from 2.59 to 4.32. A xenolith sample from the Morovis stock yields the highest Na₂O content (5.56 wt.%) within the other xenolith samples. Most plutonic and xenolith samples range in wt.% TiO₂ from 0.33 to 0.99 with the exception of the Tibes stock where values range from 1.23 to 2.31. Plutonic and xenolith samples yield wt.% P₂O₅ values from 0.09 to 0.44.

The wt.% SiO₂ values for the CIP ranges from 54.66 (diorite from San Lorenzo batholith) to 66.54 (granodiorite from Utuado pluton). The highest Zr content reported from the CIP was 132 ppm for Ciales stock (wt.% SiO₂= 65.05) and the lowest Zr values was 39 ppm for diorite sample from San Lorenzo batholith (wt.% SiO₂= 54.66). The wt.% SiO₂ values for the SIP ranges from 49.94 (Tibes diorite) to 66.46 (Tea diorite porphyry). Tibes stock is the only gabbro sample within the 3 igneous provinces. The highest Zr content reported from the SIP was 192 ppm for Las Tunas stock (wt.% SiO₂= 61.54) and the lowest Zr values was 44 ppm for diorite from Tibes stock (wt.% SiO₂= 50.41). The Rio Blanco pluton, the only sample analyzed from the NIP, yields a wt.% SiO₂ value of 61.46 with a Zr content of 89 ppm.

The average wt.% SiO₂ for the analysis of these plutonic rocks, excluding the Tibes stock values, is 60.22% which is comparable to the mean of 62.4 wt.% SiO₂ for published chemical analysis of these rocks (Cavosie et al., 2008).

4.5 Oxygen isotopes analysis

This section includes the $\delta^{18}\text{O}$ analyses for 41 intrusive rock samples from the three igneous provinces of Puerto Rico (Table 4). From this total, 24 new samples were collected during this study and the remaining 17 samples are from the UPRM archive (Smith et al., 1998; Schellekens et al., 1998). Samples from the UPRM collection were only analyzed for $\delta^{18}\text{O}$ quartz and whole rock; the remaining sample sizes weren't large enough for zircon or titanite separation. The UPRM archive samples have published geochemical data that were used to get a general idea of distribution and composition of the plutonic rocks in Puerto Rico (Frost et al., 1998; Schellekens, 1998a; Smith et al., 1998).

Whole rock

$\delta^{18}\text{O}(\text{WR})$ analyses were performed on 40 whole rock samples including the mafic xenoliths (Table 4). Measured $\delta^{18}\text{O}(\text{WR})$ values vary considerably among the plutonic suite of Puerto Rico with values ranging from 6.23‰ (Tibes stock) to 11.42‰ (Rincon porphyry) (Fig. 70C). Qualitative analysis of rocks with elevated $\delta^{18}\text{O}(\text{WR})$ in thin section demonstrates

variable amounts of alteration. Some of the highest $\delta^{18}\text{O}(\text{WR})$ values can be explained as a product of sub-solidus rock alteration. A quantitative value of this alteration is calculated with the following equation (Valley et al., 1994; Lackey et al., 2005; Valley et al., 2005):

$$\Delta^{18}\text{O}(\text{Zrc-WR}) = \delta^{18}\text{O}(\text{Zrc}) - \delta^{18}\text{O}(\text{WR}) \approx -0.0612(\text{wt.}\% \text{SiO}_2) + 2.50\text{‰}$$

The predicted $\delta^{18}\text{O}(\text{WR})$ is calculated based on the measured value for $\delta^{18}\text{O}(\text{Zrc})$. This value is then compared to the measured $\delta^{18}\text{O}(\text{WR})$. The difference between the calculated and measured $\delta^{18}\text{O}(\text{WR})$ is the product of subsolidus alteration of $\delta^{18}\text{O}(\text{WR})$ (Lackey et al., 2005). $\delta^{18}\text{O}(\text{Zrc})$ is used in this calculation since it records magmatic $\delta^{18}\text{O}$; it is not affected by subsolidus alteration.

The petrographic analyses (See section 4.1) were used to qualitatively assess the measured $\delta^{18}\text{O}(\text{WR})$ values and to explain the elevated $\delta^{18}\text{O}(\text{WR})$ values. The Las Tunas, Rincon porphyry, Tea Diorite, Maguayo porphyry, Coamo Arriba, Barranquitas, Utuado and Morovis stocks all have elevated $\delta^{18}\text{O}(\text{WR}) > 7.5\text{‰}$. Minerals (plagioclase, K-feldspar) in the Morovis (Fig. 36, 37), Coamo Arriba (Fig. 59) and Las Tunas (Fig. 16) stocks are severely altered (almost entirely replaced by sericite). The $\delta^{18}\text{O}$ of these minerals are the product of alteration and show that measured $\delta^{18}\text{O}(\text{WR})$ doesn't reflect the magmatic $\delta^{18}\text{O}(\text{WR})$ composition of these samples.

Zircon

Zircons from 14 samples were analyzed for oxygen isotope ratio (Table 4). Oxygen isotope analysis of zircon is used to “see through” alteration in rocks, including hydrothermal alteration and metamorphism, where the $\delta^{18}\text{O}(\text{WR})$ is reset (Valley, 2003). The $\delta^{18}\text{O}(\text{Zrc})$ values range from 5.33‰ (Cuyon and Tibes stock) to 7.17‰ (Las Tunas stock). Samples from Morovis, Ciales, Caguas, Barranquitas and Las Tunas stocks have considerably elevated values (6.32 to 7.17‰) from the predicted primitive mantle values, $5.3 \pm 0.6\text{‰}$, 2SD (Valley et al., 1998). Samples from San Lorenzo batholith, Utuado, Rio Blanco, Vieques, Tibes, Tea diorite, Cuyon and Coamo Arriba stocks preserve primitive mantle zircon values, ranging from 5.33 to

5.77‰. Figure 70B shows a histogram of the distribution of $\delta^{18}\text{O}(\text{Zrc})$ values for plutonic rocks of Puerto Rico. Values in the shaded area represent mantle-equilibrated $\delta^{18}\text{O}(\text{Zrc})$ ($5.3 \pm 0.6\text{‰}$) values. The five additional samples with higher values represent elevated $\delta^{18}\text{O}(\text{Zrc})$ values indicative of crustal contamination (Valley et al., 2005).

Quartz

Values of $\delta^{18}\text{O}(\text{Qtz})$ were analyzed for 28 samples of plutonic rock (Table 4). $\delta^{18}\text{O}(\text{Qtz})$ values range from 8.30‰ (Coamo Arriba stock) to 10.12‰ (Ciales stock). $\delta^{18}\text{O}(\text{Qtz})$ values for the largest plutonic bodies of Puerto Rico (San Lorenzo and Utuado plutons) range from 8.5 to 9.6‰. The Ciales stock yields the highest $\delta^{18}\text{O}(\text{Qtz})$ value of 10.12‰. Figure 70D shows a histogram of the distribution of $\delta^{18}\text{O}(\text{Qtz})$ values for plutonic rocks. Three of the samples with elevated $\delta^{18}\text{O}(\text{Qtz})$ correspond to elevated $\delta^{18}\text{O}(\text{Zrc})$ values ($>5.3 \pm 0.6\text{‰}$). Comparisons of $\delta^{18}\text{O}(\text{Qtz})$ with $\delta^{18}\text{O}(\text{Zrc})$ are discussed in the following sections to determine the apparent closing temperatures for the quartz-zircon pairs.

Titanite

The $\delta^{18}\text{O}(\text{Tnt})$ was analyzed for 6 samples of plutonic rocks (Table 4). $\delta^{18}\text{O}(\text{Tnt})$ values range from 4.15‰ (Utuado pluton) to 5.51‰ (Ciales stock). The magnitude of titanite values analyzed in this study mimics the general trend of $\delta^{18}\text{O}(\text{Zrc})$. Plutons with primitive $\delta^{18}\text{O}(\text{Zrc})$ yield lower $\delta^{18}\text{O}(\text{Tnt})$ values: 4.15‰ (Utuado), 4.23‰ (Vieques), and 4.31‰ (San Lorenzo); whereas plutons with 'high' $\delta^{18}\text{O}(\text{Zrc})$ yield higher $\delta^{18}\text{O}(\text{Tnt})$ values of 5.11‰ (Caguas), 5.28‰ (Morovis), and 5.51‰ (Ciales). Figure 70A shows a histogram with the distribution $\delta^{18}\text{O}(\text{Tnt})$ values for plutonic rocks. Comparisons of $\delta^{18}\text{O}(\text{Tnt})$ with $\delta^{18}\text{O}(\text{Zrc})$ are discussed in the following section to determine the apparent closing temperatures for the titanite-zircon pairs.

$\delta^{18}\text{O}$ values for coexisting zircon, quartz and titanite

Experimental analyses of oxygen isotope fractionation of coexisting minerals allow an empirical calibration of the oxygen isotope partitioning (King et al., 2001; Valley et al., 2003). The fractionation of $\delta^{18}\text{O}$ between coexisting minerals can be used to determine the apparent closure temperatures of oxygen isotope exchange during the cooling history of the magma. These temperatures can be reset by subsolidus alteration. The $\Delta^{18}\text{O}$ fractionation of coexisting pairs of minerals is presented in Table 5 and is discussed in the following section.

Chapter 5

DISCUSSION

Puerto Rico is a complex island arc terrane with plutonic intrusive activity from 85 Ma to 38 Ma (Cavosie et al., 2008). These plutonic intrusions are heterogeneously distributed among the three igneous provinces and exposed plutons vary from ~1 to 500 km² (stock to batholith scale). The origin of these rocks has been intensively studied by several authors but is still speculative since the parental magmas for these plutons have not been identified. This thesis was designed to place better constraints and new ideas on the origin of the granitic rocks from this island arc. This section includes a discussion of petrographic analyses, WR major elements, and $\delta^{18}\text{O}$ of WR, zircon, quartz and titanite that were used to constrain the origin of these granitoids.

5.1 Oxygen isotopes of whole rock

Measured $\delta^{18}\text{O}(\text{WR})$ values for plutonic samples among the three igneous provinces vary considerably, ranging from 6.23‰ to 11.42‰ over a range of wt.% SiO₂ of 48.84 to 70.49 % (Fig. 71; Table 4). Qualitative petrographic analyses of these granitic rocks reveals that samples with $\delta^{18}\text{O}(\text{WR}) > 7.5\text{‰}$ are partially to pervasively altered whereas samples with $\delta^{18}\text{O}(\text{WR}) < 7.5\text{‰}$ are generally better preserved (Fig. 70C). $\delta^{18}\text{O}(\text{WR})$ values for samples from the major intrusions, including San Lorenzo batholith, Utuado, Vieques, Caguas and Rio Blanco stocks, yield primitive $\delta^{18}\text{O}(\text{WR})$ values, ranging from 6.24 to 7.72‰, for a range of wt.% SiO₂ 58.03 to 66.54‰. Other stocks (<20 km²) yield higher $\delta^{18}\text{O}(\text{WR})$ values, ranging from 7.47 to 10.27‰. San Lorenzo batholith samples (PP-1, PRP-11, PRP-105) and Las Tunas, Rincon porphyry, Tea Diorite, Maguayo porphyry, Coamo Arriba, Barranquitas, Utuado and Morovis stocks all have elevated $\delta^{18}\text{O}(\text{WR}) > 7.5\text{‰}$, which is interpreted to result from moderate to pervasive alteration observed in thin section.

$\delta^{18}\text{O}(\text{WR})$ values from mafic xenoliths collected from the San Lorenzo, Utuado, Rio Blanco, Morovis and Vieques plutons range from 5.92 to 8.88‰ over a range of 51.42 to 56.77 wt. % SiO₂ (Fig. 72). Mafic xenoliths from 3 granitoids (Utuado, San Lorenzo diorite, Rio Blanco) yield $\Delta^{18}\text{O}(\text{WR granitoid} - \text{WR mafic xenolith})$ from 0.42 to 0.58‰. The largest

$\Delta^{18}\text{O}(\text{WR granitoid} - \text{WR mafic xenolith})$ value was measured in the Morovis stock, where the $\Delta^{18}\text{O}(\text{WR granitoid} - \text{WR mafic xenolith})$ is 1.2‰ due to pervasive alteration of the WR granitoid. The host rock-xenolith pair from the Vieques pluton yielded the smallest $\Delta^{18}\text{O}$, 0.06 ‰. Petrographic analysis of the xenoliths reveals igneous textures (e.g., oscillatory zoning in plagioclase) and assemblages dominated by hornblende + plagioclase, indicative of an igneous origin in a hydrous melt. The xenolith results $\delta^{18}\text{O}$ (with the exception of Vieques) are consistent with the derivation of the granitoid plutons from gabbroic parental melts represented by the xenoliths. The small fractionations of $\Delta^{18}\text{O}(\text{WR granitoid} - \text{WR mafic xenolith})$ are permissible for magmatic processes such as partial melting or fractional crystallization. It is thus possible that the mafic xenoliths represent the elusive gabbroic source(s) for the granitoids in Puerto Rico.

5.2 Oxygen isotopes of zircon, quartz and titanite.

Oxygen isotopes of zircon

Zircon was selected for $\delta^{18}\text{O}$ analysis because of its capacity for retaining magmatic $\delta^{18}\text{O}$ values, as whole rock values can be affected by subsolidus alteration. From a total of 14 zircon samples analyzed in this study, 9 samples yield primitive (mantle-like) $\delta^{18}\text{O}(\text{Zrc})$ values (Fig. 70B). $\delta^{18}\text{O}(\text{Zrc})$ values for the Upper Cretaceous intrusions Caguas, Ciales, Morovis and Las Tunas stock are elevated (relative to $\delta^{18}\text{O} = 5.3 \pm 0.6\text{‰}$, 2SD; Valley et al., 1998) from primitive mantle values. Other plutons like Coamo Arriba, San Lorenzo, and Vieques, intruded over the same time interval (85.6 ± 1.3 to 67.1 ± 1.6 Ma) yet preserve primitive $\delta^{18}\text{O}(\text{Zrc})$ values ranging from 5.34 to 5.71‰. The only Paleocene intrusion (Tibes stock) and 3 Eocene intrusions (Tea Road, Cuyon, and Rio Blanco) yield primitive mantle values of $\delta^{18}\text{O}(\text{Zrc})$ from 5.33‰ to 5.62‰. The Barranquitas stock with U/Pb zircon age of 47.7 ± 1.6 Ma yields elevated $\delta^{18}\text{O}(\text{Zrc})$ of 6.75‰. Two samples of the largest intrusion, the San Lorenzo batholith ($\sim 500 \text{ km}^2$), yield values of $\delta^{18}\text{O}(\text{Zrc}) = 5.63 \pm 0.04\text{‰}$ for granodiorite and $\delta^{18}\text{O}(\text{Zrc}) = 5.51 \pm 0.10\text{‰}$ for diorite. Cathodoluminescence images of zircon from both samples of the San Lorenzo Batholith show simple igneous zoning patterns (Fig. 65a-b)

The oldest intrusion analyzed in this study is the Coamo Arriba stock with a U/Pb zircon age of 85.6 ± 1.3 Ma (Table 6) (Cavosie et al., 2008), and $\delta^{18}\text{O}(\text{Zrc}) = 5.34 \pm 0.10\%$. This event was followed by the crystallization of the Ciales, Morovis and Las Tunas stocks (83.9 to 79 Ma, Cavosie et al., 2008) which have elevated $\delta^{18}\text{O}(\text{Zrc})$ values relative to mantle values ($5.3 \pm 0.6\%$, 2SD) suggesting a time period where high $\delta^{18}\text{O}$ materials (e.g., sediments or altered ocean crust) were incorporated into magmas, enriching the $\delta^{18}\text{O}$ of the magma. The two largest intrusions of the island arc terrane, San Lorenzo batholith and Utuado pluton yield primitive $\delta^{18}\text{O}(\text{Zrc})$ values (5.51 to 5.71%) which constrain that there were no sediment incorporation into these magmas.

The Caguas stock was emplaced at 66.8 Ma and yields an enriched $\delta^{18}\text{O}(\text{Zrc})$ value (6.32%) suggesting incorporation of crustal material during subduction activity. Tibes stock was emplaced at 60.5 ± 1.2 Ma (Cavosie et al., 2008) with $\delta^{18}\text{O}(\text{Zrc})$ value of 5.33% . This Paleocene intrusion doesn't have $\delta^{18}\text{O}$ enrichment and is the only plutonic body reported during this time period. From 60.5 Ma to ~ 48 Ma there is no record of plutonic activity in Puerto Rico. The Eocene intrusions Rio Blanco, Cuyon, and Tea Road have primitive $\delta^{18}\text{O}(\text{Zrc})$ values. Barranquitas stock has elevated $\delta^{18}\text{O}(\text{Zrc})$ values of 6.75% . This stock yield an age of 47.7 Ma which is the same as the Rio Blanco stock (47.7 Ma) and Cuyon stock (47.6 Ma) but in contrast to the Barranquitas stock, these plutons have primitive $\delta^{18}\text{O}(\text{Zrc})$ values. Tea Diorite is the youngest intrusion studied in this research project, at 38.4 Ma (Cavosie et al., 2008), and has a $\delta^{18}\text{O}(\text{Zrc}) = 5.62\%$; wt.% $\text{SiO}_2 = 66.46$.

The few plutons from the SIP show large variability in their $\delta^{18}\text{O}(\text{Zrc})$ values. The Tibes stock shows primitive $\delta^{18}\text{O}(\text{Zrc})$ values and Las Tunas stock shows the highest $\delta^{18}\text{O}(\text{Zrc})$ value for the entire island arc.

Oxygen isotopes of quartz

The values of $\delta^{18}\text{O}(\text{Qtz})$ range from 8.30% (Coamo Arriba stock) to 10.12% (Ciales stock). The main batholiths San Lorenzo and Utuado yield $\delta^{18}\text{O}(\text{Qtz}) = 8.31$ to 8.58% . These values are in disequilibrium compared with $\delta^{18}\text{O}(\text{Zrc})$ values, ($\Delta^{18}\text{O}_{\text{Qtz-Zrc}}$) (Table 5). This disequilibrium is explained by the fact that the rates of oxygen diffusion for quartz and zircon are different. Farver and Yund (1991) explain that oxygen isotope diffusion in quartz is fast relative

to zircon, and it continues exchanging oxygen at lower temperatures. Experimental and empirical analysis of oxygen diffusion in zircon show slow rates and the closure temperature for oxygen exchange is relatively high ($>750^{\circ}\text{C}$) (Watson and Cherniak, 1997; Valley et al., 2003; Peck et al., 2003; Lackey, 2005). Most $\Delta^{18}\text{O}(\text{Qtz-Zrc})$ values for the plutonic rocks of Puerto Rico are in disequilibrium and this can be explained by resetting of $\delta^{18}\text{O}(\text{Qtz})$ during post magmatic cooling. Possible exceptions are the San Lorenzo batholith ($\Delta^{18}\text{O}(\text{Qtz-Zrc})= 2.85\text{‰}$), Tea diorite stock ($\Delta^{18}\text{O}(\text{Qtz-Zrc})= 2.88\text{‰}$) and Rio Blanco pluton ($\Delta^{18}\text{O}(\text{Qtz-Zrc})=2.90\text{‰}$) where oxygen isotope fractionation between zircon and quartz is close to expected values (2.64‰; Valley et al., 2003) for this mineral pair fractionations. Petrographic analyses of these plutons show no profound alteration which supports the primary (magmatic) values.

Oxygen isotopes of titanite

Titanite was found only in plutons from the CIP, with wt.% SiO_2 values ranging from 62.96 to 66.54. The values of $\delta^{18}\text{O}(\text{Tnt})$ range from 4.15 (Utuaedo pluton) to 5.51‰ (Ciales stock). $\delta^{18}\text{O}(\text{Tnt})$ values for the Ciales and Morovis stocks are similar but not identical, probably affected by the degree of alteration of the samples. Titanite has an oxygen diffusion rate different than zircon. Titanite has a faster oxygen diffusion compared to zircon and the closure temperature is lower (King et al., 2001; Valley et al., 2003; Lackey et al., 2005).

$\delta^{18}\text{O}(\text{WR})$ vs. $\delta^{18}\text{O}(\text{Zrc})$

The $\delta^{18}\text{O}(\text{WR})$ values can be affected by low temperature processes that alter the minerals, increasing the $\delta^{18}\text{O}$ values. One method to evaluate the $\delta^{18}\text{O}$ WR values is by making a comparison with the $\delta^{18}\text{O}$ zircon (Fig. 73). An example of the systematics for zircon, quartz, and whole rock in magmatic equilibrium is a diagram from Lackey (2005) (Fig. 4). This diagram represents the values for quartz and zircon as a function of wt. % SiO_2 . The fractionations between $\Delta^{18}\text{O}(\text{Qtz-WR})$ and $\Delta^{18}\text{O}(\text{Zrc-WR})$ remain the same regardless of the bulk WR $\delta^{18}\text{O}$. Low $\delta^{18}\text{O}(\text{WR})$ values can represent alteration of the magmas, and show non-equilibrium fractionation of oxygen isotopes between zircon and the whole rock.

Evaluation of the $\Delta^{18}\text{O}(\text{WR-Zrc})$ to evaluate the subsolidus alteration of the rocks is based on the equation:

$$\Delta^{18}\text{O}(\text{WR-Zrc}) = \delta^{18}\text{O}(\text{WR}) - \delta^{18}\text{O}(\text{Zrc}) \approx 0.0612(\text{wt.}\% \text{ SiO}_2) - 2.50\text{‰}$$

(Valley et al., 1994; Lackey et al., 2005; Valley et al., 2005)

This equation was characterized based on solidus temperatures for rock compositions from gabbro to high-silica granite. An example for determining subsolidus alteration: Caguas stock, a rock with wt.% $\text{SiO}_2 = 64.91$, $\delta^{18}\text{O}(\text{Zrc}) = 6.32\text{‰}$, and $\delta^{18}\text{O}(\text{WR}) = 7.47\text{‰}$ (measured value). Using the equation from Valley et al. (2005) a value of $\delta^{18}\text{O}(\text{WR})$ is calculated (7.79‰) using the wt.% SiO_2 and $\delta^{18}\text{O}(\text{Zrc})$. The difference of the calculated $\delta^{18}\text{O}(\text{WR})$ value and measured $\delta^{18}\text{O}(\text{WR})$ is attributed to subsolidus alteration of $\delta^{18}\text{O}(\text{WR})$; in this example $7.79\text{‰} - 7.47\text{‰} = 0.32$, which represents slight subsolidus alteration. Comparison of measured $\delta^{18}\text{O}(\text{WR})$ and calculated $\delta^{18}\text{O}(\text{WR})$ for this suite of rocks shows values ranging from undetectable to 3.93‰ (Table 5). Figure 73 show that most plutons in Puerto Rico have experienced low-temperature alteration of the WR.

Fractionation of $\delta^{18}\text{O}$ between coexisting minerals

$\delta^{18}\text{O}$ values for coexisting mineral pairs are compared to determine their oxygen fractionation (exchange) and their isotopic equilibrium during crystallization:

$$\Delta^{18}\text{O}_{\text{A-B}} = \delta^{18}\text{O}_{\text{A}} - \delta^{18}\text{O}_{\text{B}} \approx 1000 \ln (\alpha_{\text{A-B}}) = A_{(\text{A-B})} * 10^6 / T^2 \text{ (Valley et al., 2003)}$$

Equilibrium fractionations are calculated using temperature dependance:

$$1000 \ln (\alpha_{\text{A-B}}) = A_{(\text{A-B})} * 10^6 / T^2$$

In this expression, T is temperature (in kelvin), A is the experimentally determined coefficient, and $1000 \ln (\alpha_{\text{A-B}})$ is the fractionation between two minerals, A and B. A-coefficients for oxygen isotopes used in this study are: quartz-zircon = 2.64, quartz-titanite = 3.66, and zircon-titanite = 1.02 (Valley et al., 2003).

The above equation was used to determine the apparent crystallization temperatures of the system based on the mineral fractionations. A line that intersects the origin in a graph has a 0.0‰ fractionation; this is used to create isotherms for coexisting mineral pairs and to estimate their apparent crystallization temperature based on their $\delta^{18}\text{O}$ fractionation. If values of coexisting minerals move along the same isotherm this may represent magmatic variation. Values located on different isotherms may represent fast/slow cooling or alteration (e.g., meteoric water) (Lackey et al., 2005).

The range of apparent crystallization temperatures based on quartz-zircon fractionation is from 689°C for the San Lorenzo granodiorite to 609 °C for the Ciales granodiorite (Fig. 74). The Utuado (613 °C) and Ciales plutons (609 °C) have lower apparent temperatures than assumed magmatic temperatures for similar composition rocks from the Sierra Nevada batholith (e.g., 850 - 650°C; Lackey et al., 2005). Given that zircon has been demonstrated by experimental and empirical studies to retain magmatic $\delta^{18}\text{O}$ values (Valley et al., 2003; Lackey et al., 2005), changes in primary $\delta^{18}\text{O}(\text{Qtz})$ values are likely the cause of low apparent temperatures. The Utuado pluton is the second largest intrusion in the island arc and the lower apparent temperature for quartz-zircon fractionation may be explained by slower cooling of the magma allowing oxygen exchange in quartz for a longer time period. The lower apparent temperature for Ciales stock may also be explained by continuous exchange of $\delta^{18}\text{O}$ in quartz during slow cooling, however the exposed Ciales stock is much smaller than the Utuado pluton.

Zircon-titanite fractionations yield an apparent crystallization temperature range from 645°C for the Caguas pluton to 535°C for the Utuado pluton (Fig. 75). The apparent temperatures for the Vieques (541 °C) and Utuado (535°C) plutons are low compared to magmatic temperatures. Analyses of oxygen isotope fractionation between zircon-titanite fractionation from Sierra Nevada batholith (Lackey et al., 2005) and Idaho batholith (King et al., 2001) have demonstrated different apparent temperatures for primary (igneous) and secondary (metamorphic) titanite. Petrographic analyses of plutonic samples of the island arc show no evidence of metamorphic titanite (Fig. 42). A comparison of the apparent temperatures of zircon-titanite with the results for primary and secondary titanite from Lackey et al. (2005), shows that the low apparent temperatures for the island arc plutons from Puerto Rico (645 to 535°C) are higher than the highest apparent temperatures recorded by secondary (metamorphic) titanite from the Sierra Nevada batholith, which supports the interpretation that the titanite

analyzed in this study is primary (igneous). The fact that the lowest apparent temperatures are found in large plutonic bodies (Vieques, 541°C and Utuado 535°C) may again be explained by slow cooling of the magma, allowing oxygen isotope exchange in titanite for a longer time. The highest apparent zircon-titanite temperatures recorded (Ciales, 641°C and Caguas 645°C) are consistent with the closure temperature of titanite to oxygen diffusion of ~ 650 °C suggested by King et al. (2001).

The fractionations for quartz-titanite show an apparent crystallization temperature range from 664°C for the San Lorenzo granodiorite to 589°C for Utuado pluton (Fig. 76). The fractionations between quartz-titanite for Utuado and Vieques plutons show an apparent temperature (589 to 607 °C) that is lower than expected magmatic temperatures. These lower temperatures may again be explained by a slow cooling based on the size of these plutons, allowing oxygen isotope exchange in quartz and titanite for a longer time period. No evidence of secondary titanite was found in petrographic analyses. These results may also be explained by subsolidus alteration of quartz, resetting $\delta^{18}\text{O}(\text{Qtz})$ values.

Figure 77 shows SiO_2 (wt.%) vs. $\delta^{18}\text{O}$ (‰) values for whole rock, quartz, titanite and zircon for the six titanite-bearing plutonic samples analyzed in this study. All samples mimic the general trend of oxygen isotope enrichment where $\delta^{18}\text{O}(\text{Tnt}) < \delta^{18}\text{O}(\text{Zrc}) < \delta^{18}\text{O}(\text{WR}) < \delta^{18}\text{O}(\text{Qtz})$ with the exception of the Morovis stock, where the $\delta^{18}\text{O}(\text{WR})$ value is higher than $\delta^{18}\text{O}(\text{Qtz})$. Petrographic analysis of this pluton show pervasively alteration in thin section which indicates that the measured $\delta^{18}\text{O}(\text{WR})$ does not represent magmatic $\delta^{18}\text{O}$.

5.3 Origin of plutonism in Puerto Rico

The magmatic evolution of Puerto Rico as recorded by plutonic activity can be divided in three major events, Santonian, Late Campanian-Maastrichtian and Eocene intrusions (Cavosie et al., 2008). The first record of plutonism in the island arc is the Coamo Arriba stock (85.6 \pm 1.3 Ma). Simultaneously with this Santonian age intrusion was the intrusion of the Morovis and Ciales stocks (85.3 \pm 1.8 Ma; 83.9 \pm 1.7 Ma respectively) (Fig. 78). The Coamo Arriba stock is

compositionally different (Fig. 69), both in major/minor element composition and $\delta^{18}\text{O}(\text{Zrc})$, than the Morovis and Ciales stocks. After a hiatus of ~ 10 Ma, the largest two intrusions, San Lorenzo and Utuado plutons were emplaced during the Campanian-Maastrichtian. Samples from the San Lorenzo batholith yield similar ages, 75.1 ± 2.1 Ma (granodiorite) and 74.1 ± 1.4 Ma (quartz diorite). Previously, Lower Cretaceous ages were determined for this batholith [amphibole K-Ar ages 100 ± 15 Ma; 109 ± 9 Ma (Cox et al., 1977)] but these values were not duplicated. K-Ar ages of hornblende (78.4 ± 1.6 Ma and 70.6 ± 3.2 Ma) overlaps with zircon ages. Along the western and eastern margins of the San Lorenzo batholith two stocks were emplaced during the Maastrichtian, the Caguas and Vieques pluton (67.1 ± 1.6 Ma and 66.8 ± 1.2 Ma). The Vieques pluton (separated from the main island) has been previously described as part of the CIP based on the compositional and age similarities with the San Lorenzo batholith (Cavosie et al., 2008). The Eocene intrusions Rio Blanco, Cuyon and Barranquitas stocks comprised the final events of plutonic activity in Central and Eastern Puerto Rico.

The SIP, which has been described as a separate unit from the rest of the island based on composition and tectonic setting (Schellekens, 1998a; Jolly et al., 2007) has three reported zircon ages that do not correlate with any other plutonic activity in the rest of the island. The oldest intrusion age for the SIP is 79.0 ± 2.1 Ma for Las Tunas stock (Cavosie et al., 2008). This event was followed by the Paleocene Tibes stock (60.5 ± 1.6 Ma). The youngest zircon age reported in Puerto Rico is Tea Diorite (38.4 ± 0.8 Ma), which represents the end of magmatism in the island.

5.4 Tectonic model for isotopically bimodal plutons

Plutonic rocks in Puerto Rico show a remarkable limited range in WR major, minor, and trace elements, suggesting a common origin. Analysis of these plutonic intrusions based on their geographic location among the three igneous provinces, $\delta^{18}\text{O}(\text{Zrc})$ values and their age of crystallization shows a continuous and complex magmatic history during the evolution of this Cretaceous island arc (Fig. 79). The first record of plutonism in Puerto Rico (85 to 80 Ma) is recorded by simultaneous intrusion of isotopically ($\delta^{18}\text{O}$) primitive (mantle-like) and elevated (crustal contaminated) plutons that are closely spaced (Fig. 79). This scenario is well

documented in the CIP. The Coamo Arriba pluton (85.6 ± 1.3 Ma, $\delta^{18}\text{O}(\text{Zrc})= 5.34\text{‰}$), and Ciales and Morovis stocks (83.9 ± 1.7 Ma, $\delta^{18}\text{O}(\text{Zrc})= 6.73\text{‰}$; 83.5 ± 1.8 Ma, $\delta^{18}\text{O}(\text{Zrc})= 6.69\text{‰}$) have dramatically different oxygen isotope ratios despite being intruded over the same time interval in nearly the same location. The same scenario occurred during emplacement of the largest plutons in Puerto Rico approximately 10 Ma later. Samples from the San Lorenzo batholith (74.1 ± 1.3 Ma, $\delta^{18}\text{O}(\text{Zrc})= 5.34\text{‰}$; 75.1 ± 2.1 Ma, $\delta^{18}\text{O}(\text{Zrc})= 5.63\text{‰}$), Utuado pluton (70.8 ± 1.2 Ma, $\delta^{18}\text{O}(\text{Zrc})= 5.71\text{‰}$) and Vieques pluton (67.1 ± 1.6 Ma, $\delta^{18}\text{O}(\text{Zrc})= 5.77\text{‰}$) all have primitive $\delta^{18}\text{O}$ in contrast with the Caguas stock (66.8 ± 1.2 Ma, $\delta^{18}\text{O}(\text{Zrc})= 6.32\text{‰}$) which has an elevated $\delta^{18}\text{O}$ over the same time interval (75 – 67 Ma). The final record of plutonism in Central Puerto Rico during Eocene (~47 Ma) still produced isotopically bimodal plutons in close proximity to each other. The Rio Blanco pluton (47.7 ± 2.1 Ma, $\delta^{18}\text{O}(\text{Zrc})= 5.54\text{‰}$) and Cuyon stock (47.6 ± 0.8 Ma, $\delta^{18}\text{O}(\text{Zrc})= 5.33\text{‰}$) overlap in age with the Barranquitas stock (47.7 ± 1.6 Ma, $\delta^{18}\text{O}(\text{Zrc})= 6.75\text{‰}$) which has elevated $\delta^{18}\text{O}(\text{Zrc})$ despite separated by less than 10 km. A model is proposed to explain the generation of isotopically bimodal plutons during the magmatic evolution of the island arc (Fig. 80).

A crustal component (with elevated $\delta^{18}\text{O}$ material) is needed to satisfy that some of the plutons have enriched $\delta^{18}\text{O}(\text{Zrc})$ values, and this crustal component persisted during the complete evolution of the arc from ~85 to 47 Ma. It has been proposed by several authors that before a polarity reversal takes place, a breakage of what is the backarc (it will become the forearc after the polarity reversal) will break (fault) on a weak zone (young and thin lithosphere backarc) where the new subduction will take place (Stern, 2004). Stern (2004) described the Cenozoic example of the Solomon convergent margin with the Ontong Java Plateau where the new subduction zone formed behind the magmatic arc. He classified this example as an induced nucleation subduction zone (INSZ) polarity reversal. It is possible that during this breakage of the oceanic crust (which is composed of altered basalt and materials with elevated $\delta^{18}\text{O}$ values) a “crustal slab” gets incorporated into the subduction zone providing elevated $\delta^{18}\text{O}$ values to the heating source and the magma chamber (Fig. 80). Note that there is a concentration of elevated $\delta^{18}\text{O}(\text{Zrc})$ values at the north part of the CIP (present geographic location) (Fig. 79). This region represents an area where crustal recycling was taking place during the entire magmatic evolution of the arc.

One aspect to be considered for regional tectonic changes is the controversial polarity reversal of the Caribbean and the over which it occurred. The data from this study does not allow a precise age estimate for polarity reversal but the following statements can be made: (1) The continuous process whereby isotopically bimodal plutons were generated during the evolution of the island arc limits any major tectonic change to have occurred prior to ~85 Ma (2) The Izu-Bonin-Mariana (IBM) is an oceanic island arc of ~2500 km in length that trends south of Japan and exposes early volcanic arc rocks (Ishizuka et al., 2006). Ar-Ar dating of these early volcanic rocks yield ages of 48-46 Ma. Haraguchi et al. (2003) described the earliest plutonic bodies of the IBM as ~38 Ma tonalites from the Komahashi-Daini Seamount. The IBM arc thus demonstrates a time span of ~ 10 Ma between the earliest stages of forearc igneous activity and the emplacement of large plutonic bodies. A comparison of the Greater Antilles island arc magmatism with the IBM may indicate that the initiation of subduction (or polarity reversal) in Puerto Rico, having in mind that the first record of plutonism is 85.6 Ma (Coamo Arriba stock), began at approximately 95 Ma (Cavosie et al., 2008).

Other aspects to consider for the tectonic changes resulting in changes in magmatism in the island arc prior to ~85 Ma is a proposed ridge subduction beneath Dominican Republic at ~90 Ma. Escuder-Virujete et al. (2007) described changes in composition of volcanic rocks in the Tiro Formation from tholeiitic volcanics to a sequence of adakites, high-Mg andesites, and Nb-enriched basalts. Adakite rocks indicate melting of a subducting slab, magnesian andesites are the product of hybridization of the mantle wedge with the adakite liquids, and Nb-enriched basalts are the melts of the remnant from hybridization (Escuder-Virujete et al., 2007). This model provides a slab window beneath the arc forming at ~90 Ma at the northwest area of Puerto Rico which provided a higher heat flow. This change of heat flow may be associated with changes of plate velocities of the arc during that time and these changes may have caused the hypothesized crustal scale fault proposed in the model (Fig. 80) for the origin of plutonic rocks of Puerto Rico (isotopically bimodal plutons along the evolution of the arc).

Figure 80 E shows a schematic diagram of the current level of exposure for the island arc where mid-crust granitoids has been exposed. No published geophysical data is available to explain the actual geometry of the island arc at depth.

Additional findings

The Ciales and Morovis stocks are exposed as separate plutons separated by ~2 km. Berryhill (1965) and others have speculated that the two bodies are connected at shallow depth. This hypothesis was evaluated with the results of this study using for 4 lines of evidence: (1) petrographic analysis of Ciales sample (06CS-01) and Morovis (06MS-01) shows similar mineralogical composition; (2) chemical composition by XRF analysis (Table 3) for both samples show similar weight percentages for major and trace elements; (3) U/Pb geochronology of zircons from these plutons yields identical ages within the error of 83.5 ± 1.8 Ma for Morovis stock and 83.9 ± 1.7 Ma for Ciales stock (Cavosie et al., 2008); (4) $\delta^{18}\text{O}(\text{Zrc})$ analyses yield values of 6.69 ± 0.04 ‰ for Morovis stock and 6.73 ± 0.04 ‰ for Ciales stock which are identical values within the uncertainty. This evidence suggests that both stocks are part of the same magmatic system and are connected at shallow depth.

REFERENCES

- Barabas, H.B., 1982. Potassium-Argon dating of magmatic events and hydrothermal activity associated with porphyry copper mineralization in West Central Puerto Rico. *Economic Geology*, v. 77, 109-126.
- Berryhill, H.L., Jr., and Glover, L., III, 1960. Geology of the Cayey quadrangle, Puerto Rico: U.S. Geological Survey Miscellaneous Geologic Investigations Series Map I-319, scale 1:20,000.
- Berryhill, H. L., 1965. Geology of the Ciales quadrangle, Puerto Rico: U.S. Geological Survey Bulletin 1184, 116p.
- Bindeman, I.N., Valley, J.W., Wooden, J.L., and Persing, H.M., 2001. Post-caldera volcanism: In situ measurement of U-Pb age and oxygen isotope ratio in Pleistocene zircons from Yellowstone caldera. *Earth Planetary Science Letters*, v. 189, 197-206.
- Briggs, R.P., 1971. Geologic map of the Orocovis quadrangle, Puerto Rico: U.S. Geological Survey Miscellaneous Geologic Investigations Map I-615, scale 1:20,000.
- Briggs, R.P., and Akers, J.P., 1965. Hydrogeologic map of Puerto Rico and adjacent islands: U.S. Geological Survey Hydrologic Investigations Atlas HA- 197, 1965, scale 1: 240000.
- Briggs, R.P., and Gelabert, P.A., 1962. Preliminary report of the geology of the Barranquitas quadrangle, Puerto Rico: U.S. Geological Survey Miscellaneous Geologic Investigations Map I-336, scale 1:20,000.
- Broedel, C.H., 1961. Preliminary geologic map showing iron and copper prospects in the Juncos quadrangle, Puerto Rico: U.S. Geological Survey Miscellaneous Geologic Investigations Map I-326, scale 1:20,000.
- Burke, K., 1988. Tectonic evolution of the Caribbean. *Annual Reviews of Earth and Planetary Science*, v. 16, 201-230.
- Burke, K., Fox, P.J., and Sengör, A.M.C., 1978. Buoyant ocean floor and the evolution of the Caribbean. *Journal of Geophysical Research*, v. 83, 3949-3954.
- Cavosie, A.J., Perez, R.J., Valencia, V.A., and Gehrels, G.E. Magmatic evolution in the Great Antilles island arc: Zircon geochronology of metaluminous I-type oceanic arc granitoids in Puerto Rico, USA. *Earth Planetary Science Letters*, in review.

- Cavosie, A.J., Wilde, S.A., Liu, D., Weiblen, P.W., Valley, J.W., 2004. Internal zoning and U-Th-Pb chemistry of Jack Hills detrital zircons: a mineral record of Early Archean to Mesoproterozoic (4348-1576 Ma) magmatism, *Precambrian Research*, v.135, 251-279.
- Cavosie, A.J., Valley, J.W., Wilde, S.A., E.I.M.F., 2005. Magmatic $\delta^{18}\text{O}$ in 4400-3900 Ma detrital zircons: A record of the alteration and recycling of crust in the Early Archean. *Earth Planetary Science Letters*, v. 235, 663-681.
- Chen, J., 1969. Petrological and chemical studies of Utuado pluton, Puerto Rico. *Acta Geologica Taiwanica*, No. 13, 21-41.
- Cox, D.P., Marvin, R.F., M'Gonigle, J.W., McIntyre, D.H., and Rogers, C.L., 1977. Potassium-Argon geochronology of some metamorphic, igneous, and hydrothermal events in Puerto Rico and the Virgin Islands. *U.S. Geological Survey Journal of Research*, v. 5, 689-703.
- Curet, A.F., 1986. Geologic map of the Mayagüez and Rosario quadrangles, Puerto Rico: U.S. Geological Survey Miscellaneous Geologic Investigations Map I-421, scale 1:20,000.
- Draper, G., Guitierrez, G., and Lewis, J.F., 1996. Thrust emplacement of the Hispaniola peridotite belt: orogenic expression of the mid-Cretaceous Caribbean arc polarity reversal? *Geology*, v. 24, 1143-1146.
- Eiler, J.M., 2001. Oxygen isotope variations of basaltic lavas and upper mantle rock. In: Valley, J.W., Cole D.R. (eds) *Stable Isotope Geochemistry, Reviews in Mineralogy and Geochemistry*, v. 43. Mineralogical Society of America/Geochemical Society, Washington, DC, 319-364.
- Erikson, J.P., Pindell, J.L. and Larue, D.K., 1990. Mid-Eocene – Early Oligocene sinistral transcurrent faulting in Puerto Rico associated with formation of the northern Caribbean plate boundary. *Journal of Geology*, v. 98, 365-384.
- Frost, C.D., Schellekens, J. H., and Smith, A. L., 1998. Nd, Sr, and Pb isotopic characterization of Cretaceous and Paleogene volcanic and plutonic island arc rocks from Puerto Rico. *Geological Society of America, Special Paper 322*, 123-132.
- Ghosh, N., Hall, S.A., Casey, J.F. and Burke, K., 1994. Magnetic stripes of the Caribbean ocean floor: Formation of the Farallon-Phoenix-Pacific triple junction (abstract). *Eos (Transactions, American Geophysical Union)*, v. 75, p. 594.

- Glover, L., 3rd, 1971. Geology of the Coamo area, Puerto Rico and its relation to the volcanic arc-trench association. U.S. Geological Survey Professional Paper 636, 102p.
- Glover, L., 3rd, and Mattson, P.H., 1973. Geologic map of the Rio Descalabrado quadrangle, Puerto Rico: U.S. Geological Survey Miscellaneous Geologic Investigations Map I-735, scale 1:20,000.
- Gottfried, D., Jaffe, H.W., and Senftle, F.E., 1959. Evaluation of the lead-alpha (Larsen) method for determining ages of igneous rocks. U.S. Geological Survey Bulletin 1097-A, 19 p.
- Govindaraju, K., 1994. Geostandards Newsletter, v. 18. Special Issue, 1-158.
- Gradstein, F.M., Ogg, J.G., Smith, A.G., Agterberg, F.P., Bleeker, W., Cooper, R.A., Davydov, V., Gibbard, P., Hinnov, L.A., House, M.R., Lourens, L., Luterbacher, H.P., McArthur, J., Melchin, M.J., Robb, L.J., Shergold, J., Villeneuve, M., Wardlaw, B.R., Ali, J., Brinkhuis, H., Hilgen, F.J., Hooker, J., Howarth, R.J., Knoll, A.H., Laskar, J., Monechi, S., Plumb, K.A., Powell, J., Raffi, I., Röhl, U., Sadler, P., Sanfilippo, A., Schmitz, B., Shackleton, N.J., Shields, G.A., Strauss, H., Van Dam, J., van Kolfschoten, T., Veizer, J., and Wilson, D., 2004. *A Geologic Time Scale 2004*. Cambridge University Press, 589 p.
- Haraguchi, S., Ishii, T., Kimura, J.I., Ohara, Y., 2003. Formation of tonalite from basaltic magma at the Komahashi-Daini Seamount, northern Kyushu-Palau Ridge in the Philippine Sea, and growth of Izu-Ogasawara (Bonin)-Mariana arc crust. *Contribution to Mineralogy and Petrology*. 145: 151–168.
- Hoskin, P.W.O. and Schaltegger, U., 2003. The composition of zircon and igneous and metamorphic petrogenesis. In: J.M. Hanchar and P.W.O. Hoskin, Editors, *Reviews in Mineralogy and Geochemistry*. Mineralogical Society of America, v. 53, 27–62.
- Ishizuka, O., Kimura, J.-I., Li, Y.B., Stern, R.J., Reagan, M.K., Taylor, R.N., Ohara, Y., Bloomer, S.H., Ishii, T., Hargrove, U.S.III, Haraguchi, S., 2006. Early stages in the evolution of Izu-Bonin arc volcanism: New age, chemical, and isotopic constraints. *Earth and Planetary Science Letters*, v. 250, 385-401.
- Jolly, W.T., Lidiak, E.G., Schellekens, J.H. and Santos, H., 1998a. Volcanism, tectonics, and stratigraphic correlations in Puerto Rico. Geological Society of America, Special Paper 322, 1-24.

- Jolly, W.T., Lidiak, E.G., Dickin, A.P., and Wu, T-W, 1998b. Geochemical diversity of Mesozoic island arc tectonic blocks in eastern Puerto Rico. Geological Society of America, Special Paper 322, 67-98.
- Jolly, W.T., Schellekens, J.H., Dickin, A.P., 2007. High-Mg andesites and related lavas from southwest Puerto Rico (Greater Antilles Island Arc): Petrogenetic links with emplacement of the Late Cretaceous Caribbean mantle plume. *Lithos* 98, 1–26.
- Jolly, W.T., Lidiak, E.G., and Dickin, A.P., 2008. Bimodal volcanism in northeast Puerto Rico and the Virgin Islands (Greater Antilles Island Arc): Genetic links with Cretaceous subduction of the mid-Atlantic ridge Caribbean spur. *Lithos*, doi: 10.1016/j.lithos.2007.10.008
- Jones, L.M., and Kesler, S.E., 1980. Strontium isotope geochemistry of intrusive rocks, Puerto Rico, Greater Antilles. *Earth and Planetary Science Letters*, v. 50(1), 219-224.
- Johnson, D.M., Hooper, P.R., and Conrey, R.M., 1999. XRF Analysis of Rocks and Minerals for Major and Trace Elements on a Single Low Dilution Li-tetraborate Fused Bead. *Advances in X-ray Analysis*, v. 41, 843-867.
- Kesler, S.E., and Sutter, J.F., 1979. Compositional evolution of intrusive rocks in the eastern Greater Antilles island arc. *Geology*, v. 7, 197-200.
- King, E.M., and Valley, J.W., 2001. The source, magmatic contamination, and alteration of the Idaho batholith. *Contributions to Mineralogy and Petrology*, v. 142, 72-88.
- King, E.M., Valley, J.W., Davis, D.W., and Edwards, G.R., 1998. Oxygen isotope ratios of Archean plutonic zircons from granite-greenstone belts of Superior Province: Indicator of magmatic source. *Precambrian Research*, v. 92, 365-387.
- Krushensky, R.D., and Monroe, W.H., 1978. Geologic Map of the Peñuelas and Punta Cuchara quadrangles, Puerto Rico. U.S. Geological Survey Miscellaneous Geologic Investigations Map I-1142, scale 1:20,000.
- Lackey J.S., 2005. The magmatic and alteration history of the Sierra Nevada batholith as recorded by oxygen isotope ratios in zircon, titanite, garnet, and quartz. [PhD Thesis], University of Wisconsin, Madison. 345p.

- Lackey J. S., Valley, J. W., Saleeby, J. B., 2005. Supracrustal input to magmas in the deep crust of Sierra Nevada batholith: Evidence from high- $\delta^{18}\text{O}$ zircon. *Earth and Planetary Science Letters*, v. 235, 315-330.
- Larue, D.K., Joyce, J., and Ryan, H.F., 1991. Neotectonics of the Puerto Rico Trench: Extensional tectonism and forearc subsidence, in Larue, D.K., and Draper, G., eds., *Transactions, 12th Caribbean Geological Conference: Coral Gables, Florida, Miami Geological Society*, 231-247.
- Lidiak, E.G., 1991. Depth of emplacement of granitoid plutonic rocks in the eastern Greater Antilles island arc. *Transactions of the 12th Caribbean Geological Conference, St. Croix, U.S.V.I., Miami Geological Society*, 259-267.
- Malfait, B.T., and Dinkelman, M.G., 1972. Circum Caribbean tectonic and igneous activity and the evolution of the Caribbean Plate. *Geological Society of America Bulletin*, v. 83, 251-272.
- Mattson, P.H., 1960. Geology of the Mayagüez area, Puerto Rico. *Geological Society of America Bulletin*, v. 71, 319-362.
- Mattson, P.H., 1964. Petrography and structure of serpentinite from Mayagüez, Puerto Rico. In Burke, C.A., ed., *A study of serpentinite. NAS-NRC Publication*, v. 1188, 7-24.
- Mattson, P.H., 1973. Middle Cretaceous nappe structures in Puerto Rico ophiolites and their relation to the tectonic history of the Greater Antilles: *Geological Society of America Bulletin*, v. 84, 21- 38.
- Mattson, P.H., 1979. Subduction, buoyant braking, flipping, and strike-slip faulting in the northern Caribbean. *Journal of Geology*, v. 87, 293-304.
- M'Gonigle, J.W., 1978. Geologic map of the Humacao quadrangle, Puerto Rico: U.S. Geological Survey Miscellaneous Investigations Series Map I-1070, scale 1:20,000.
- M'Gonigle, J.W., 1979. Geologic map of the Naguabo and part of the Puerto Puerca quadrangles, Puerto Rico: U.S. Geological Survey Miscellaneous Investigations Series Map I-1099, scale 1:20,000.

- McIntyre, D.H., 1971. Geologic map of the Central La Plata quadrangle, Puerto Rico: U.S. Geological Survey Miscellaneous Investigations Series Map I-660, scale 1:20,000.
- McIntyre, D.H., 1974. Concepcion and Palma Escrita Formations, western Puerto Rico: U.S. Geological Survey Bulletin, v. 1394-D, D1-D9.
- McIntyre, D.H., 1975. Geologic map of the Maricao quadrangle Puerto Rico: U.S. Geological Survey Miscellaneous Geologic Investigations Map I-918, scale 1:20,000.
- McIntyre, D.H., Aaron, J.M., and Tobisch, O.T., 1970. Cretaceous and Lower Tertiary stratigraphy of northwestern Puerto Rico: U.S. Geological Survey Bulletin, v. 1294-D, 16p.
- Monani, S., and Valley, J.W., 2001. Oxygen isotope ratios of zircon: Magma genesis of low $\delta^{18}\text{O}$ granites from the British Tertiary Igneous Province, western Scotland, Earth and Planetary Science Letter, v. 184, 377-392.
- Monroe, S.C., and Suda, C.E., 1995. Final report Barranquitas area. Cominco American, Company internal report. 57p.
- Montgomery, H.M., Pessagno, E.A., Jr., and Pindell, J.L., 1994. A 195 Ma Terrane in a 165 Ma sea: Pacific origin of the Caribbean Plate: GSA Today, v.4, no. 1, 1, 3-6.
- Nelson, A.E., 1967. Geologic map of the Utuado quadrangle, Puerto Rico: U.S. Geological Survey Miscellaneous Geologic Investigations Map I- 480, scale 1:20,000.
- Nesse, W.D., 2004. Introduction to Optical Mineralogy. Third Ed. Oxford University Press. Oxford.
- O'Connor, Y.L., and Morrison, J., 1999. Oxygen isotope constraints on the petrogenesis of the Sybille Intrusion of the Proterozoic Laramie anorthosite complex. Contributions to Mineralogy and Petrology, v. 136, 81-91.
- Ortiz, D.M., 2006. U-Pb geochronology constraints on the sources of detrital zircon in the Cotui Limestone, southwest Puerto Rico. [Senior thesis]. University of Puerto Rico Mayagüez. 39p.
- Page, F.Z., Ushikubo, T., Kita, N.T., Riciputi, L.R., and Valley, J.W., 2007. High-precision oxygen isotope analysis of picogram samples reveals 2 μm gradients and slow diffusion in zircon. American Mineralogist, v. 92, 1772-1775.

- Pease, M.H., 1968. Cretaceous and Lower Tertiary stratigraphy of the Naranjito and Aguas Buenas quadrangles and adjacent areas, Puerto Rico: U.S. Geological Survey Bulletin, v. 1253, 57p.
- Pease, M.H., and Briggs, R.P., 1960. Geology of the Comerío quadrangle, Puerto Rico: U.S. Geological Survey Miscellaneous Geologic Investigations Map I-320, scale 1:20,000.
- Peck, W.H., King, E.M., and Valley J.W., 2000. Oxygen isotope perspective on Precambrian crustal growth and maturation. *Geology*, v. 28, 363-366.
- Peck, W. H., Valley J.W., Wilde S. A., and Graham C. M., 2001. Oxygen isotope ratios and rare earth elements in 3.3 to 4.4 Ga zircons: Ion microprobe evidence for high $\delta^{18}\text{O}$ continental crust and oceans in the Early Archean. *Geochimica et Cosmochimica Acta*, 65: 22: 4215-4229.
- Pindell, J.L., 1985. Alleghenian reconstruction and the subsequent evolution of the Gulf of Mexico, Bahamas, and proto-Caribbean: *Tectonics* v. 4, 1-39.
- Pindell, J.L., 1993. Regional synopsis of Gulf of Mexico and Caribbean evolution. In: Pindell, J.L., Perkins, R.F. (eds.), 1993. Mesozoic and Early Cenozoic development of the Gulf of Mexico and Caribbean region- A context for hydrocarbon exploration: Selected papers presented at the GCSSEPM Foundation thirteenth annual research conference, Gulf Coast Section SEPM, 251-274.
- Pindell, J.L., 1994. Evolution of the Gulf of Mexico and the Caribbean: in Donovan S.K. and Jackson, T. A. (eds.) *Caribbean Geology: an introduction*, University of the West Indies Publishers Association/University of the West Indies Press, Kingston, Jamaica, 13-39.
- Pindell, J.L, and Barret, S.F., 1990. Geological evolution of the Caribbean region: a plate tectonic perspective, in G. Dengo and J.E., Case (eds.) *The Caribbean Region, the Geology of North America*. Geological Society of America, v. H, 405-432.
- Pindell, J.L., and Dewey, J.F., 1982. Permo-Triassic reconstruction of western Pangea and the evolution of the Gulf of Mexico/Caribbean region. *Tectonics*, v. 1, 179-212.
- Pindell, J.L. and Kennan, L., 2001. Kinematic evolution of the Gulf of Mexico and Caribbean. In: *Transactions Petroleum systems of deep-water basins; global and Gulf of Mexico experience*, GCSSEPM 21st Annual Research conference, December 2-5: Houston, Texas, GCSSEPM, 193-220.

- Pindell, J.L., Kennan, L., Stanek, K.P., Maresch, W.V., and Draper, G.G., 2006. Foundations of Gulf of Mexico and Caribbean Evolution: eight controversies resolved. *Acta Geologica*, v. 4, 303-341.
- Rogers, C.L., 1977. Geologic map of the Punta Guayanés quadrangle, Puerto Rico: U.S. Geological Survey Miscellaneous Investigations Series Map I-998, scale 1:20,000.
- Rogers, C.L., 1979. Geologic map of the Caguas quadrangle, Puerto Rico: U.S. Geological Survey Miscellaneous Investigations Series Map I-1152, scale 1:20,000.
- Rogers, C.L., Cram, C.M., Pease, M.H., Jr., and Tischler, M.S., 1979. Geologic map of the Yabucoa and Punta Tuna quadrangles, Puerto Rico: U.S. Geological Survey Miscellaneous Investigations Series Map I-1086, scale 1:20,000.
- Sampayo, M.M., 1992. Stratigraphy and sedimentology of the Monte Grande Formation, southwest Puerto Rico [M.S. Thesis]: Boulder, University of Colorado, 109p.
- Santos, H., 1990. The stratigraphy, paleoenvironments, and biofacies of the Cotui Limestone: Cretaceous of Southwestern Puerto Rico [M.S. Thesis] University of Colorado, Boulder, CO, 109 p.
- Santos, H., 1999. Stratigraphy and Depositional History of the Upper Cretaceous Strata in the Cabo Rojo-San German Structural Block, Southwestern Puerto Rico [Ph.D. Thesis], University of Colorado, Boulder, CO. 105 p.
- Schellekens, J. H., 1991. Late Jurassic to Eocene geochemical evolution of volcanic rocks of Puerto Rico. *Geophysical Research Letters*, v. 18, 553-556.
- Schellekens, J.H., 1993. Geochemical evolution of volcanic rocks in Puerto Rico. [PhD Thesis]: University of Syracuse. Syracuse, New York, 289 p.
- Schellekens, J. H., 1998a. Geochemical evolution and tectonic history of Puerto Rico. *Geological Society of America, Special Paper 322*, 35-66.
- Schellekens, J.H., 1998b. Composition, Metamorphic grade, and origin of Metabasites in the Bermeja Complex, Puerto Rico. *International Geology Review*, v.40, 722-747.
- Schellekens, J.H., and Joyce, J., 1999. Geological Processes and Evolution of the Northeastern Caribbean. Field guide to the Eighteen Annual Symposium on Caribbean Geology. Department of Geology, University Puerto Rico, Mayagüez. 30p.
- Schellekens, J.H., Montgomery, H., Joyce, J., and Smith, A. L., 1990. Late Jurassic to Late Cretaceous development of island arc crust in southwestern Puerto Rico, in Larue, D.K.,

- and Draper, G., eds., Transactions, 12th Caribbean Geological Conference, St. Croix, U.S. Virgin Islands, August 1989, 268-281.
- Seiders, V.M., 1971a. Geologic map of the Gurabo quadrangle Puerto Rico: U.S. Geological Survey Miscellaneous Geologic Investigations Map I-657, scale 1:20,000.
- Seiders, V.M., 1971b. Geologic map of the El Yunque quadrangle Puerto Rico: U.S. Geological Survey Miscellaneous Geologic Investigations Map I-658, scale 1:20,000.
- Smith, A.L., Schellekens, J. H., and Muriel-Diaz, A., 1998. Batholiths as markers of tectonic change in the northeastern Caribbean. Geological Society of America, Special Paper 322, 99-122.
- Smith, A.L., and Schellekens, J.H., 1994. Batholith emplacement in the northeastern Caribbean: Markers of tectonic changes (abs.): Eos, Transactions, American Geophysical Union, v. 75, 594.
- Spicuzza, M.J., Valley, J.W., and McConnel, V.S., 1998. Oxygen isotope analysis of whole rock via laser fluorination: an air-lock approach. Geological Society of America- Abstracts with Programs, v. 30, no. 7, 80.
- Stern, R.J., 2004. Subduction initiation: spontaneous and induced. Earth and Planetary Science Letters, v. 226, 275-292.
- Streckeisen, A.L., 1973. Plutonic rocks, classification and nomenclature recommended by the IUGS subcommission on the systematics of igneous rocks. Geotimes, v. 18, 26-30.
- Tobisch, O.T., and Turner, M.D., 1971. Geologic map of the San Sebastian quadrangle, Puerto Rico: U.S. Geological Survey Miscellaneous Investigations Map I- 661, scale 1:20,000.
- Valley, J.W., 2003. Oxygen isotopes in zircon. In: Hanchar J.M, Hoskin WO (eds) Zircon, Reviews in Mineralogy and Geochemistry, v. 53. Mineralogical Society of America/Geochemical Society, Washington, DC, 343-385.
- Valley, J.W., Chiarenzelli, J.R., and McLelland, J.M., 1994. Oxygen isotope geochemistry of zircon. Earth and Planetary Science Letters, v.126, 187-206.
- Valley, J.W., Kitchen, N., Kohn M., Niendorf, C.R., and Spicuzza, M.J., 1995. UWG-2, a garnet standard for oxygen isotope ratios: strategies for high precision and accuracy with laser heating. Geochimica. Cosmochimica Acta, v. 59, 5223-5231.

- Valley, J.W., Kinny, P.D., Schulze, D.J., and Spicuzza, M.J., 1998. Zircon megacrysts from kimberlite: oxygen isotope variability among mantle melts. *Contribution to Mineralogy and Petrology*, v. 133, 1-11.
- Valley, J.W., Bindeman, I.N., Peck, W.H., 2003. Empirical calibration of oxygen isotope fractionation in zircon. *Geochimica et Cosmochimica Acta*, v. 6 No. 17, 3257-3266.
- Valley, J.W., Lackey, J.S., Cavosie, A.J., Clechenco, C., Spicuzza, M.J., Basei, M.A.S., Bindeman, I.N., Ferreira, V.P., Sial, A.N., King, E.M., Peck, W.H., Sinha, A.K., Wei, C.S., 2005. 4.4 billion years of crustal maturation from oxygen isotope ratios of zircon. *Contribution to Mineralogy and Petrology*, v. 150, 561-580.
- Valley, J.W., Peck, W.H., King, E.M., Wilde, S.A., 2002. A cool early Earth. *Geology*, v. 30, 351-354.
- Volckmann, R.P., 1984a. Upper Cretaceous stratigraphy of southwest Puerto Rico, in *Stratigraphic notes 1983: U.S. Geological Survey Bulletin*, v. 1537- A, A73-A83.
- Volckmann, R.P., 1984b. Geologic map of the Cabo Rojo and Parguera quadrangles, southwest Puerto Rico: Geological Survey Miscellaneous Geologic Investigations Map I-1557, scale 1:20,000.
- Volckmann, R.P., 1984c. Geologic map of the San German quadrangle, southwest Puerto Rico: U.S. Geological Survey Miscellaneous Geologic Investigations Map I-1558, scale 1:20,000.
- Weaver, J.D., 1958. Utuado pluton, Puerto Rico. *Geological Society of America Bulletin*, v. 69, 1125-1142.
- White, R.V., Tarney, J., Kerr, A.C., Saunders, A.D., Kempton, P.D., Pringle, M.S., and Klaver G.T., 1999. Modification of an oceanic plateau, Aruba, Dutch Caribbean: Implications for the generation of continental crust. *Lithos*, v. 46, 43-68.
- Wilde, S.A., Valley, J.W., Peck, W.H., and Graham, C.M., 2001. Evidence from detrital zircons for the existence of continental crust and oceans on the Earth 4.4 Gyr ago. *Nature*, v. 409, 175-178.

TABLES

Table 1. Location of the plutonic igneous rocks collected for this study.

Sample	Rock type	Quadrangle	Map Unit	Latitude longitude	Roads
BA-2	diorite	Barranquitas	qp	Not available	PR 771
06CA-01	quartz diorite	Barranquitas	hd	N18°08.512 W66°21.809	PR 555
06CG-01	granodiorite	Caguas	Kgc	N18°14.481 W66°00.579	PR 189
06CS-01	granodiorite	Ciales	TKg	N18°20.173 W66°27.799	PR 145
06CY-01	quartz diorite	Cayey	Thqd	N18°06.399 W66°14.789	PR 162
06IV-01	granodiorite	Isla Vieques	-----	N18°07.009 W65°31.206	PR 994
06LT-01	diorite	San German	Kti	Not available	PR 3306
06MS-01	granite	Ciales	TKg	N18°18.044 W66°24.616	PR 155
06RB-01	granodiorite	El Yunque	Tqd	N18°17.126 W66°47.398	PR 191
06RP-01	porphyritic diorite	Rincón*	-----	N18°18.201 W66°14.097	PR 429
06SL-01	quartz diorite	Yabucoa	Kd	N18°04.295 W65°59.511	PR 181
06SL-02	mafic xeno.	Juncos	N/A	N18°09.005 W65°58.810	PR 181
06SL-03	granodiorite	Juncos	Tkgd	N18°09.005 W65°58.810	PR 181
06TD-01	porphyritic diorite	San German	Tkqd	N18°03.516 W67°00.590	PR 118
06TS-01	diorite/gabbro	Peñuelas	Thd	N18°04.823 W66°38.181	PR 503
06TS-06	diorite/gabbro	Peñuelas	Thd	N18°04.693 W66°38.182	PR 503
06UP-01	mafic xeno.	Utuaado	N/A	N18°16.065 W66°42.514	PR 111
06UP-02	granodiorite	Utuaado	TKu	N18°16.065 W66°42.514	PR 111
06ZB-01	diorite	Rio Descalabrado	Kca	N18°06.071 W66°24.540	PR 153

*= no published geologic map

xeno= xenolith

Table 2. Starting sample weights and minerals successfully concentrated from each sample.

Sample	Rock type	Weight (kg)	Whole rock	Zircon	Quartz	Titanite
06SL-03	granodiorite	5.0	X	X	X	X
06UP-02	granodiorite	5.0	X	X	X	X
06MS-01	granite	5.3	X	X	X	X
06IV-01	granodiorite	5.3	X	X	X	X
06CG-01	granodiorite	5.1	X	X	X	X
06CS-01	granodiorite	4.9	X	X	X	X
06RB-01	granodiorite	5.2	X	X	X	Trace
06SL-01	quartz diorite	4.9	X	X	X	
06CA-01	quartz diorite	5.2	X	X	X	
06CY-01	quartz diorite	5.0	X	X	X	
06TD-01	porphyritic diorite	1.2	X	X	X	
06TS-06	diorite/gabbro	5.1	X	X		
BA-2	diorite	3.7	X	X		
06LT-01	porphyritic diorite	5.1	X	X		
06RP-01	porphyritic diorite	5.1	X	Trace		
06CA-03	diorite	5.1	X	Trace		
06TS-01	diorite/gabbro	5.0	X	Trace		

Table 3. Chemical composition of plutonic rocks of the CIP, SIP and NIP.

Sample	DL ¹	CIP							
		06SL-01	06SL-02	06SL-03	06UP-01	06UP-02	06CG-01	06IV-01	06IV-02
Unnormalized Major Elements (Weight %):									
SiO ₂	0.58	53.52	50.54	62.67	55.24	64.73	62.92	61.30	51.65
TiO ₂	0.02	0.66	0.76	0.46	0.97	0.41	0.42	0.51	0.77
Al ₂ O ₃	0.16	18.22	18.37	16.90	14.22	15.90	16.20	16.68	16.93
FeO*	0.20	8.28	8.89	4.23	7.40	3.31	4.17	5.24	9.05
MnO	0.00	0.19	0.25	0.14	0.23	0.08	0.12	0.13	0.30
MgO	0.08	3.95	4.43	1.64	6.66	1.88	1.73	2.23	4.59
CaO	0.06	9.36	9.55	5.73	6.44	4.33	4.82	5.80	7.43
Na ₂ O	0.05	3.15	3.98	3.62	4.37	4.05	3.57	3.32	3.17
K ₂ O	0.03	0.38	0.61	2.18	1.41	2.41	2.83	1.99	2.68
P ₂ O ₅	0.01	0.19	0.22	0.14	0.35	0.19	0.16	0.15	0.17
Total		97.91	97.61	97.72	97.29	97.29	96.94	97.36	96.73
Normalized Major Elements (Weight %):									
SiO ₂	0.19	54.66	51.78	64.14	56.77	66.54	64.91	62.96	53.40
TiO ₂	0.01	0.68	0.78	0.47	0.99	0.42	0.43	0.53	0.80
Al ₂ O ₃	0.08	18.61	18.82	17.29	14.61	16.34	16.71	17.13	17.50
FeO*	0.18	8.46	9.11	4.33	7.60	3.40	4.30	5.38	9.35
MnO	0.00	0.20	0.26	0.14	0.23	0.08	0.12	0.14	0.31
MgO	0.07	4.03	4.53	1.68	6.85	1.93	1.79	2.29	4.74
CaO	0.04	9.56	9.79	5.86	6.62	4.45	4.97	5.96	7.68
Na ₂ O	0.04	3.22	4.07	3.70	4.50	4.17	3.68	3.41	3.27
K ₂ O	0.02	0.39	0.63	2.23	1.45	2.48	2.92	2.04	2.77
P ₂ O ₅	0.00	0.19	0.23	0.15	0.36	0.19	0.17	0.16	0.18
		100.00	100.00	100.00	100.00	100.00	100.00	100.00	100.00
Unnormalized Trace Elements (ppm):									
Ni	3.5	6.1	8.3	bd	48	13	bd	4.8	12
Cr	3.0	2.6	2.9	3.0	198	17	8.2	7.8	61
Sc	1.6	25	26	10	32	8.4	9.3	15	31
V	5.0	233	267	93	209	85	102	127	222
Ba	11.7	358	204	1299	549	1039	1525	798	1037
Rb	1.7	4.8	2.5	37	33	57	69	35	34
Sr	4.6	471	567	509	463	685	658	417	378
Zr	3.9	39	57	101	92	99	108	97	26
Y	1.2	18	19	20	22	9.2	15	18	32
Nb	1.2	bd	bd	2.6	6.7	3.2	2.6	1.6	3.4
Ga	2.7	17	18	16	16	17	16	16	15
Cu	7.4	69	185	14	78	368	11	25	7.3
Zn	3.3	84	101	58	109	44	53	58	104
Pb	2.6	bd	2.5	3.6	6.5	14	16	bd	2.8
La	5.7	6.5	bd	8.4	28	21	13	8.0	14
Ce	7.9	14	17	16	61	37	29	13	30
Th	1.6	1.1	2.5	1.1	4.4	8.3	5.0	2.4	1.3
Nd	4.3	8.1	8.9	12	30	13	12	7.6	19
1= Detection limit for each element at 2 standard deviation									
* = Total Fe expressed as FeO									
bd = below detection									

Table 3. Chemical composition of plutonic rocks of the CIP, SIP and NIP (cont.)

Sample	DL ¹	CIP				NIP		
		06CS-01	06CY-01	06MS-01	06MS-01b	06CA-01	06RB-01	06RB-02
Unnormalized Major Elements (Weight %):								
SiO ₂	0.58	62.23	63.46	62.54	50.25	52.69	60.47	50.74
TiO ₂	0.02	0.48	0.41	0.38	0.74	0.48	0.48	0.79
Al ₂ O ₃	0.16	16.13	16.47	16.28	18.81	17.68	17.11	18.48
FeO*	0.20	4.09	4.88	3.68	9.23	6.07	6.26	8.56
MnO	0.00	0.08	0.06	0.11	0.28	0.34	0.16	0.31
MgO	0.08	2.32	1.87	1.47	4.08	3.65	2.55	6.36
CaO	0.06	2.36	5.49	4.01	4.60	5.86	6.91	9.90
Na ₂ O	0.05	3.89	3.69	3.68	5.28	3.88	3.20	3.02
K ₂ O	0.03	3.82	0.89	4.10	1.39	1.32	1.14	0.43
P ₂ O ₅	0.01	0.26	0.15	0.19	0.32	0.15	0.11	0.09
Total		95.66	97.36	96.44	94.99	92.11	98.39	98.68
Normalized Major Elements (Weight %):								
SiO ₂	0.19	65.05	65.17	64.85	52.91	57.20	61.46	51.42
TiO ₂	0.01	0.50	0.42	0.39	0.78	0.52	0.49	0.80
Al ₂ O ₃	0.08	16.86	16.91	16.88	19.80	19.19	17.39	18.73
FeO*	0.18	4.28	5.01	3.82	9.72	6.59	6.37	8.68
MnO	0.00	0.08	0.06	0.11	0.30	0.36	0.16	0.31
MgO	0.07	2.42	1.92	1.52	4.30	3.96	2.59	6.44
CaO	0.04	2.47	5.64	4.16	4.84	6.36	7.02	10.03
Na ₂ O	0.04	4.07	3.79	3.82	5.56	4.21	3.25	3.06
K ₂ O	0.02	3.99	0.92	4.26	1.46	1.43	1.16	0.44
P ₂ O ₅	0.00	0.27	0.15	0.20	0.34	0.17	0.11	0.09
		100.00	100.00	100.00	100.00	100.00	100.00	100.00
Unnormalized Trace Elements (ppm):								
Ni	3.5	bd	bd	bd	14	13	bd	33
Cr	3.0	3.8	bd	6.4	3.8	33	5.1	53
Sc	1.6	8.0	6.9	8.7	17	16	13	28
V	5.0	101	85	85	196	131	132	240
Ba	11.7	1214	311	1380	373	213	292	129
Rb	1.7	85	21	98	45	27	28	6.3
Sr	4.6	580	368	765	848	300	233	270
Zr	3.9	132	123	109	101	53	89	74
Y	1.2	19	17	16	7.3	13	19	23
Nb	1.2	6.7	2.0	4.5	bd	1.3	1.4	2.0
Ga	2.7	17	16	16	24	16	15	17
Cu	7.4	36	53	280	1120	bd	27	67
Zn	3.3	48	22	50	192	226	61	94
Pb	2.6	3.8	bd	3.4	3.6	bd	bd	bd
La	5.7	26	12	19	13	bd	5.9	bd
Ce	7.9	47	23	37	20	13	12	10
Th	1.6	5.8	2.1	3.2	2.4	bd	bd	bd
Nd	4.3	21	14	18	6.4	6.7	7.2	10
1= Detection limit for each element at 2 standard deviation								
* = Total Fe expressed as FeO								
bd = below detection								

Table 3. Chemical composition of plutonic rocks of the CIP, SIP and NIP (cont.)

Sample	DL ¹	SIP					
		BA-2	06LT-01	06TD-01	06TS-06	06TS-11	06TS-12
Unnormalized Major Elements (Weight %):							
SiO ₂	0.58	55.71	57.76	62.88	48.84	49.41	46.94
TiO ₂	0.02	0.52	0.78	0.31	1.20	1.51	2.24
Al ₂ O ₃	0.16	16.93	15.79	16.73	21.52	16.54	13.91
FeO*	0.20	5.33	5.49	2.84	7.83	10.16	12.37
MnO	0.00	0.12	0.13	0.12	0.13	0.20	0.21
MgO	0.08	4.37	2.51	1.01	3.10	6.06	6.31
CaO	0.06	7.80	5.46	5.43	11.04	10.33	11.66
Na ₂ O	0.05	3.13	3.21	4.08	3.17	2.54	2.56
K ₂ O	0.03	0.67	2.44	1.06	0.71	0.83	0.56
P ₂ O ₅	0.01	0.10	0.29	0.15	0.25	0.43	0.13
Total		94.68	93.86	94.61	97.80	98.02	96.90
Normalized Major Elements (Weight %):							
SiO ₂	0.19	58.84	61.54	66.46	49.94	50.41	48.44
TiO ₂	0.01	0.55	0.83	0.33	1.23	1.54	2.31
Al ₂ O ₃	0.08	17.88	16.83	17.68	22.01	16.88	14.36
FeO*	0.18	5.63	5.85	3.00	8.01	10.37	12.77
MnO	0.00	0.13	0.14	0.12	0.13	0.21	0.22
MgO	0.07	4.62	2.67	1.07	3.17	6.18	6.51
CaO	0.04	8.24	5.82	5.73	11.29	10.54	12.04
Na ₂ O	0.04	3.30	3.42	4.32	3.24	2.59	2.64
K ₂ O	0.02	0.70	2.60	1.12	0.72	0.85	0.58
P ₂ O ₅	0.00	0.11	0.30	0.16	0.26	0.44	0.13
		100.00	100.00	100.00	100.00	100.00	100.00
Unnormalized Trace Elements (ppm):							
Ni	3.5	16	5.8	bd	20	32	41
Cr	3.0	56	8.3	bd	5.0	33	2.7
Sc	1.6	24	15	4.4	26	45	63
V	5.0	171	127	57	353	417	791
Ba	11.7	321	1049	572	233	184	93
Rb	1.7	11	51	30	14	16	8.9
Sr	4.6	328	333	528	480	319	336
Zr	3.9	74	192	93	59	44	53
Y	1.2	15	20	16	19	29	28
Nb	1.2	1.0	24	6.6	3.2	2.6	3.2
Ga	2.7	16	16	19	20	17	16
Cu	7.4	55	28	144	143	136	122
Zn	3.3	46	69	54	45	93	47
Pb	2.6	bd	bd	2.7	bd	bd	bd
La	5.7	bd	29	12	8.7	10	bd
Ce	7.9	13	53	19	17	23	16
Th	1.6	2.5	4.9	4.1	2.0	2.3	1.5
Nd	4.3	5.9	23	10	10	17	11
1= Detection limit for each element at 2 standard deviation							
* = Total Fe expressed as FeO							
bd = below detection							

Table 4. Oxygen isotope geochemistry of intrusive igneous rocks of Puerto Rico.

Sample	Rock type	Pluton/ stock	SiO ₂ wt. %	$\delta^{18}\text{O}$ Qtz (‰)	±	$\delta^{18}\text{O}$ WR (‰)	±	$\delta^{18}\text{O}$ Zrc (‰)	±	$\delta^{18}\text{O}$ Tnt (‰)	±
SIP											
05BC-02	Diorite p.	Tea Road	66.46 ²	8.50	0.10	9.31	0.15	--	--	--	--
06TD-01	Diorite p.	Tea Road	66.46					5.62	0.04	--	--
VP-118		Maguayo p.	62.36	9.95	0.10	10.70	0.03	--	--	--	--
06LT-01	Diorite	Las Tunas	61.54	--	--	11.19	0.19	7.17 ¹	0.10	--	--
06TS-11	Diorite	Tibes	50.41	--	--	6.23	0.07	--	--	--	--
06TS-01	Diorite	Tibes	49.94 ²	--	--	7.21	0.10	--	--	--	--
06TS-06	Diorite	Tibes	49.94	--	--	6.73 ¹	0.19	5.33 ¹	0.04	--	--
06TS-12	Diorite	Tibes	48.44	--	--	6.64	0.07	--	--	--	--
06RP-01	Diorite p.	Rincon p.	--	--	--	11.42	0.10	--	--	--	--
CIP											
PP-1 ³	Granodiorite	San Lorenzo	70.49	8.89	0.10	9.19	0.07	--	--	--	--
PRP-105 ³		San Lorenzo	70.00	8.55	0.10	8.15	0.19	--	--	--	--
PRP-11 ³		San Lorenzo	65.66	9.58	0.10	7.83	0.02	--	--	--	--
PRP-1 ³		San Lorenzo	64.84	8.82	0.10	7.13 ¹	0.19	--	--	--	--
PRP-100 ³		San Lorenzo	64.62	8.48	0.10	7.14	0.02	--	--	--	--
06SL-03	Granodiorite	San Lorenzo	64.14	8.48	0.04	6.96	0.10	5.63 ¹	0.04	4.31	0.04
PRP-2 ³		San Lorenzo	61.68	8.86	0.10	7.16	0.02	--	--	--	--
PRP-103 ³		San Lorenzo	60.98	9.09	0.10	6.56	0.02	--	--	--	--
PRP-104 ³		San Lorenzo	60.05	8.39	0.10	6.27	0.19	--	--	--	--
PRP-6 ³		San Lorenzo	59.08	9.18	0.10	6.39	0.02	--	--	--	--
PRP-5 ³		San Lorenzo	58.03	9.03	0.10	6.24	0.02	--	--	--	--
06SL-01	Diorite	San Lorenzo	54.66	8.63	0.10	6.34	0.10	5.51 ¹	0.10	--	--
06UP-02	Granodiorite	Utuaado	66.54	9.07	0.04	7.72	0.10	5.71 ¹	0.04	4.15 ¹	0.04
PRP-27 ³		Utuaado	61.85	9.18	0.04	7.72	0.02	--	--	--	--
8690 ³		Utuaado	61.37	8.31	0.10	6.90	0.07	--	--	--	--
06MS-01	Granite	Morovis	64.85	9.83	0.04	10.08	0.10	6.69 ¹	0.04	5.28 ¹	0.04
MOR-1 ³		Morovis	63.18	9.92	0.04	9.68	0.07	--	--	--	--
PRP-29 ³		Morovis	62.78	9.83	0.04	9.19	0.02	--	--	--	--
06CY-01	Diorite	Cuyon	65.17	8.34	0.04	7.59	0.19	5.33 ¹	0.04	--	--
06CS-01	Granodiorite	Ciales	65.05	10.12	0.04	9.07	0.10	6.73 ¹	0.04	5.51 ¹	0.04
06CG-01	Granodiorite	Caguas	64.91	9.45	0.10	7.47	0.10	6.32 ¹	0.04	5.11 ¹	0.04
06IV-01	Granodiorite	Vieques	62.96	8.95	0.04	7.14	0.10	5.77 ¹	0.04	4.23 ¹	0.04
BA-2	Diorite	Barranquitas	58.84	--	--	9.68	0.10	6.75 ¹	0.04	--	--
06CA-01	Diorite	Coamo Arriba	57.20	8.30	0.04	10.27	0.19	5.34 ¹	0.10	--	--
NIP											
PRP-13 ³		Rio Blanco	60.07	8.77	0.04	7.23	0.15	--	--	--	--
PRP-14 ³		Rio Blanco	60.07	8.39	0.04	6.97	0.07	--	--	--	--
06RB-01	Granodiorite	Rio Blanco	61.46	8.44	0.04	6.50	0.10	5.54 ¹	0.04	--	--
Xenoliths											
06IV-02	xenolith	Vieques	53.40	--	--	7.08	0.10	--	--	--	--
06MS-01b	xenolith	Morovis	52.91	--	--	8.88	0.19	--	--	--	--
06RB-02	xenolith	Rio Blanco	51.42	--	--	5.92	0.10	--	--	--	--
06SL-02	xenolith	San Lorenzo	51.72	--	--	6.41	0.10	--	--	--	--
06UP-01	xenolith	Utuaado	56.77	--	--	7.30	0.10	--	--	--	--

¹ = Average value of two measurements² = estimated value³ = samples from UPR collection analyzed for $\delta^{18}\text{O}$ (WR) and $\delta^{18}\text{O}$ (Qtz)

wt= weight

Zrc= zircon

Tnt= titanite

Qtz= quartz

WR= whole rock

p.= porphyry

dior= diorite

meas= measured

Precision expressed as ± 2 standard deviation. Precision is assigned as the reproducibility of the oxygen isotope standard (UWG-2)

Table 5. Measured and calculated $\Delta^{18}\text{O}$ and apparent temperatures for WR, zircon, quartz and titanite.

Sample	Pluton/ stock	Meas. $\Delta_{(\text{Qtz-WR})}$	Meas. $\Delta_{(\text{WR-Zrc})}$	Calc. $\Delta_{(\text{WR-Zrc})}$	Meas. $\Delta_{(\text{Zrc-Tnt})}$	Meas. $\Delta_{(\text{Qtz-Zrc})}$	Meas. $\Delta_{(\text{Qtz-Tnt})}$	Calc. $\delta^{18}\text{O}(\text{WR})^1$	$\Delta^{18}\text{O}$ (WR calc. - WR meas.)	Qtz-Zrc ² (°C)	Zrc-Tnt ² (°C)	Qtz-Tnt ² (°C)
SIP												
06TS-06	Tibes	--	1.40	0.56	--	--	--	5.89	-0.84	--	--	--
06TD-01	Tea Road	-0.81	3.69	1.57	--	2.88	--	7.19	-2.12	--	--	--
05BC-02	Tea Road	0.40	--	--	--	--	--	--	--	--	--	--
VP-118	Maguayo p.	-0.75	--	--	--	--	--	--	--	--	--	--
CIP												
PP-1	San Lorenzo	-0.30	--	--	--	--	--	--	--	--	--	--
PRP-105	San Lorenzo	0.40	--	--	--	--	--	--	--	--	--	--
PRP-100	San Lorenzo	1.34	--	--	--	--	--	--	--	--	--	--
06SL-03	San Lorenzo	1.52	1.33	1.43	1.32	2.85	4.17	8.39	1.43	689	606	664
PRP-1	San Lorenzo	1.69	--	--	--	--	--	--	--	--	--	--
PRP-2	San Lorenzo	1.70	--	--	--	--	--	--	--	--	--	--
PRP-11	San Lorenzo	1.75	--	--	--	--	--	--	--	--	--	--
PRP-104	San Lorenzo	2.12	--	--	--	--	--	--	--	--	--	--
06SL-01	San Lorenzo	2.29	0.83	0.85	--	3.12	--	6.36	0.02	647	--	--
PRP-103	San Lorenzo	2.53	--	--	--	--	--	--	--	--	--	--
PRP-6	San Lorenzo	2.79	--	--	--	--	--	--	--	--	--	--
PRP-5	San Lorenzo	2.79	--	--	--	--	--	--	--	--	--	--
06UP-02	Utuaado	1.35	2.01	1.57	1.56	3.36	4.92	7.28	0.44	613	535	589
8690	Utuaado	1.41	--	--	--	--	--	--	--	--	--	--
PRP-27	Utuaado	1.46	--	--	--	--	--	--	--	--	--	--
06MS-01	Morovis	-0.25	3.39	1.47	1.41	3.14	4.55	8.16	1.92	644	577	624
MOR-1	Morovis	0.24	--	--	--	--	--	--	--	--	--	--
PRP-29	Morovis	0.64	--	--	--	--	--	--	--	--	--	--
06CS-01	Ciales	1.05	2.34	1.48	1.22	3.39	4.61	8.21	0.86	609	641	618
06CG-01	Caguas	1.98	1.15	1.47	1.21	3.13	4.34	7.79	0.32	645	645	645
BA-2	Barranquitas	--	2.93	1.10	--	--	--	7.85	1.83	--	--	--
06IV-01	Vieques	1.81	1.37	1.35	1.54	3.18	4.72	8.49	1.35	638	541	607
06CY-01	Cuyon	0.75	2.26	1.49	--	3.01	--	6.82	-0.77	663	--	--
06CA-01	Coamo Arriba	-1.97	4.93	1.00	--	2.96	--	6.34	-3.93	671	--	--
NIP												
PRP-14	Rio Blanco	1.42	--	--	--	--	--	--	--	--	--	--
PRP-13	Rio Blanco	1.54	--	--	--	--	--	--	--	--	--	--
06RB-01	Rio Blanco	1.94	0.96	1.26	--	2.90	--	6.80	0.30	681	--	--

¹=Calculation based on wt.%SiO₂ and $\delta^{18}\text{O}$ (Zrc) (Valley et al., 2005)

² = Apparent temperatures calculated based on equation from Valley et al. 2003

Meas.= measured

Calc.= calculated

p.=porphyry

dior.= diorite

Table 6. Zircon oxygen isotope and U-Pb ages for intrusive rock of Puerto Rico.

Sample	Pluton/stock	Rock type	SiO ₂ (wt. %)	U-Pb zircon			
				Age (Ma) ¹	±	δ ¹⁸ O (Zrc)	±
06CA-01	Coamo Arriba	quartz diorite	57.20	85.6	1.3	5.34	0.10
06MS-01	Morovis	granite	64.85	85.3	1.8	6.69	0.04
06CS-01	Ciales	granodiorite	65.05	83.9	1.7	6.73	0.04
06LT-01	Las Tunas	diorite	61.54	79.0	2.1	7.17	0.10
06SL-03	San Lorenzo	granodiorite	64.14	75.1	2.1	5.63	0.04
06SL-01	San Lorenzo	quartz diorite	54.66	74.1	1.4	5.51	0.10
06UP-02	Utuaado	granodiorite	66.54	70.8	1.2	5.71	0.04
06IV-01	Vieques	granodiorite	62.96	67.1	1.6	5.77	0.04
06CG-01	Caguas	granodiorite	64.91	66.8	1.2	6.32	0.04
06TS-06	Tibes	diorite/gabbro	49.54	60.5	1.6	5.33	0.04
BA-2	Barranquitas	diorite	58.84	47.7	1.6	6.75	0.04
06RB-01	Rio Blanco	granodiorite	61.46	47.7	2.1	5.54	0.04
06CY-01	Cuyon	diorite	65.17	47.6	0.8	5.33	0.04
06TD-01	Tea Road	porphyritic diorite	66.46	38.4	0.8	5.62	0.04

Zrc=zircon

Precision expressed as ±2 standard deviation.

¹ = Data source: Cavosie et al. 2008

FIGURE CAPTIONS

- Figure 1. Geologic map of Puerto Rico showing distribution of major igneous rocks (modified from Schellekens, 1998a; Cavosie et al., 2008). Note in particular the three major tectonic terranes. Samples analyzed in this study are labeled.
- Figure 2. Map of the Caribbean region showing major structural features that are related with the tectonic setting of the North American, South American and Caribbean Plate. Bold lines represent fault zones and “teeth” indicate polarity of subduction zone. Modified from Jolly et al., 2007.
- Figure 3. Diagram showing the $\delta^{18}\text{O}$ whole rock (‰) values for igneous (primitive and altered rocks), metamorphic (altered) and sediments (water) and the $\delta^{18}\text{O}$ values of co-existing zircon in equilibrium with these materials. Note narrow range of $\delta^{18}\text{O}$ values for zircon in equilibrium with mantle melts (Cavosie, unp.)
- Figure 4. Diagram showing the SiO_2 (wt. %) vs. $\delta^{18}\text{O}$ (‰) values for whole rock, quartz and zircon from the Tuolome intrusive suite, California (Lackey, 2005).
- Figure 5. Image of zircon grain from the Rio Blanco pluton in transmitted light (plane polarized light). Note inclusions (suspected to be apatite). Zircon is approximately 200 μm in length.
- Figure 6. A. Cathodoluminescence image of zircon from Rio Blanco pluton showing igneous growth zoning patterns with no evidence of inheritance. B. Cathodoluminescence image of zircon having complex core-rim zoning. Note the difference between core and rim. Circles are analysis spots (Page et al., 2007).
- Figure 7. Photomicrograph of polished zircons in an epoxy mount. Note label showing location of samples 06IV-01, 06LT-01, 06CS-01 and 06MS-01 (clockwise from upper left). Diameter of mount is 2.5 cm.
- Figure 8. Photograph of diorite sample from Tibes stock (06TS-01).
- Figure 9. Photomicrographs of diorite sample 06TS-01 in cross-polarized light (left) and plane polarized light (right). Subhedral plagioclase grain shows albite twinning and alteration to sericite. Also note hornblende replaced by chlorite (upper right). Scale bar = 250 μm .
- Figure 10. Photograph of diorite sample from Tibes stock (06TS-06).

Figure 11. Photomicrographs of diorite sample 06TS-06 in cross-polarized light (left) and plane polarized light (right). Highly altered plagioclase by sericite. The alteration mostly concentrates on the core of the grains. Scale bar = 250 μm .

Figure 12. Photograph of porphyritic diorite from Tea Road (06TD-01).

Figure 13. Photomicrographs of porphyritic diorite sample 06TD-01 in cross-polarized light (left) and plane polarized light (right). Subhedral plagioclase grain showing albite twinning surrounded by quartz and a groundmass mainly composed of quartz and plagioclase. Scale bar = 250 μm .

Figure 14- Photomicrograph of euhedral zircon inclusion in hornblende included in plagioclase megacryst in plane polarized light from Tea Road stock. Length of the zircon grain is 160 μm .

Figure 15. Photograph of diorite sample from Las Tunas stock (06LT-01).

Figure 16. Photomicrographs of diorite sample 06LT-01 in cross-polarized light (left) and plane polarized light (right). Highly altered subhedral plagioclase grains altered groundmass showing chlorite and magnetite. Scale bar = 250 μm .

Figure 17. Photograph of diorite sample from Rincon porphyry (06RP-01).

Figure 18. Photograph of quartz diorite sample from San Lorenzo batholith (06SL-01).

Figure 19. Photomicrographs of quartz diorite sample 06SL-01 in cross-polarized light (left) and plane polarized light (right). Note the plagioclase with oscillatory zoning. Scale bar = 250 μm .

Figure 20. Photomicrographs of quartz diorite sample 06SL-01 in cross-polarized light (left) and plane polarized light (right). Note the albite and Carlsbad twinning in the euhedral to subhedral plagioclase grains. Scale bar = 250 μm .

Figure 21. Photomicrographs of quartz diorite sample 06SL-01 in cross-polarized light (left) and plane polarized light (right). Note complex plagioclase grain showing albite twinning in the core and oscillatory zoning in the rim area. Scale bar= 250 μm .

Figure 22. Photomicrograph of titanite in plane polarized light from San Lorenzo batholith (06SL-01). The length of titanite is 145 μm .

Figure 23. Photomicrograph of zircon in plane polarized light from San Lorenzo batholith (06SL-01). The length of zircon is 145 μm .

Figure 24. Photograph of granodiorite sample from San Lorenzo batholith (06SL-03).

- Figure 25. Photomicrographs of granodiorite sample 06SL-03 in cross-polarized light (left) and plane polarized light (right). Note the subhedral plagioclase grains showing albite twinning and also the grain showing oscillatory zoning. Scale bar = 250 μm .
- Figure 26. Photomicrographs of granodiorite sample 06SL-03 in cross-polarized light (left) and plane polarized light (right). This plagioclase grain preserves oscillatory zoning which is overprinted by albite twinning. Some alteration in the grain occurs along the zoning areas. Note also irregular grain boundary. Scale bar = 250 μm .
- Figure 27. Photomicrograph of zircon in plane polarized light from San Lorenzo batholith (06SL-03). Length of zircon is 90 μm . Note low relief apatite inclusions in plagioclase.
- Figure 28. Photomicrograph of titanite in plane polarized light from San Lorenzo batholith (06SL-03). Length of titanite is 630 μm .
- Figure 29. Photomicrograph of titanite in plane polarized light from San Lorenzo batholith (06SL-03). Length of titanite is 650 μm .
- Figure 30. Photograph of granodiorite sample from Utuado pluton (06UP-02).
- Figure 31. Photomicrographs of granodiorite sample 06UP-02 in cross-polarized light (left) and plane polarized light (right). Note fractured subhedral plagioclase grain. Scale bar = 250 μm .
- Figure 32. Photomicrographs of granodiorite sample 06UP-02 in cross-polarized light (left) and plane polarized light (right). Note subhedral plagioclase grain showing oscillatory zoning. Scale bar = 250 μm .
- Figure 33. Photomicrograph of titanite in plane polarized light from Utuado pluton. Length of titanite is 720 μm .
- Figure 34. Photograph of granite sample from Morovis stock (06MS-01).
- Figure 35. Photograph of xenolith sample from Morovis stock (06MS-01b) Each unit on scale bar is 1 cm.
- Figure 36. Photomicrographs of granite sample 06MS-01 in cross-polarized light (left) and plane polarized light (right). Note orthoclase with perthitic texture and plagioclase grains. Scale bar = 250 μm .
- Figure 37. Photomicrographs of granite sample 06MS-01 in cross-polarized light (left) and plane polarized light (right). Plagioclase is highly altered to sericite. Scale bar = 250 μm .

Figure 38- Photomicrograph of titanite in plane polarized light from Morovis stock. Length of titanite is 540 μm .

Figure 39- Photomicrograph of zircon in plane polarized light from Morovis stock. Length of zircon is 70 μm .

Figure 40. Photograph of granodiorite sample from Ciales stock (06CS-01).

Figure 41. Photomicrographs of granodiorite sample 06CS-01 in cross-polarized light (left) and plane polarized light (right). Note the plagioclase pervasively altered to sericite. Scale bar = 250 μm .

Figure 42. Photomicrograph of titanite and zircon in plane polarized light from Ciales stock. Titanite is included in quartz. Length of titanite (right) is 270 μm .

Figure 43. Photomicrograph of titanite in plane polarized light from Ciales stock. Length of titanite is 220 μm .

Figure 44. Photograph of granodiorite sample from Caguas stock (06CG-01).

Figure 45. Photomicrographs of granodiorite sample 06CG-01 in cross-polarized light (left) and plane polarized light (right). Note subhedral plagioclase grain showing albite twinning. Scale bar = 250 μm .

Figure 46. Photomicrographs of granodiorite sample 06CG-01 in cross-polarized light (left) and plane polarized light (right). Note plagioclase grain with oscillatory zoning. Scale bar = 250 μm .

Figure 47. Photomicrograph of titanite in plane polarized light from Caguas stock. Length of titanite is 450 μm .

Figure 48. Photograph of granodiorite sample from Vieques pluton (06IV-01).

Figure 49. Photomicrographs of granodiorite sample 06IV-01 in cross-polarized light (left) and plane polarized light (right). Subhedral plagioclase grains showing albite twinning and oscillatory zoning with minor alteration to sericite. Note interstitial biotite grain. Scale bar = 250 μm .

Figure 50. Photomicrograph of titanite in plane polarized light from Vieques pluton. Length of titanite is 220 μm .

Figure 51. Photograph of quartz diorite sample from Cuyon stock (06CY-01).

- Figure 52. Photomicrographs of quartz diorite sample 06CY-01 in cross-polarized light (left) and plane polarized light (right). Subhedral plagioclase grain with albite twinning. Note how sericite alteration is pervasive in the core of the grain, while the rim is well preserved and relatively free of inclusions. Scale bar = 250 μm .
- Figure 53. Photomicrographs of quartz diorite sample 06CY-01 in cross-polarized light (left) and plane polarized light (right). Note subhedral plagioclase grain showing oscillatory zoning. Scale bar = 250 μm .
- Figure 54. Photograph of diorite sample from Zanja Blanca stock (06ZB-01).
- Figure 55. Photomicrographs of diorite sample 06ZB-01 in cross-polarized light (left) and plane polarized light (right). Note fractured, subhedral to anhedral plagioclase showing Carlsbad twinning. Scale bar = 250 μm .
- Figure 56. Photograph of diorite sample from Barranquitas stock (BA-2).
- Figure 57- Photomicrographs of diorite sample BA-2 in cross-polarized light (left) and plane polarized light (right). Note hornblende grain replaced by chlorite. Scale bar = 250 μm .
- Figure 58. Photograph of quartz diorite sample from Coamo Arriba stock (06CA-01).
- Figure 59. Photomicrographs of diorite sample 06CA-01 in cross-polarized light (left) and plane polarized light (right). Highly altered subhedral plagioclase grain. Note quartz grains in the groundmass surrounded by chlorite and magnetite. Scale bar = 250 μm .
- Figure 60. Photograph of granodiorite sample from Rio Blanco pluton (06RB-01). Note contact with xenolith (06RB-02).
- Figure 61. Photomicrographs of granodiorite sample 06RB-01 in cross-polarized light (left) and plane polarized light (right). Note the subhedral plagioclase grains showing oscillatory zoning. Also note the inclusion-rich, corroded core. Scale bar = 250 μm .
- Figure 62. Photomicrographs of granodiorite sample 06RB-01 in cross-polarized light (left) and plane polarized light (right). Scale bar = 250 μm .
- Figure 63. Diagram showing rock composition of plutonic rock samples based on the Q-A-P diagram. Q=quartz, P=plagioclase, A= alkali feldspar
- Figure 64. Set of representative zircon grains from the plutonic rocks of Puerto Rico. All zircon represent single generation, no inherited cores (Cavosie et al., 2008).
- Figures 65-68. Cathodoluminescence images of zircon grains, examples from each pluton analyzed. Zircons are similar within the pluton population.

Figure 69. Major and trace element variations compared with SiO₂ for plutonic and xenolith samples from the three igneous provinces.

Figure 70. Histograms showing distribution of A) $\delta^{18}\text{O}(\text{Tnt})$, B) $\delta^{18}\text{O}(\text{Zrc})$, C) $\delta^{18}\text{O}(\text{WR})$ and D) $\delta^{18}\text{O}(\text{Qtz})$ values for plutonic rocks of Puerto Rico. Note the bimodal population between primitive (mantle like) $\delta^{18}\text{O}(\text{Zrc})$ values and elevated $\delta^{18}\text{O}(\text{Zrc})$ values (crustal contaminated). High $\delta^{18}\text{O}$ plutons identified by $\delta^{18}\text{O}(\text{Zrc})$.

Figure 71. $\delta^{18}\text{O}(\text{WR})$ distribution of plutonic rocks from Puerto Rico. Note elevated values for some of the stocks, these values represent WR alteration. $\delta^{18}\text{O}(\text{WR}) > 7.5\text{‰}$ represent altered WR.

Figure 72. $\delta^{18}\text{O}(\text{WR})$ for xenoliths and granodioritic host samples. Bold lines represent the expected fractionation between mafic xenolith and granitic host rock. Dashed lines represent a higher or lower than expected fractionation.

Figure 73. Graph evaluating Low-T and Hi-T alteration of granitoids of Puerto Rico based on the calculated and measured $\delta^{18}\text{O}(\text{Zrc})$ and $\delta^{18}\text{O}(\text{WR})$. Note that most of the plutonic rocks are affected by low-temperature alteration.

Figure 74. $\delta^{18}\text{O}$ graph for coexisting quartz and zircon to determine the apparent temperatures of crystallization. Apparent temperatures range from 609 to 689°C. Isotherms calculated from Valley et al., 2003. Open symbols indicate plutons with primitive (mantle-like) $\delta^{18}\text{O}(\text{Zrc})$ and close symbols indicate plutons with elevated (crustal contamination) $\delta^{18}\text{O}(\text{Zrc})$.

Figure 75. $\delta^{18}\text{O}$ graph for coexisting zircon and titanite to determine the apparent temperatures of crystallization. Apparent temperatures range from 535 to 645°C. Isotherms calculated from Valley et al., 2003. Open symbols indicate plutons with primitive (mantle-like) $\delta^{18}\text{O}(\text{Zrc})$ and close symbols indicate plutons with elevated (crustal contamination) $\delta^{18}\text{O}(\text{Zrc})$.

Figure 76. $\delta^{18}\text{O}$ graph for coexisting quartz and titanite to determine the apparent temperatures of crystallization. Apparent temperatures range from 589 to 664°C. Isotherms calculated from Valley et al., 2003. Open symbols indicate plutons with primitive (mantle-like) $\delta^{18}\text{O}(\text{Zrc})$ and close symbols indicate plutons with elevated (crustal contamination) $\delta^{18}\text{O}(\text{Zrc})$.

Figure 77. Diagram showing wt.% SiO₂ vs. δ¹⁸O for Qtz, WR, Zircon and titanite for titanite bearing plutons analyzed in this study.

Figure 78. Oxygen isotope evolution of plutonic rocks in Puerto Rico. Note that the oldest plutons are bimodal in terms of δ¹⁸O(Zrc).

Figure 79. Map showing distribution of δ¹⁸O(Zrc) values along the island. Note the concentration of elevated δ¹⁸O(Zrc) values at the north part of the CIP.

Figure 80. Tectonic models representing isotopically bimodal plutons of Puerto Rico from ~85 to ~48 Ma. Plutons in bold are active during that time interval.

FIGURES

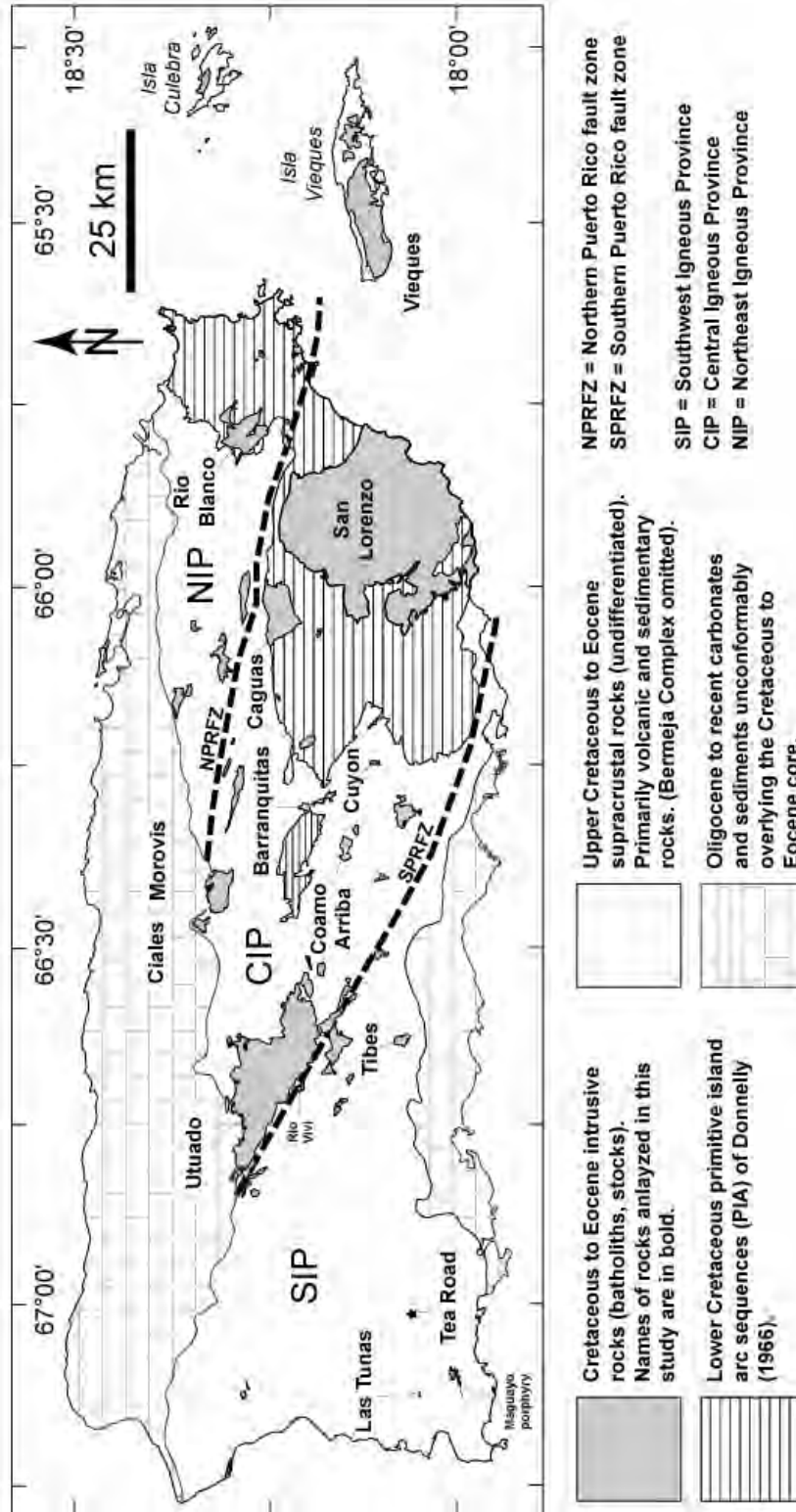


Figure 1

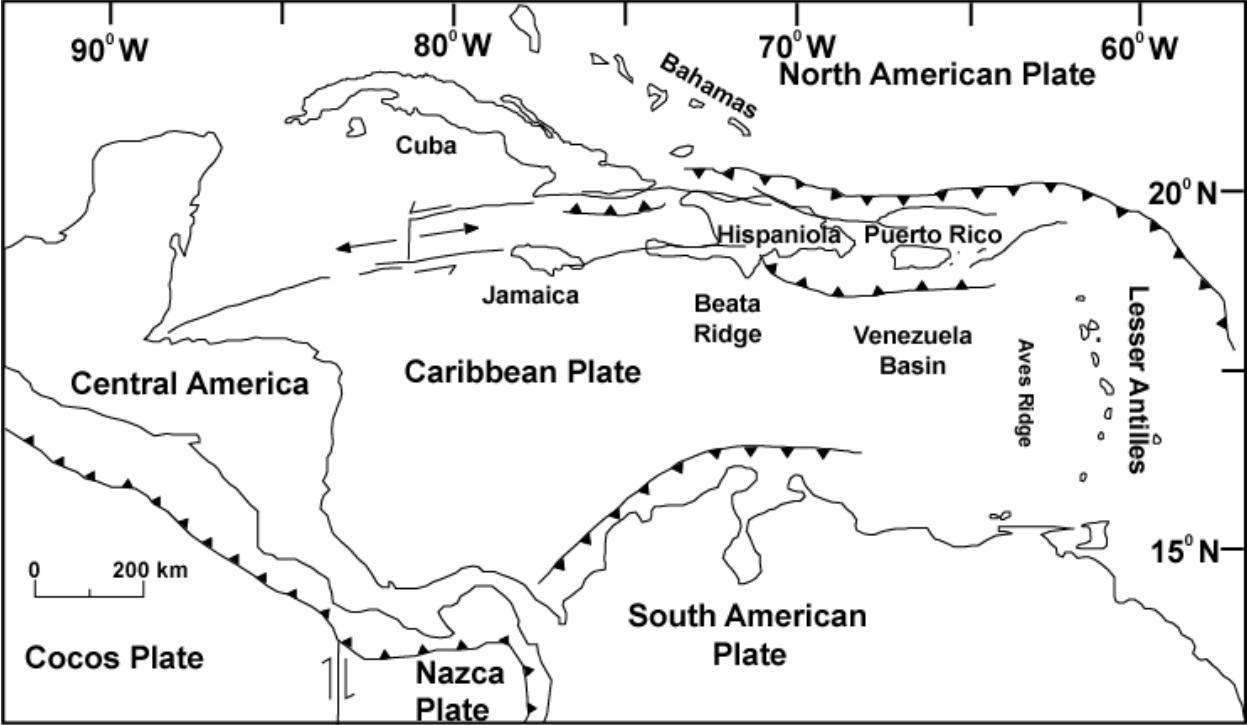


Figure 2

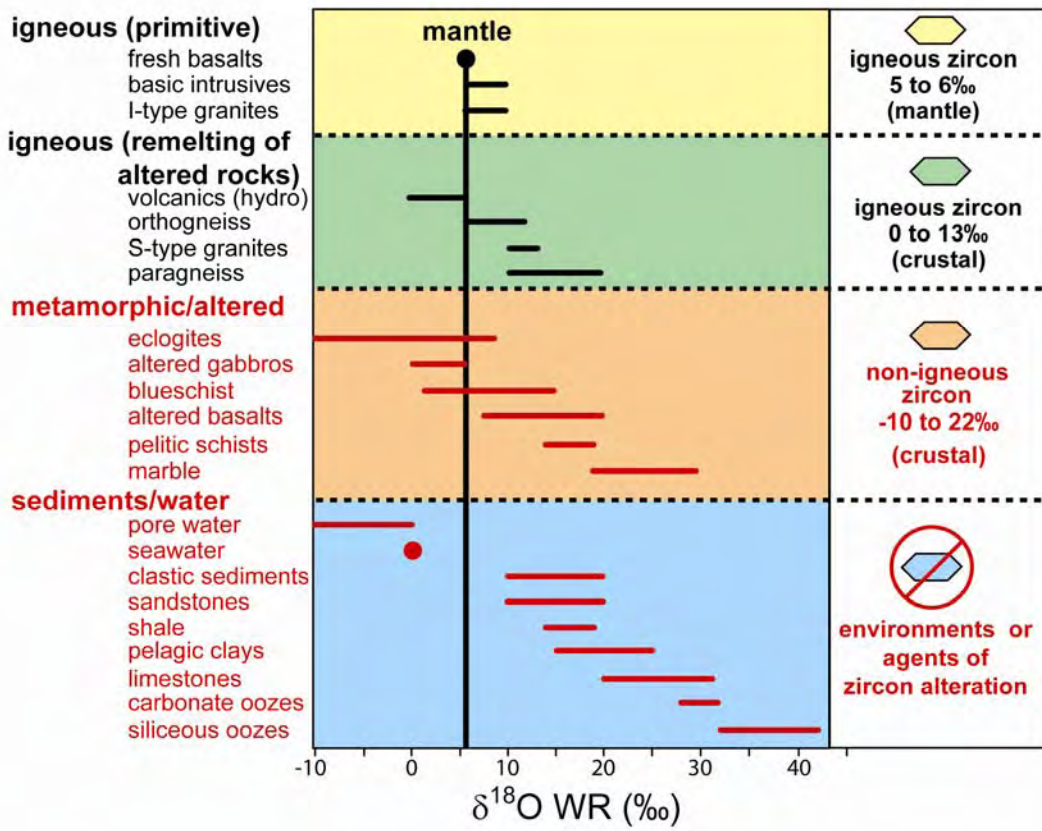


Figure 3

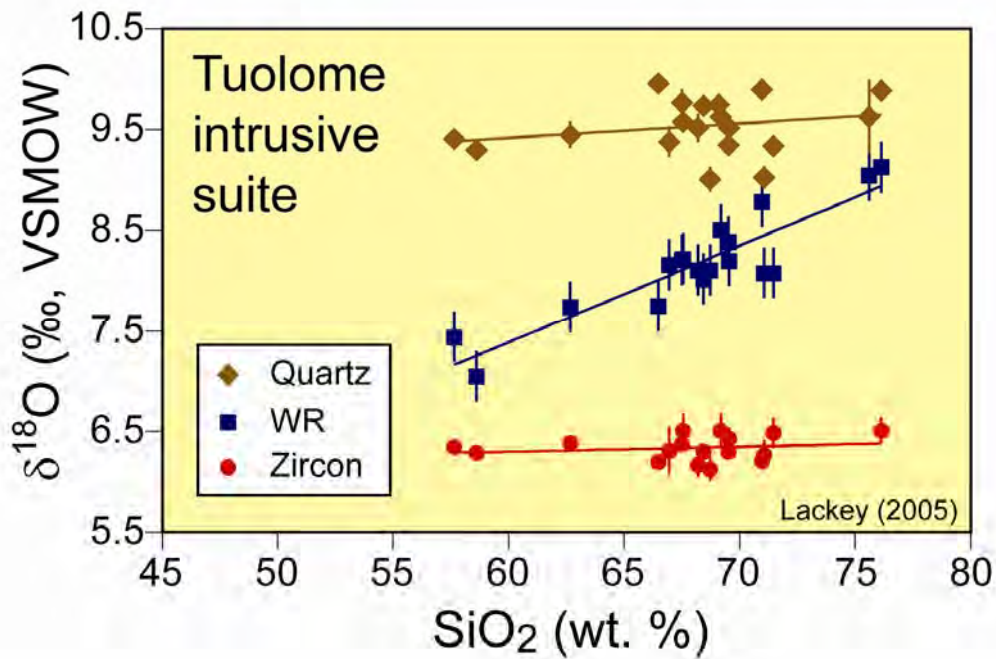


Figure 4



Figure 5

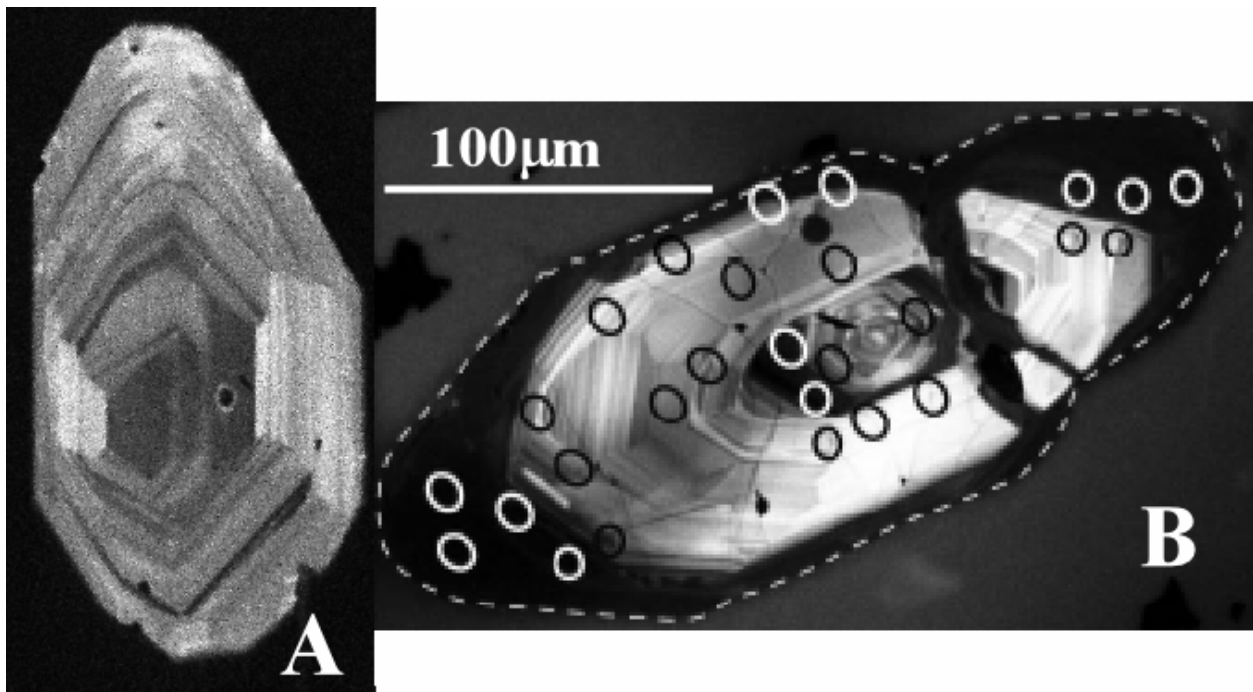


Figure 6

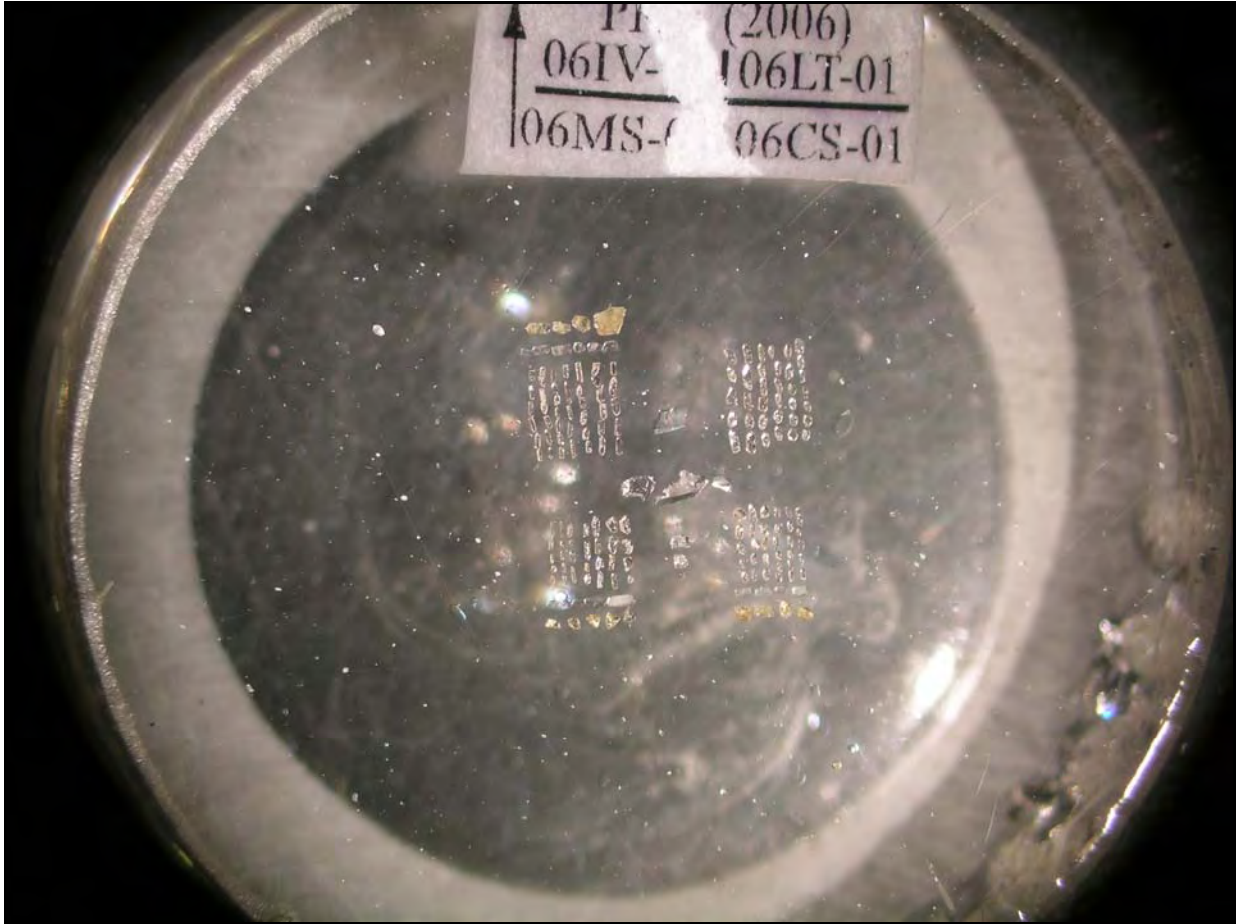


Figure 7

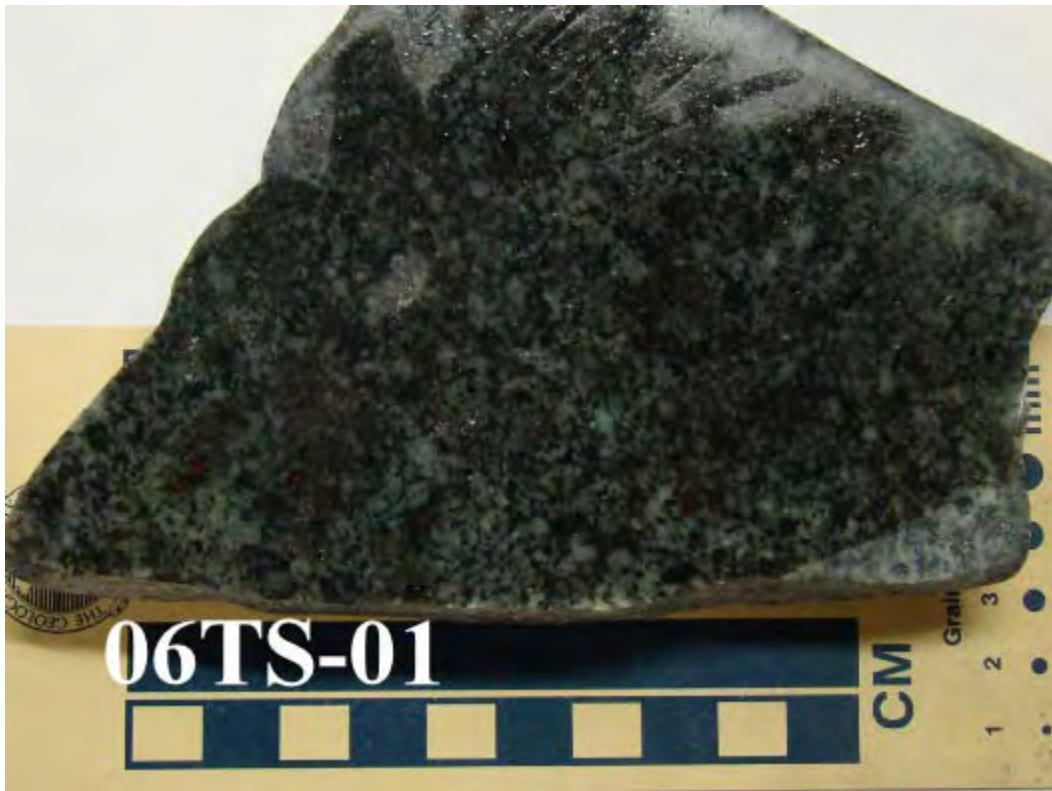


Figure 8

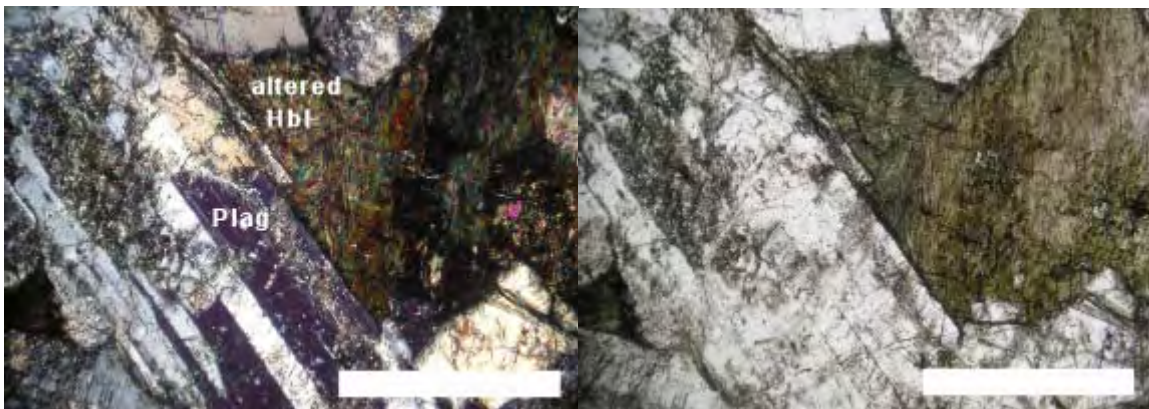


Figure 9

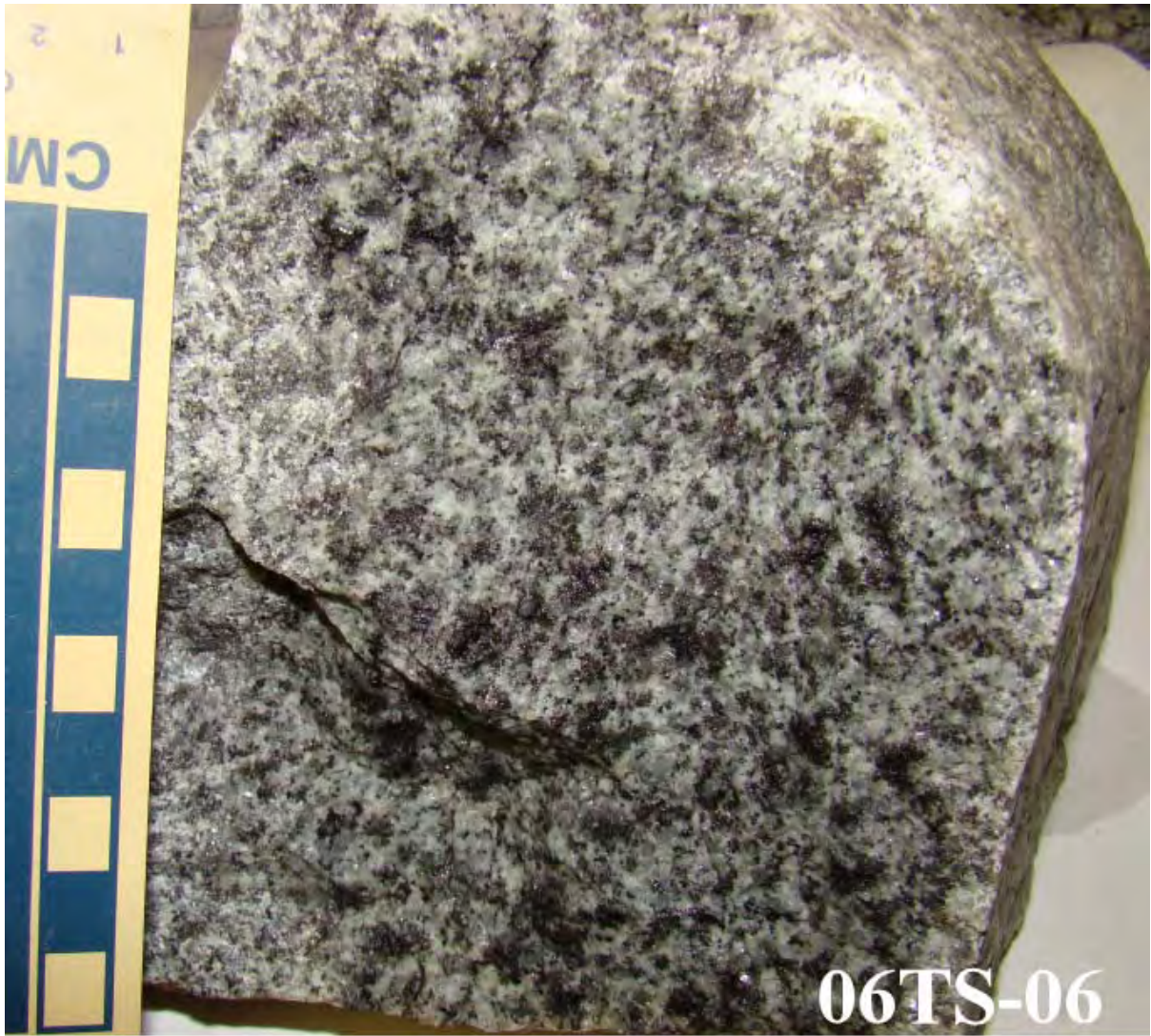


Figure 10

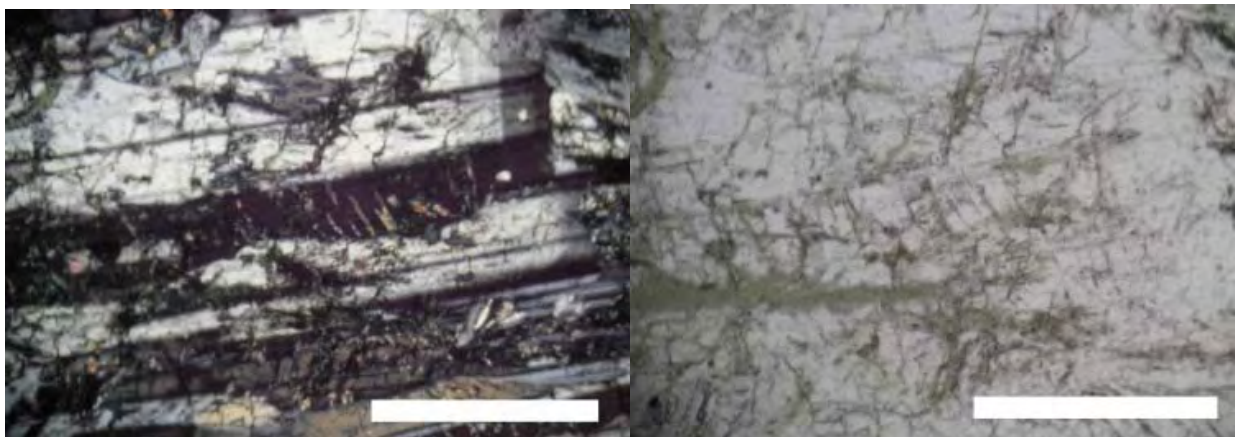


Figure 11



Figure 12



Figure 13

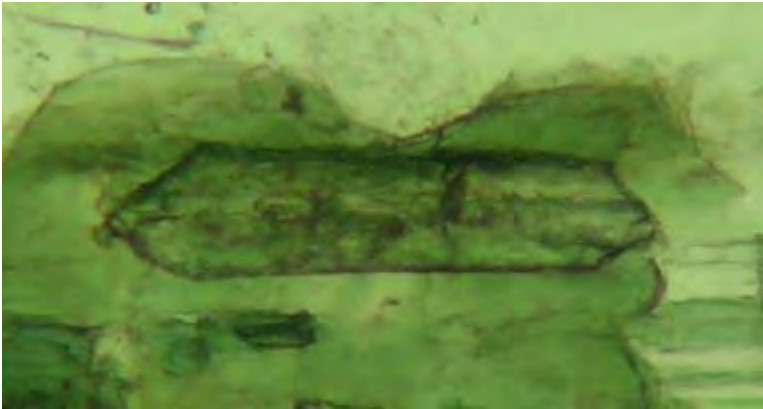


Figure 14



Figure 15

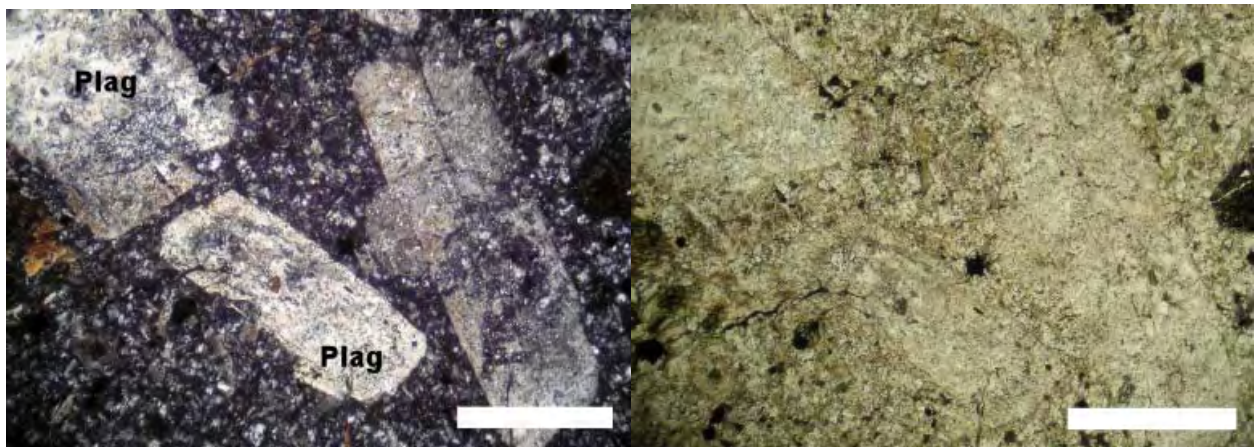


Figure 16

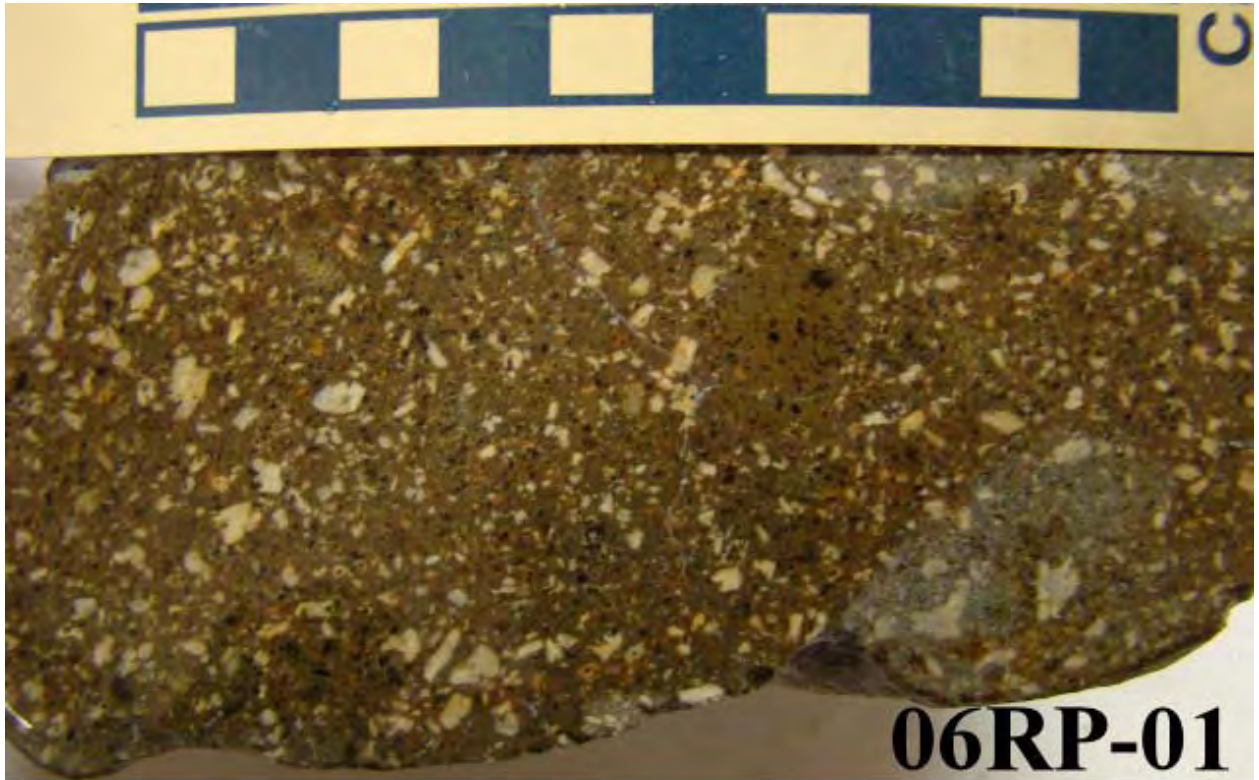


Figure 17



Figure 18

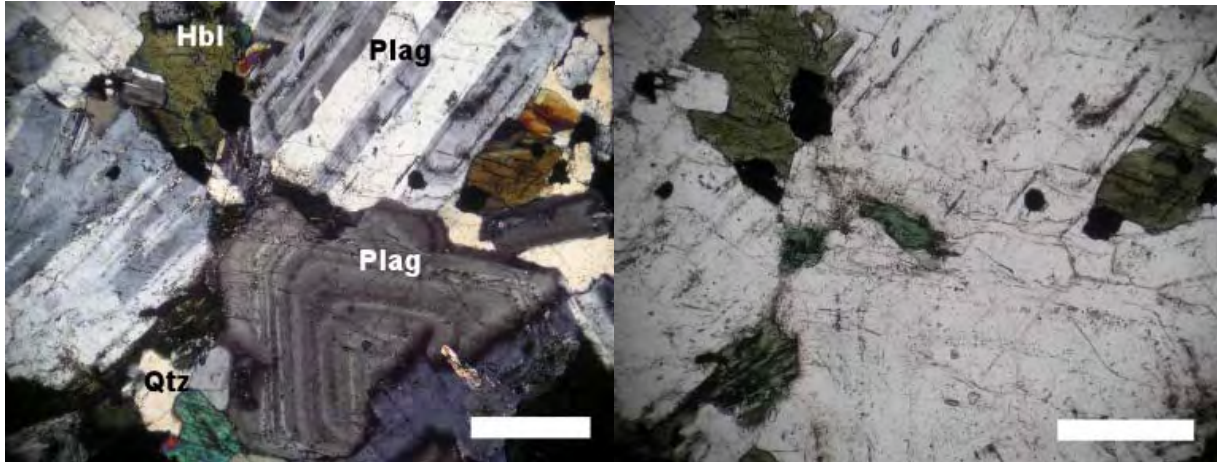


Figure 19

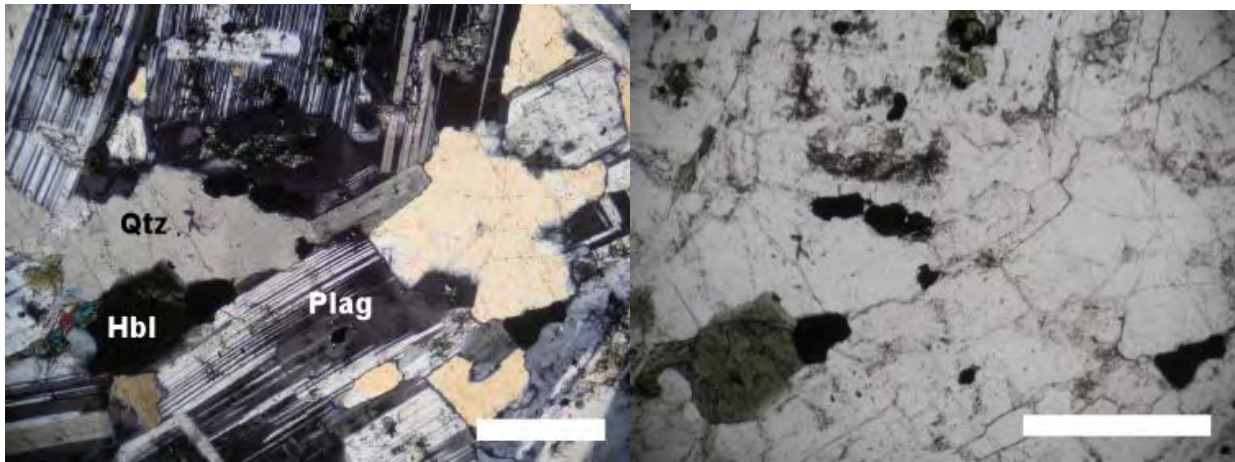


Figure 20

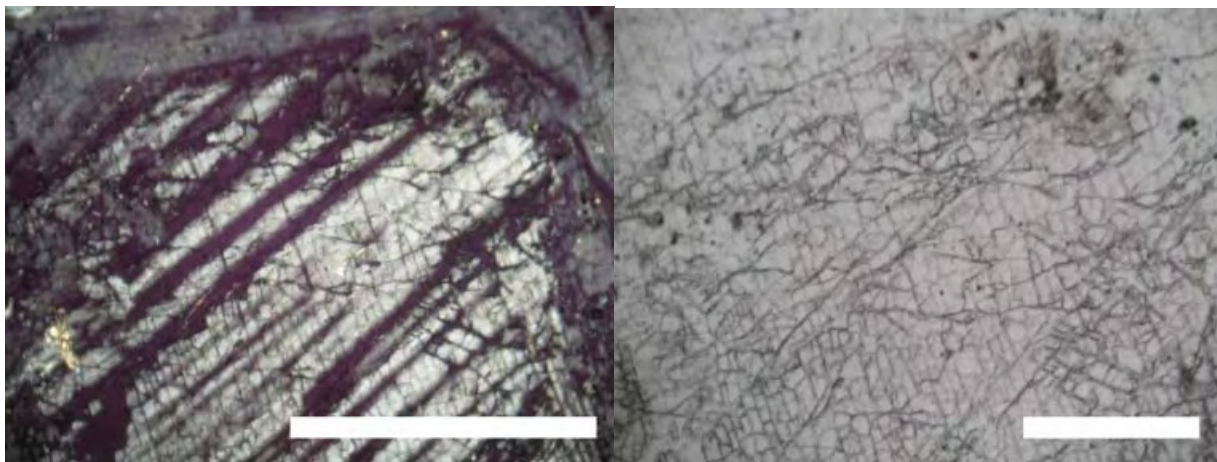


Figure 21



Figure 22

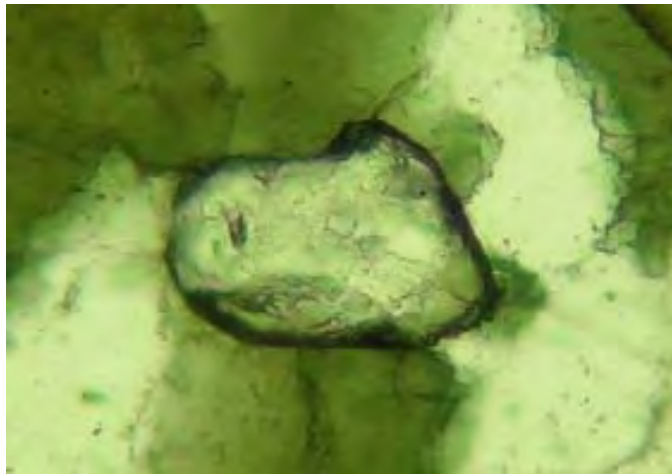


Figure 23



Figure 24



Figure 25

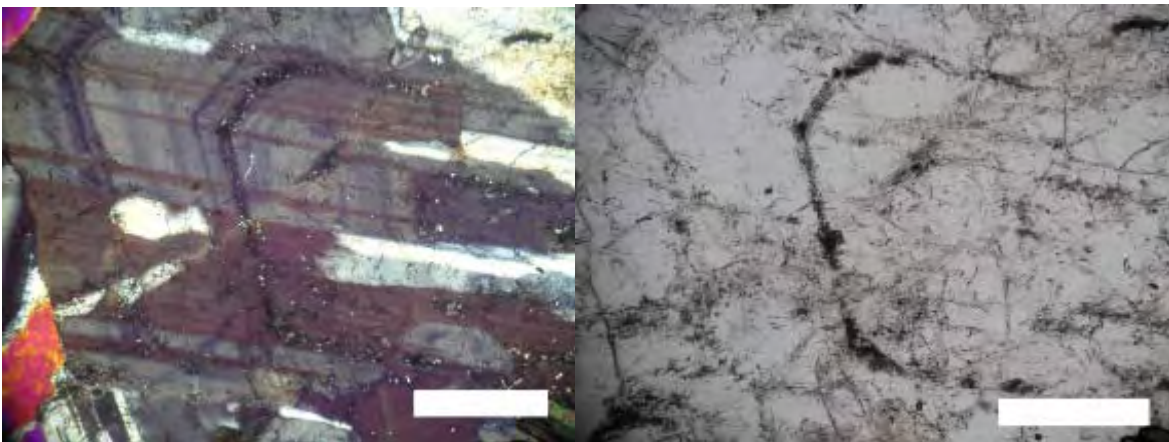


Figure 26

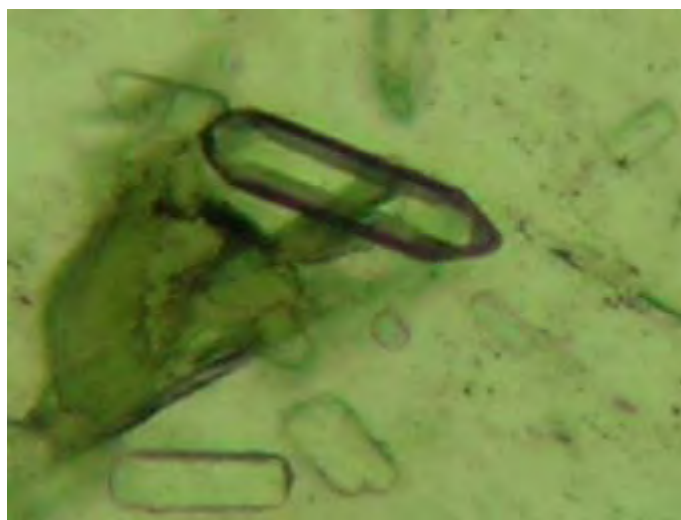


Figure 27

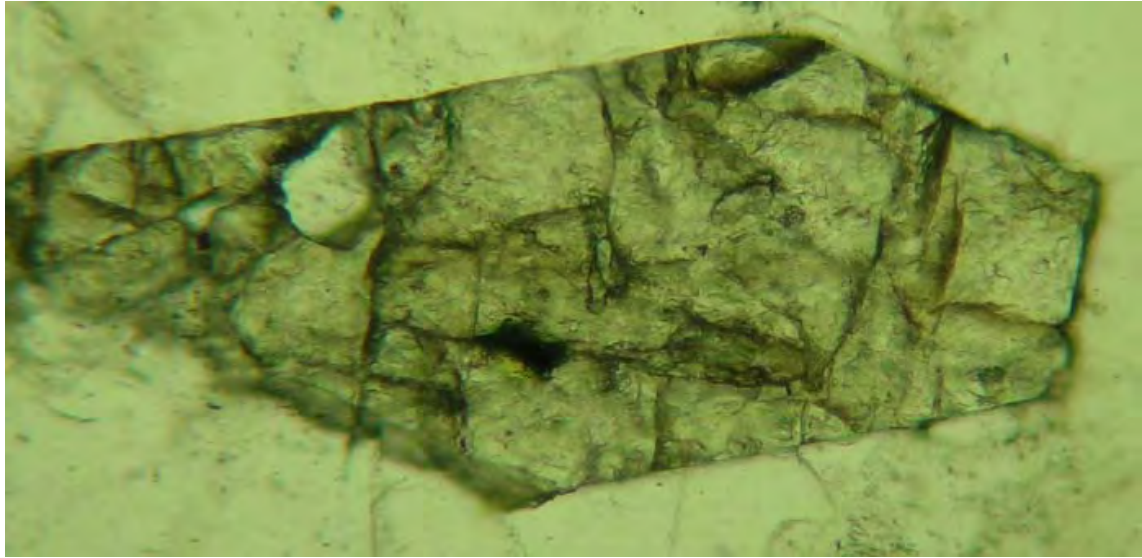


Figure 28

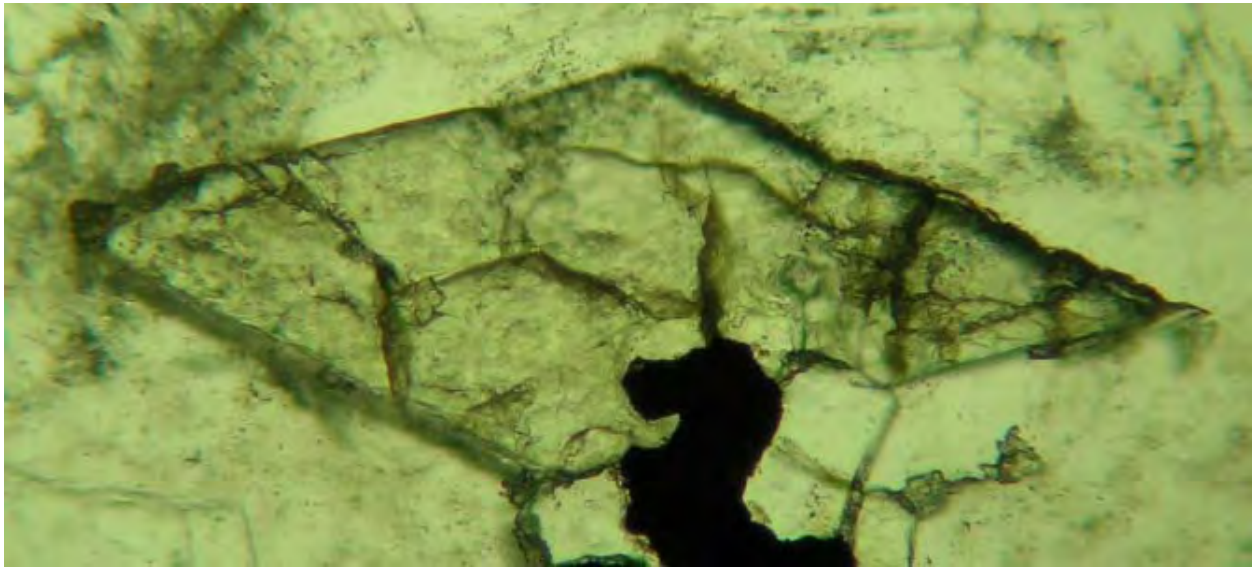


Figure 29



Figure 30

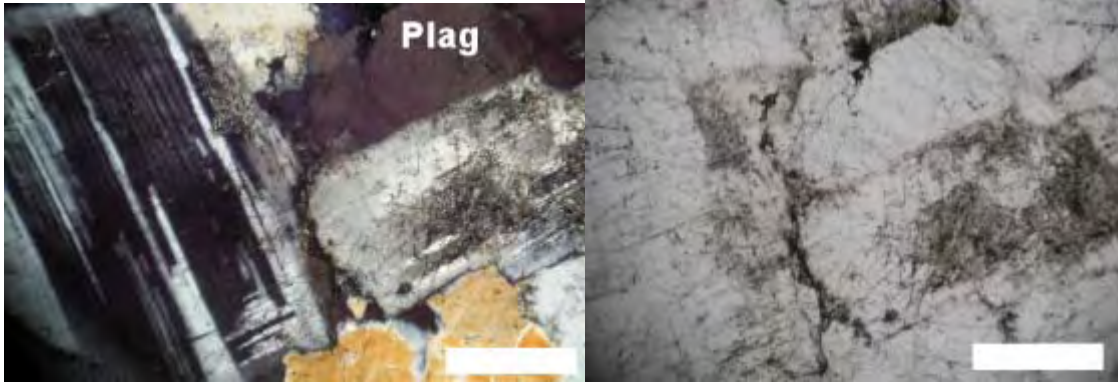


Figure 31



Figure 32

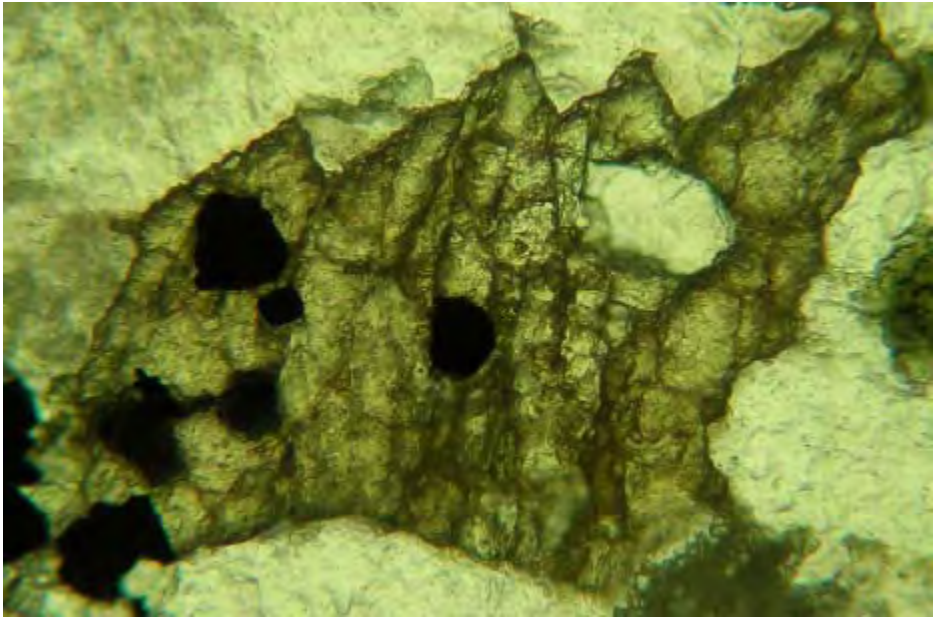


Figure 33



Figure 34

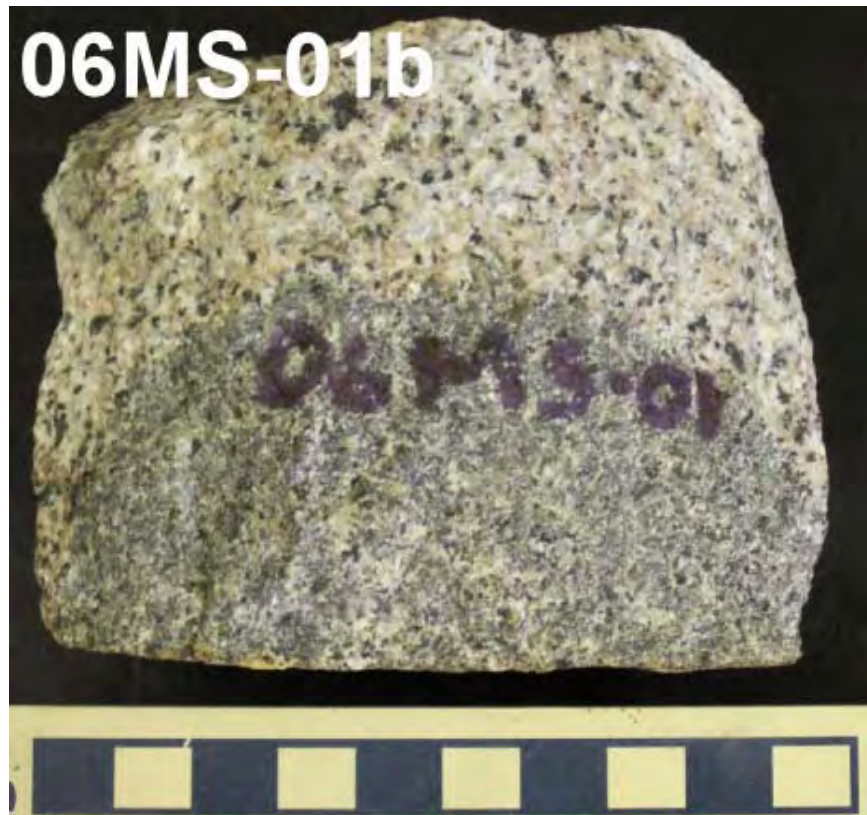


Figure 35

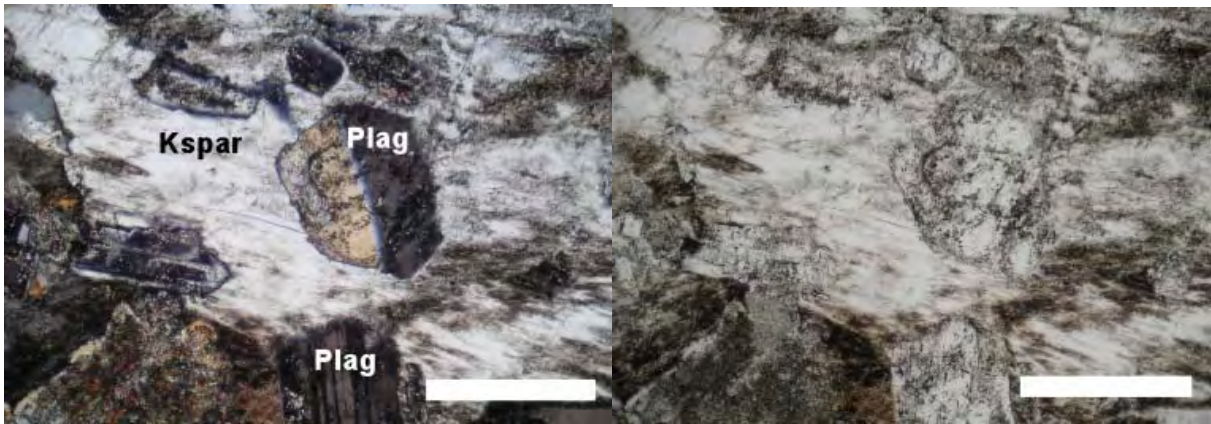


Figure 36

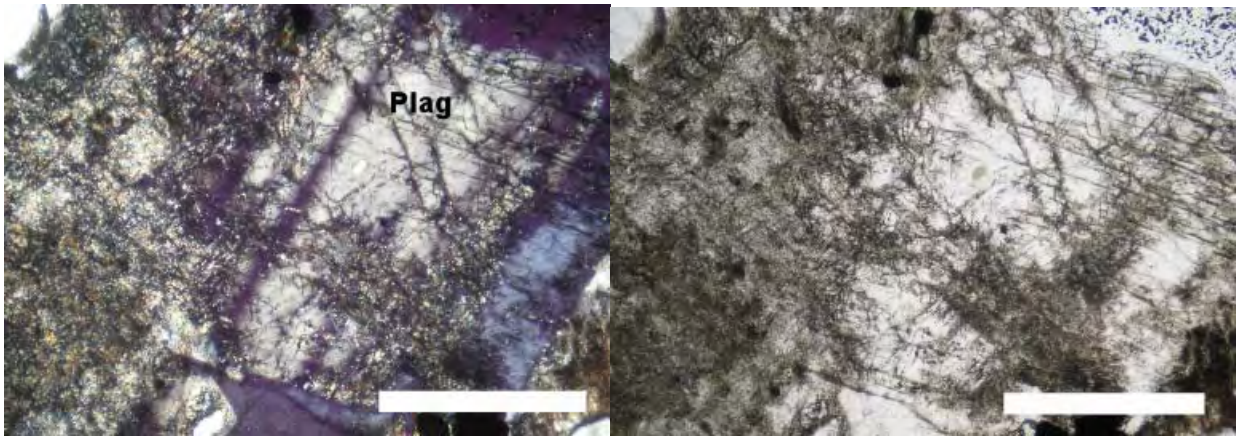


Figure 37

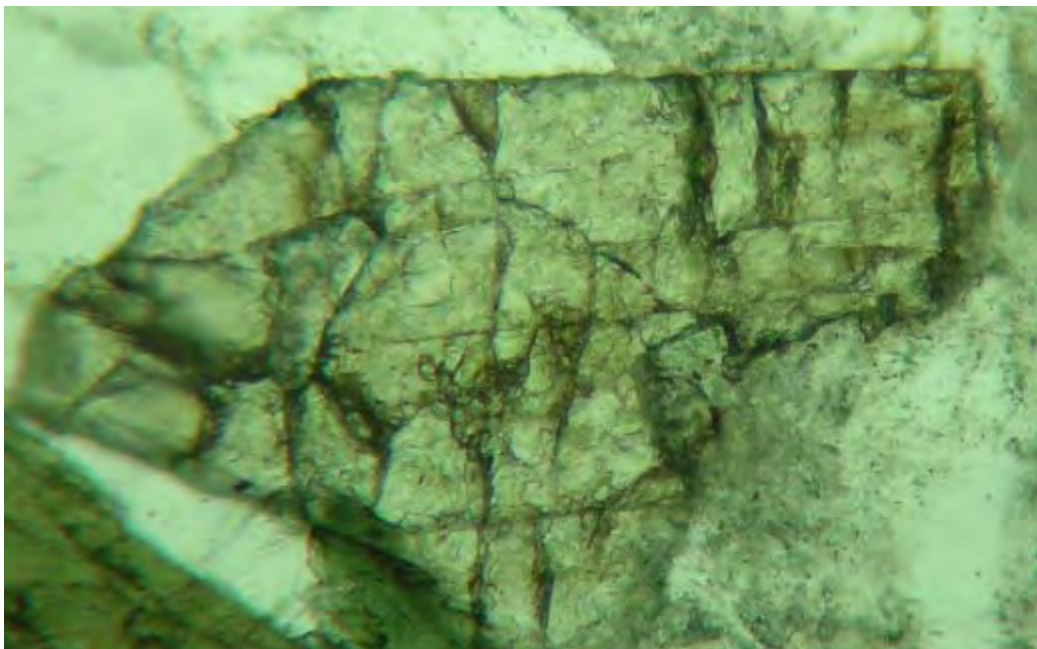


Figure 38



Figure 39



Figure 40

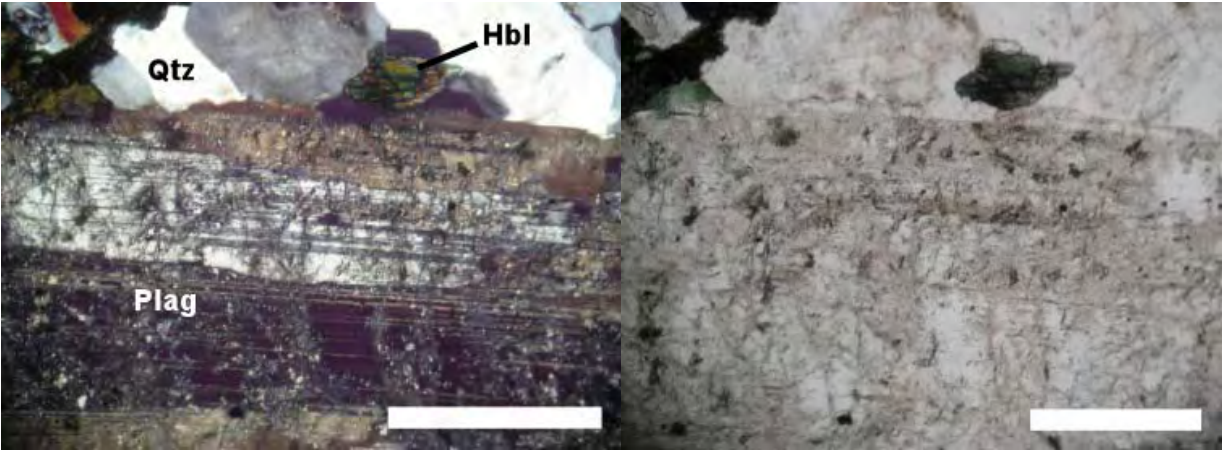


Figure 41

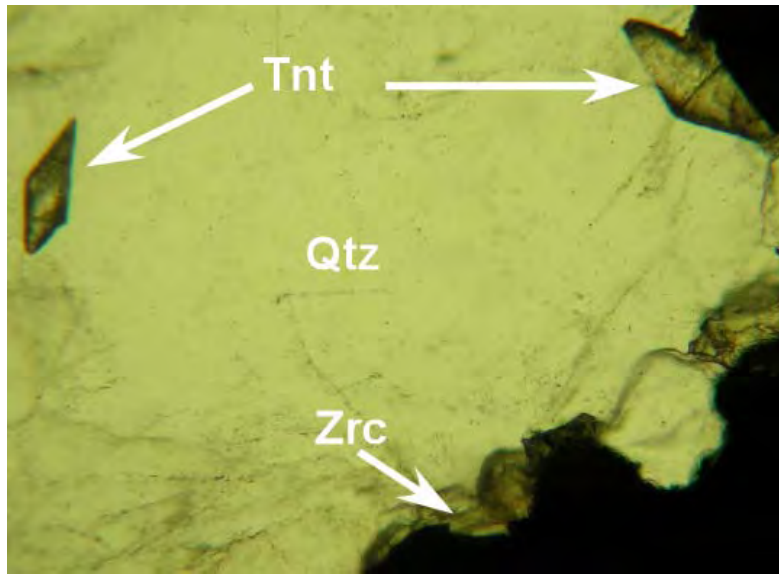


Figure 42

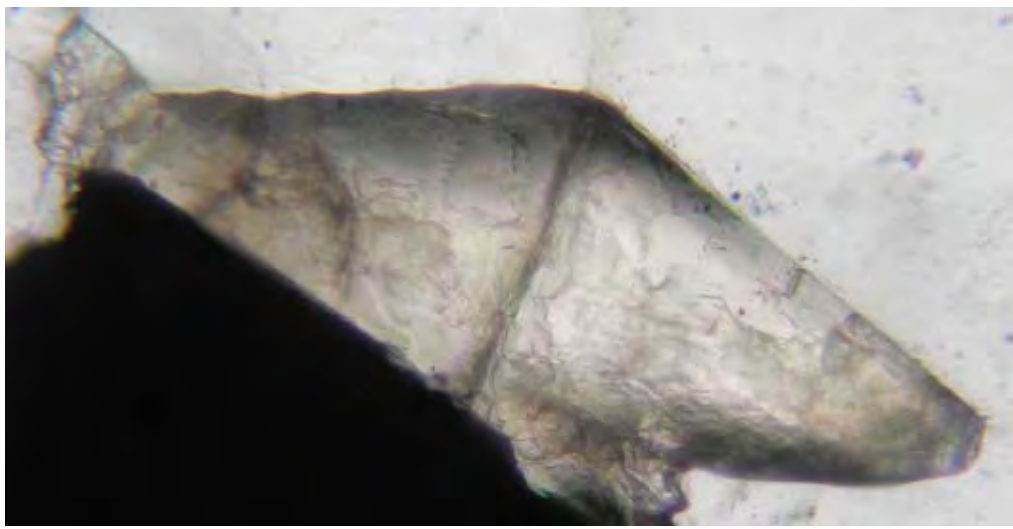


Figure 43



Figure 44

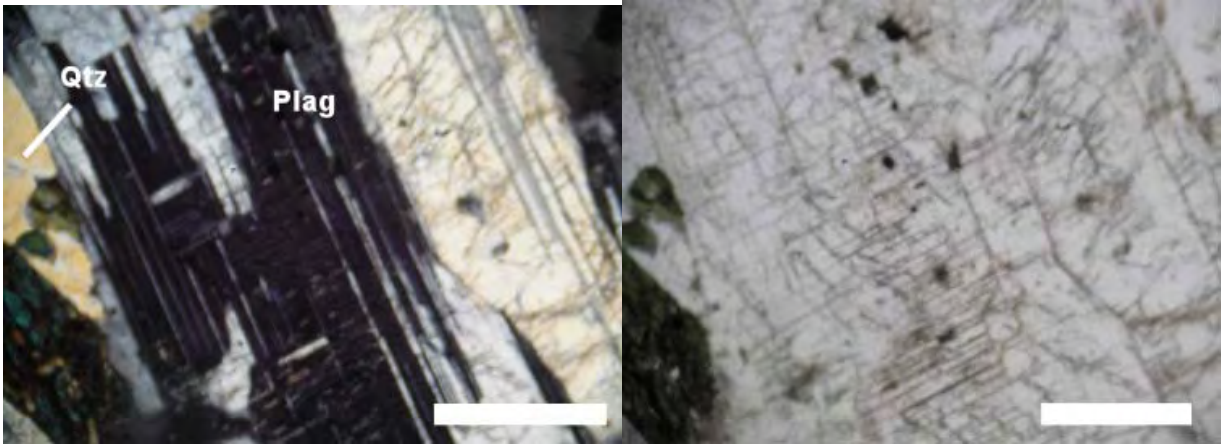


Figure 45

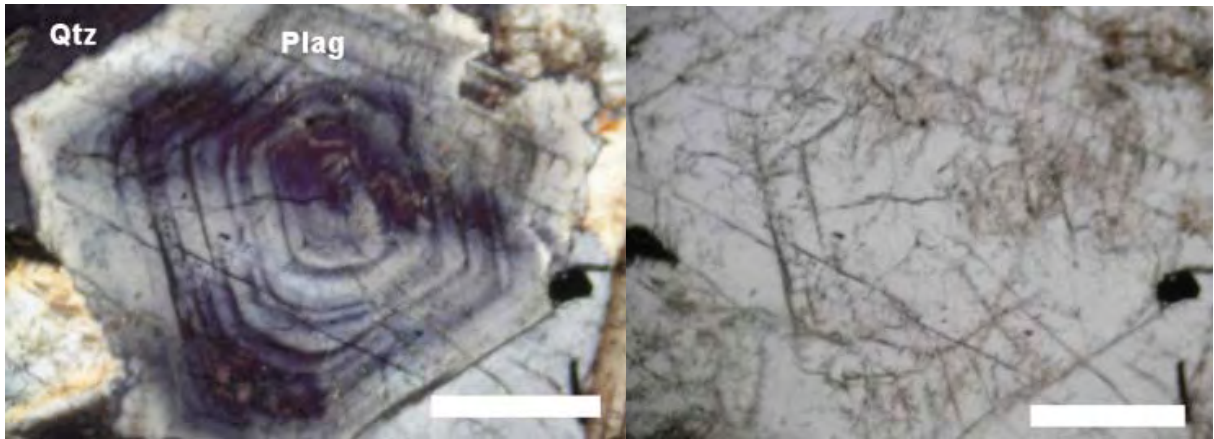


Figure 46

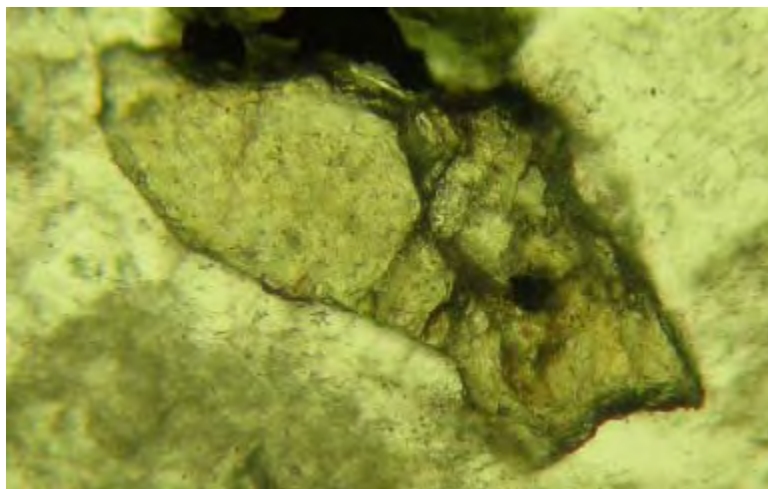


Figure 47



Figure 48

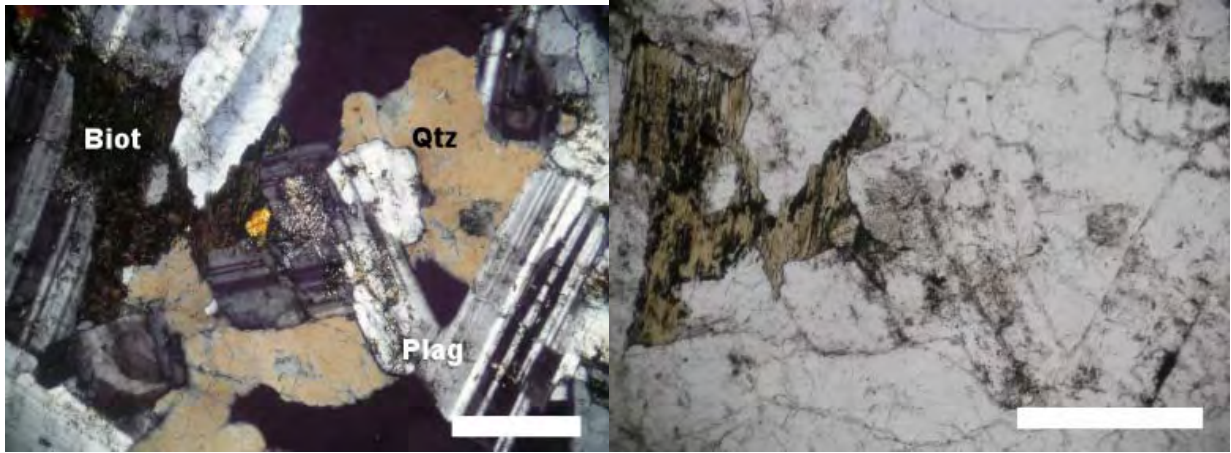


Figure 49

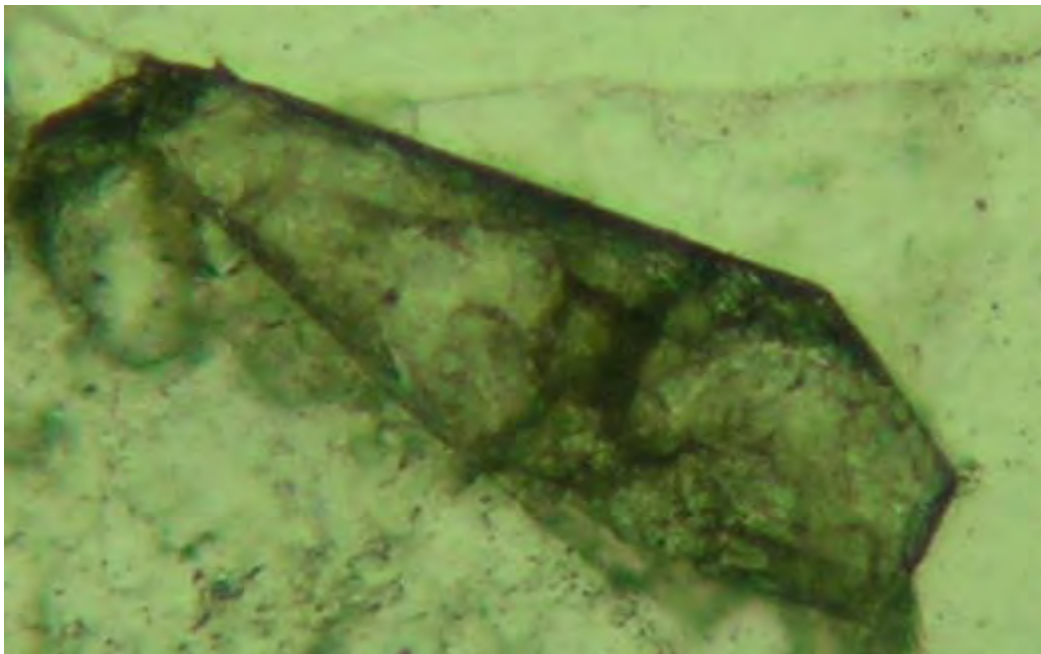


Figure 50

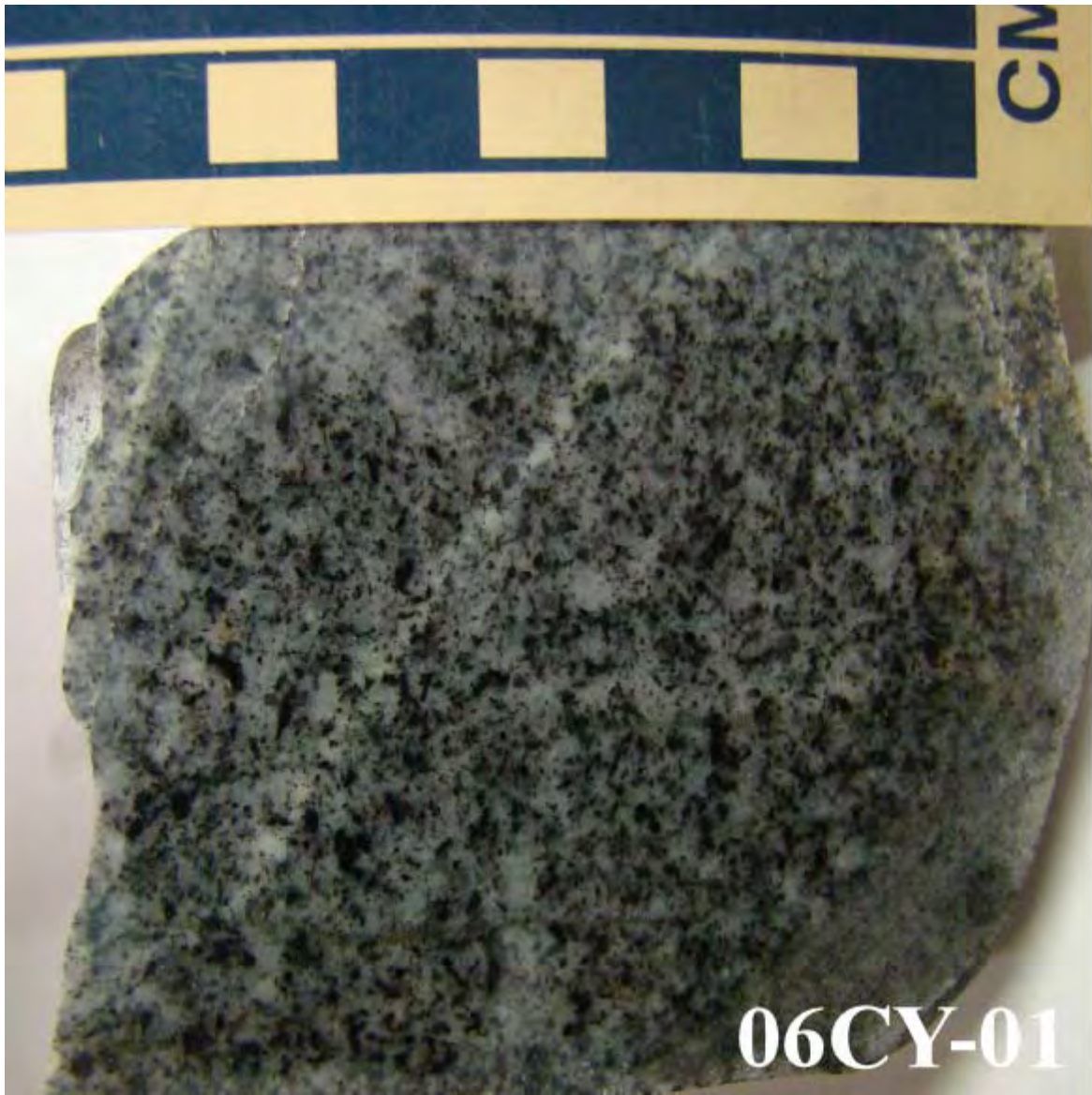


Figure 51

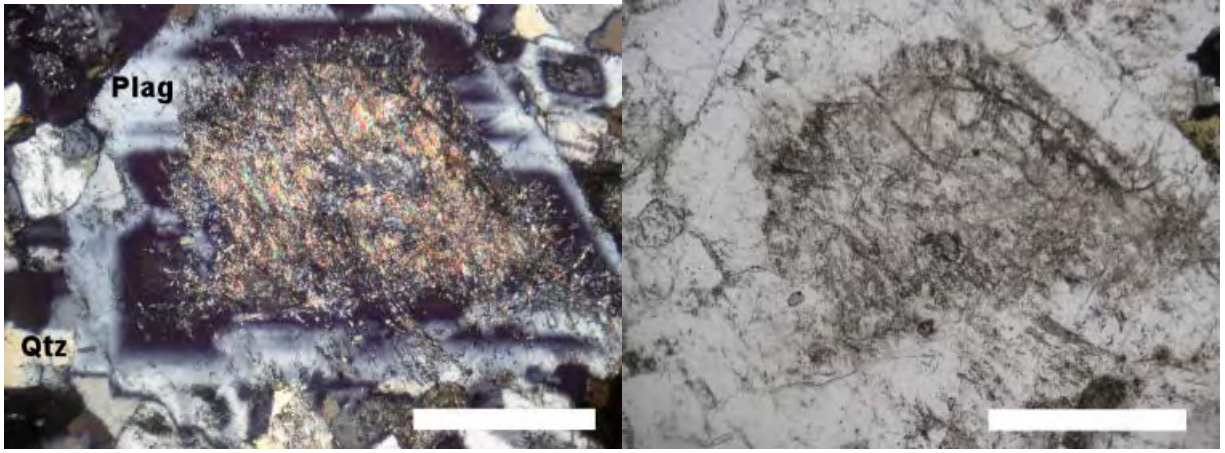


Figure 52

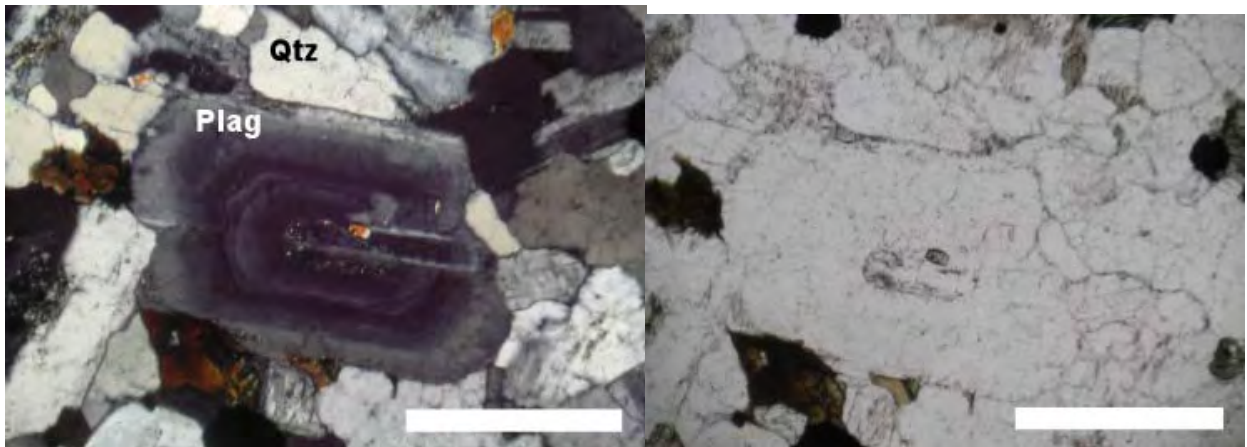


Figure 53



Figure 54

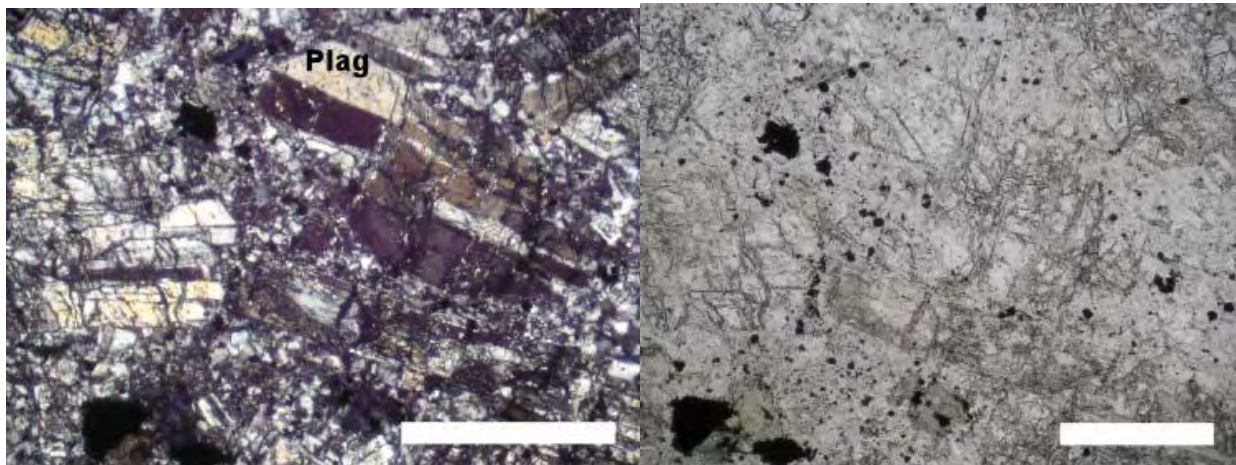


Figure 55

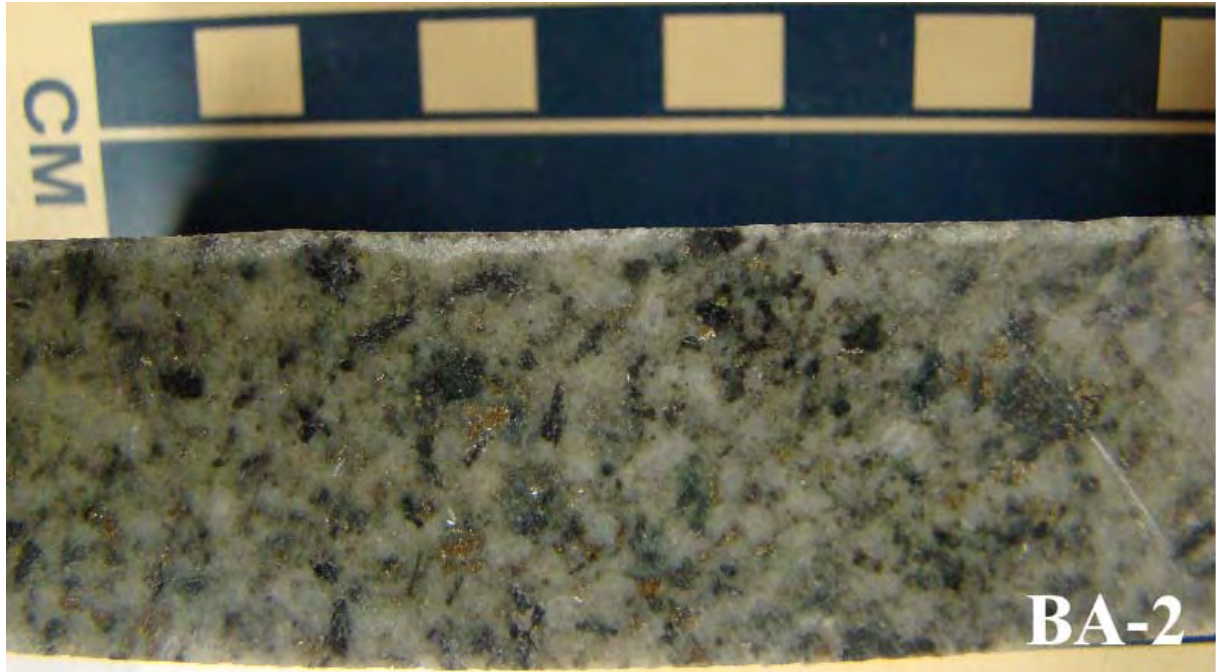


Figure 56

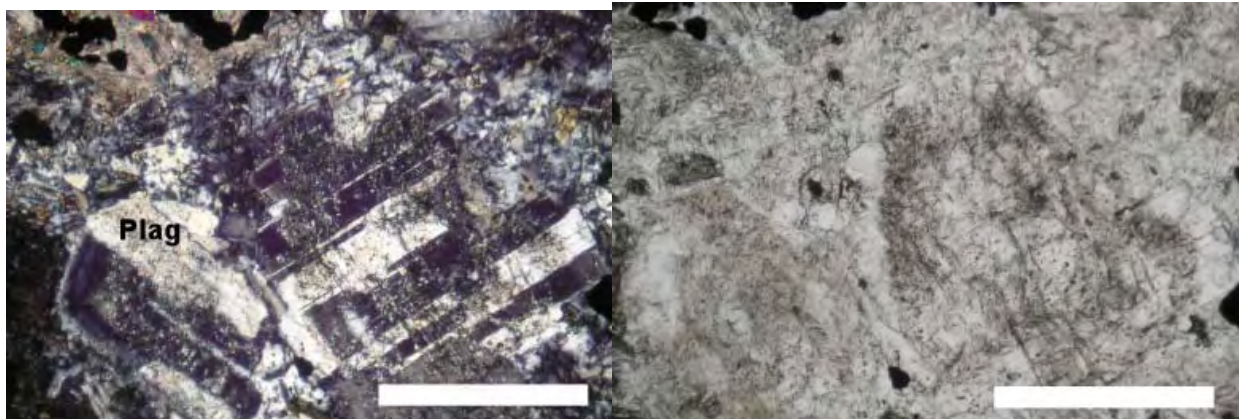


Figure 57



Figure 58

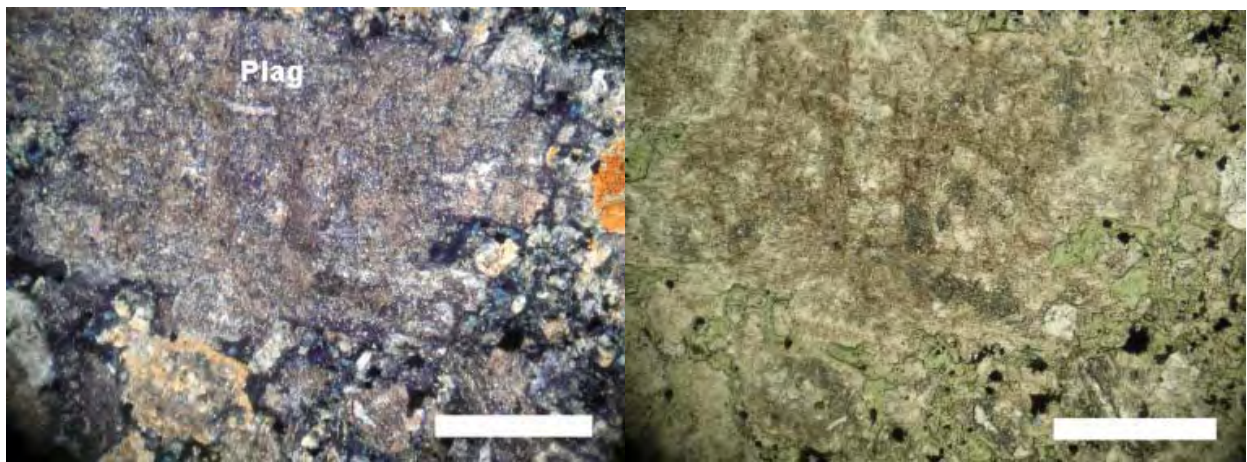


Figure 59



Figure 60

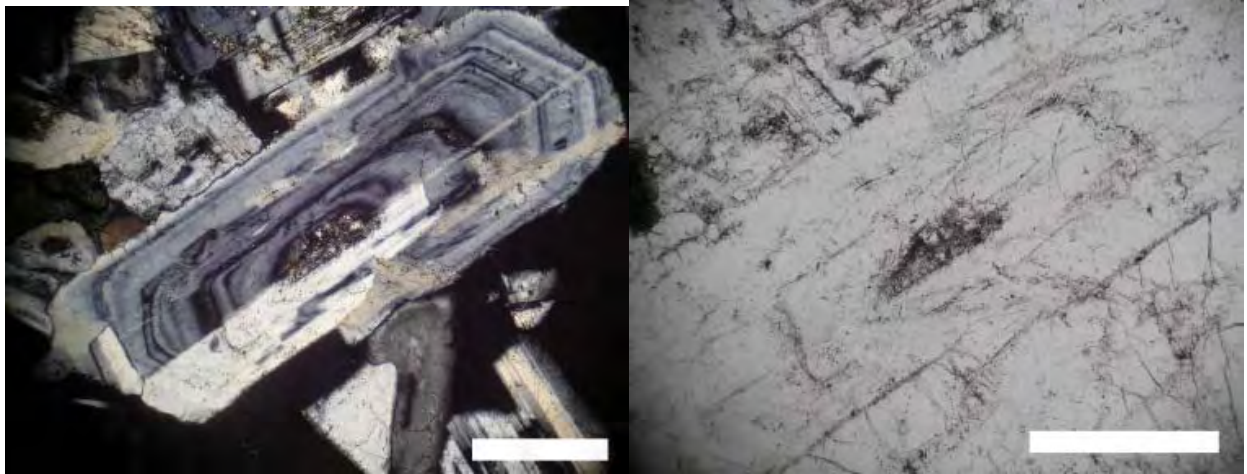


Figure 61

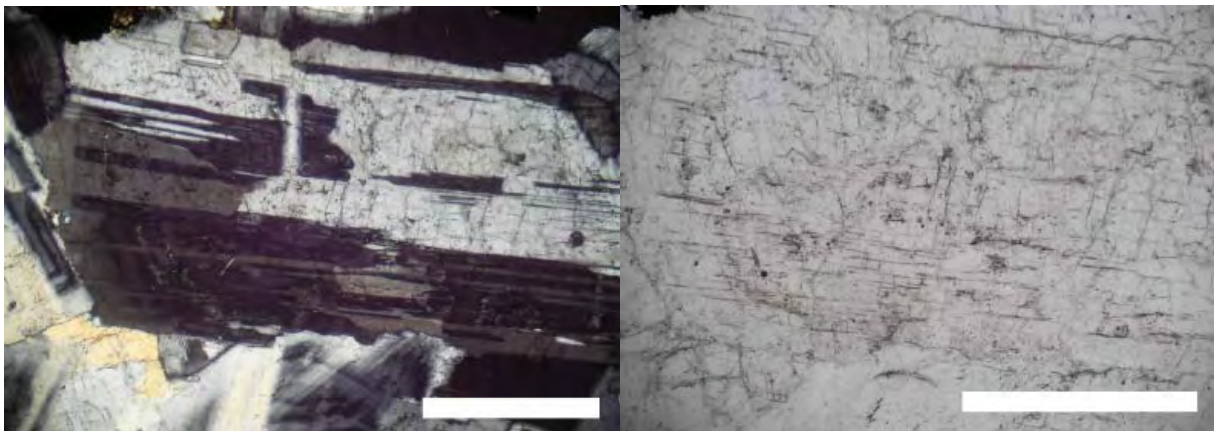


Figure 62

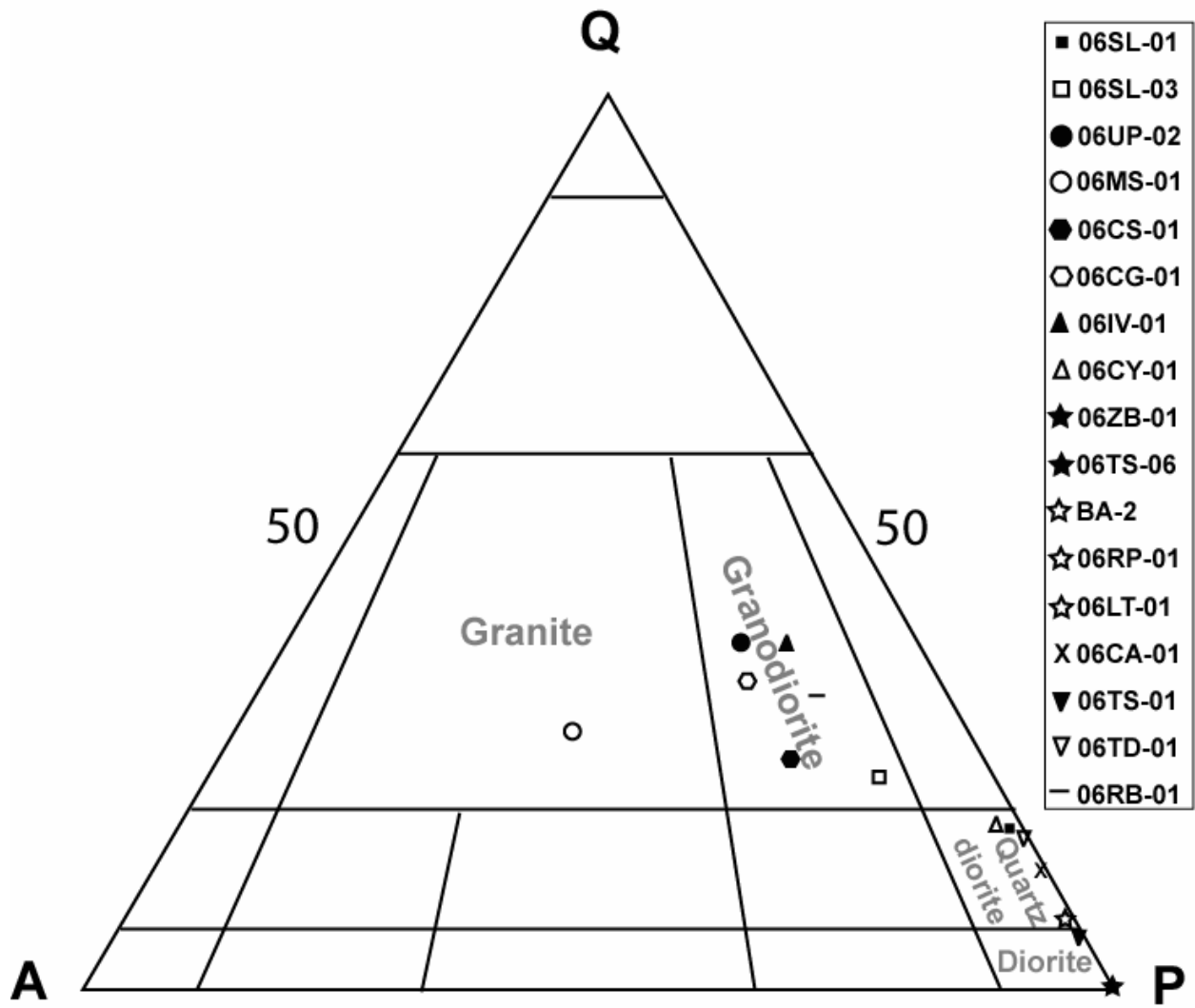


Figure 63

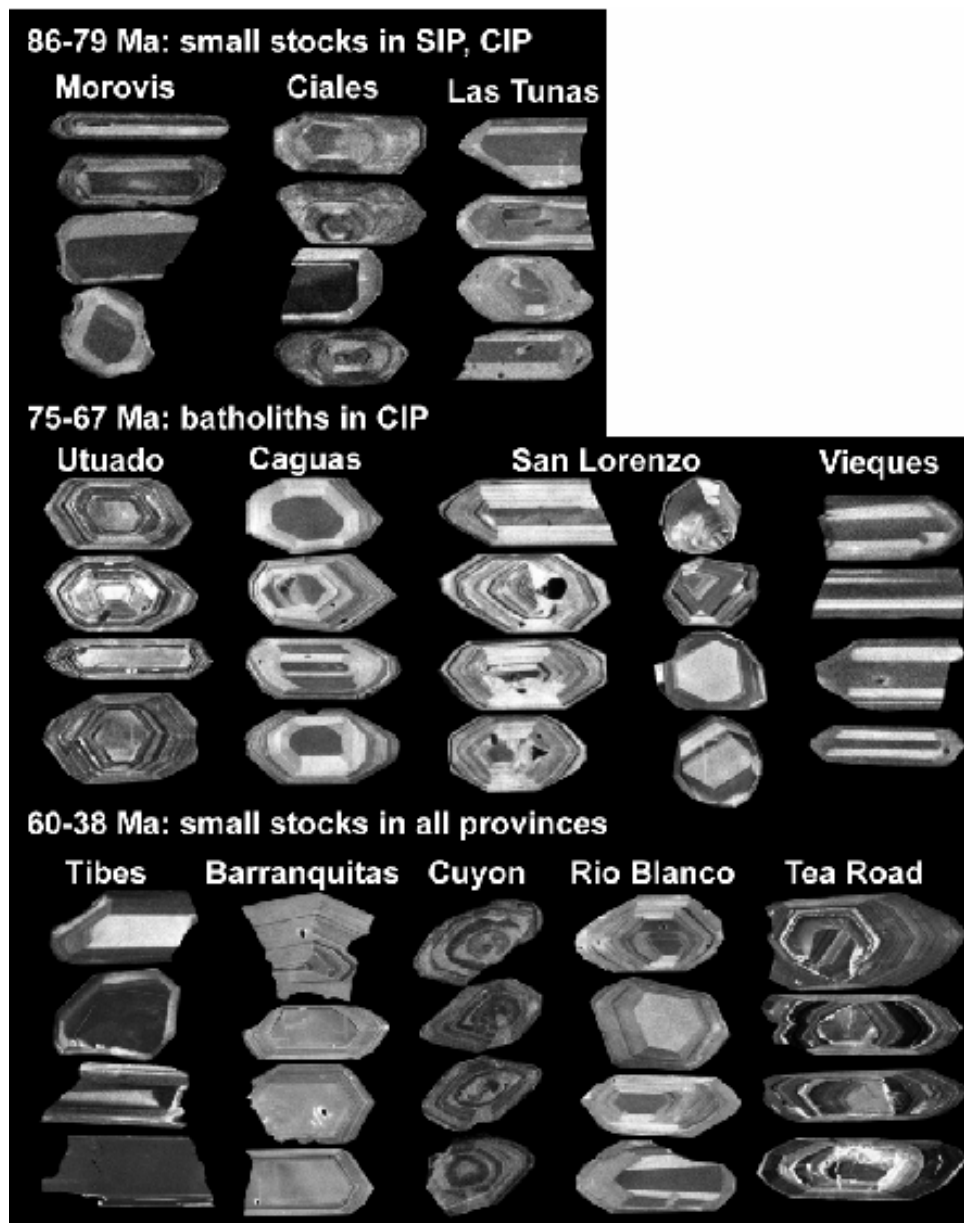


Figure 64

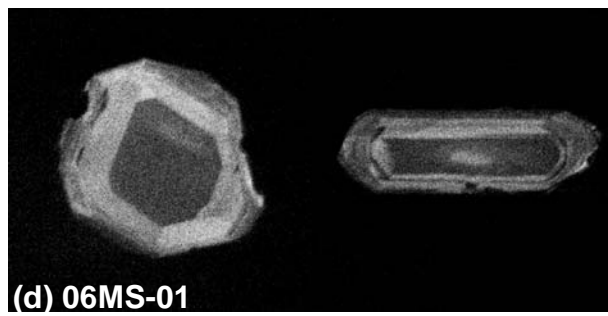
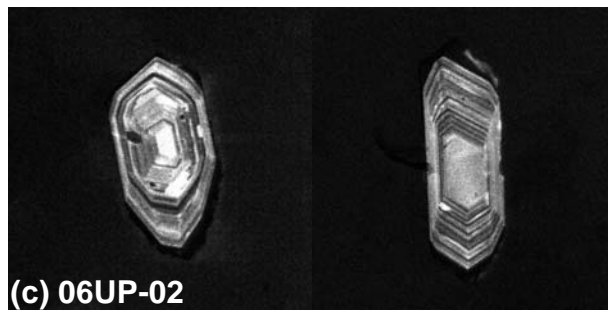
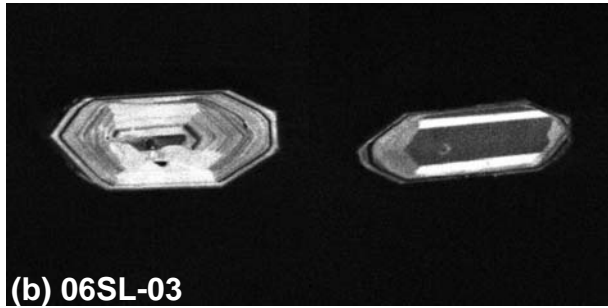
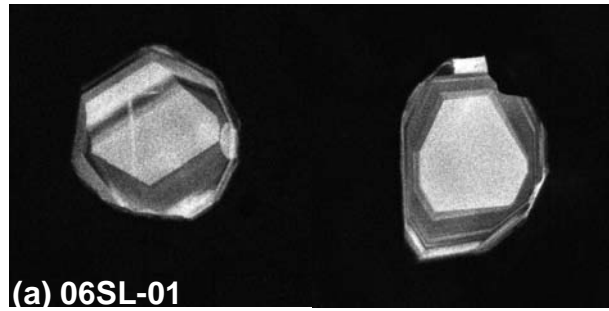


Figure 65

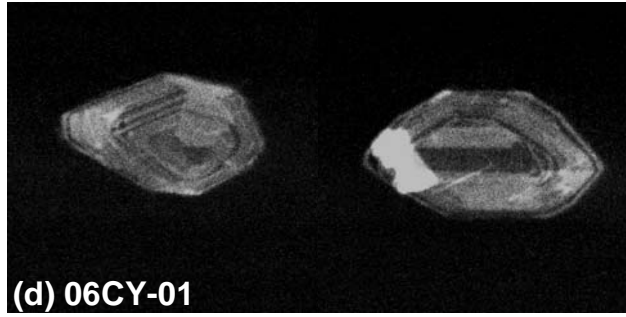
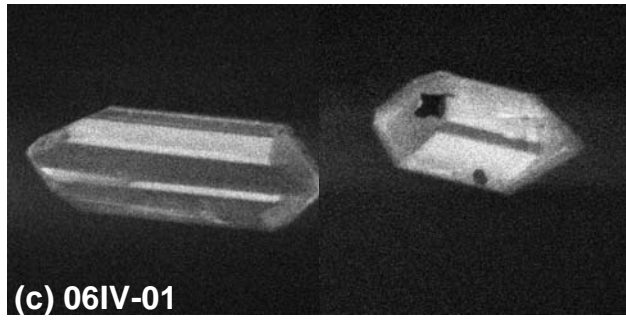
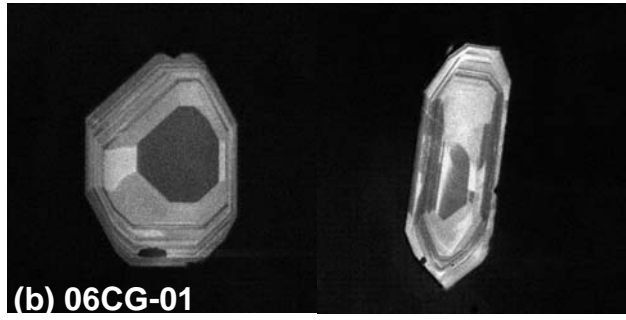
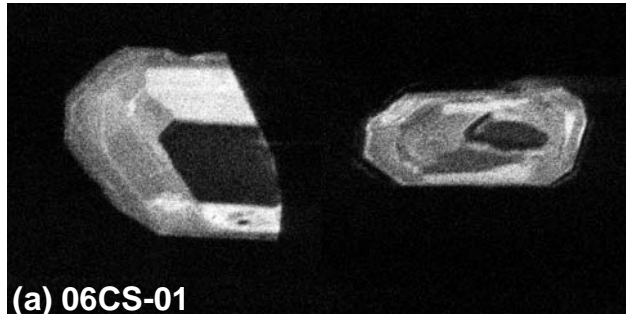


Figure 66

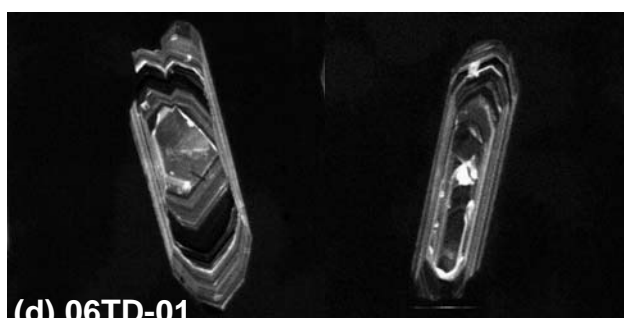
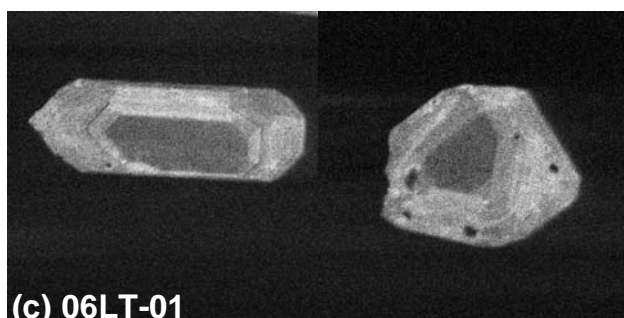
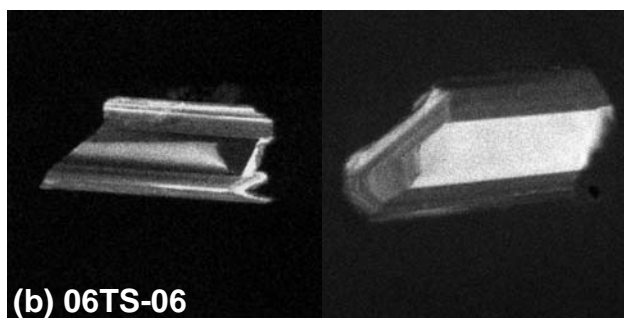
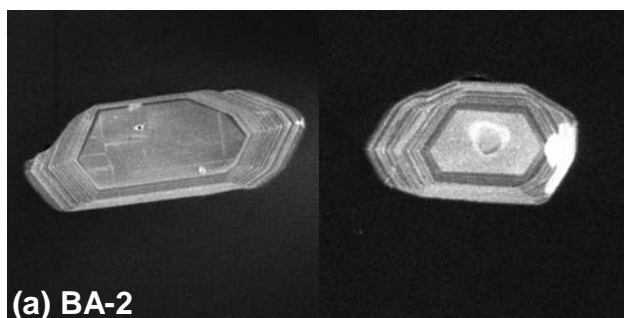


Figure 67

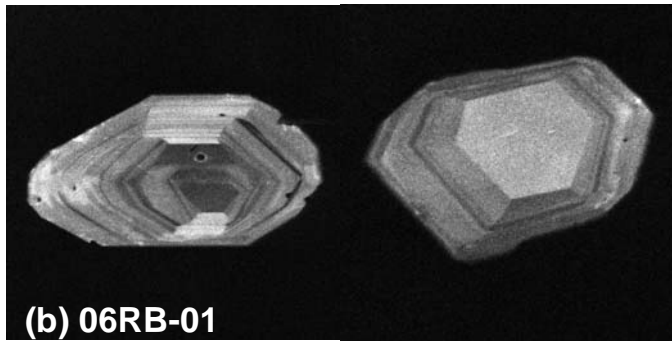
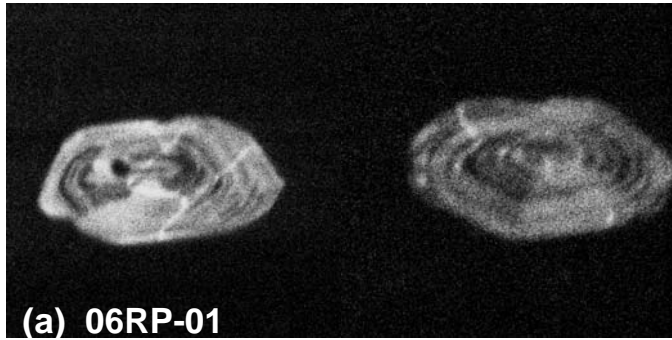


Figure 68

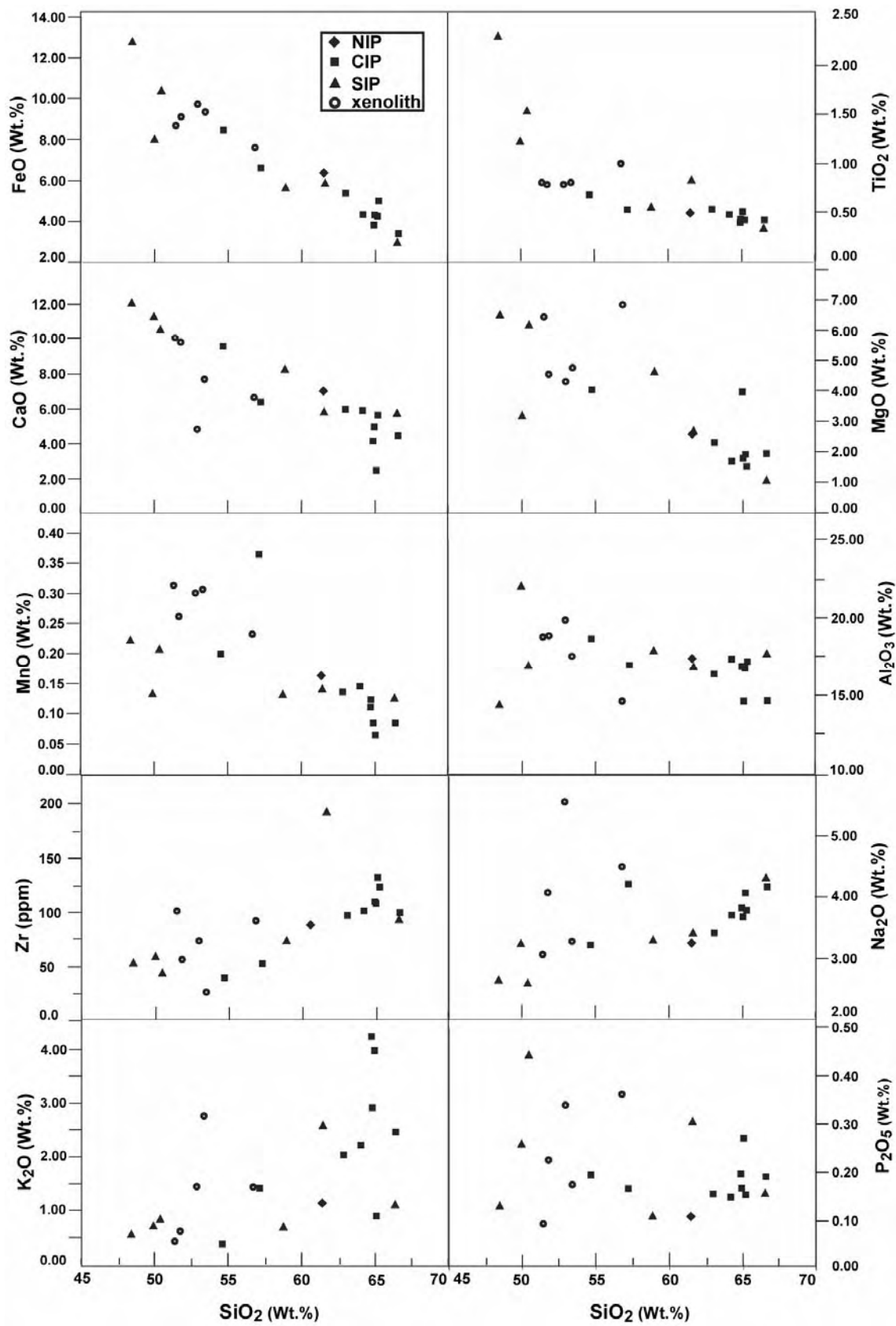


Figure 69

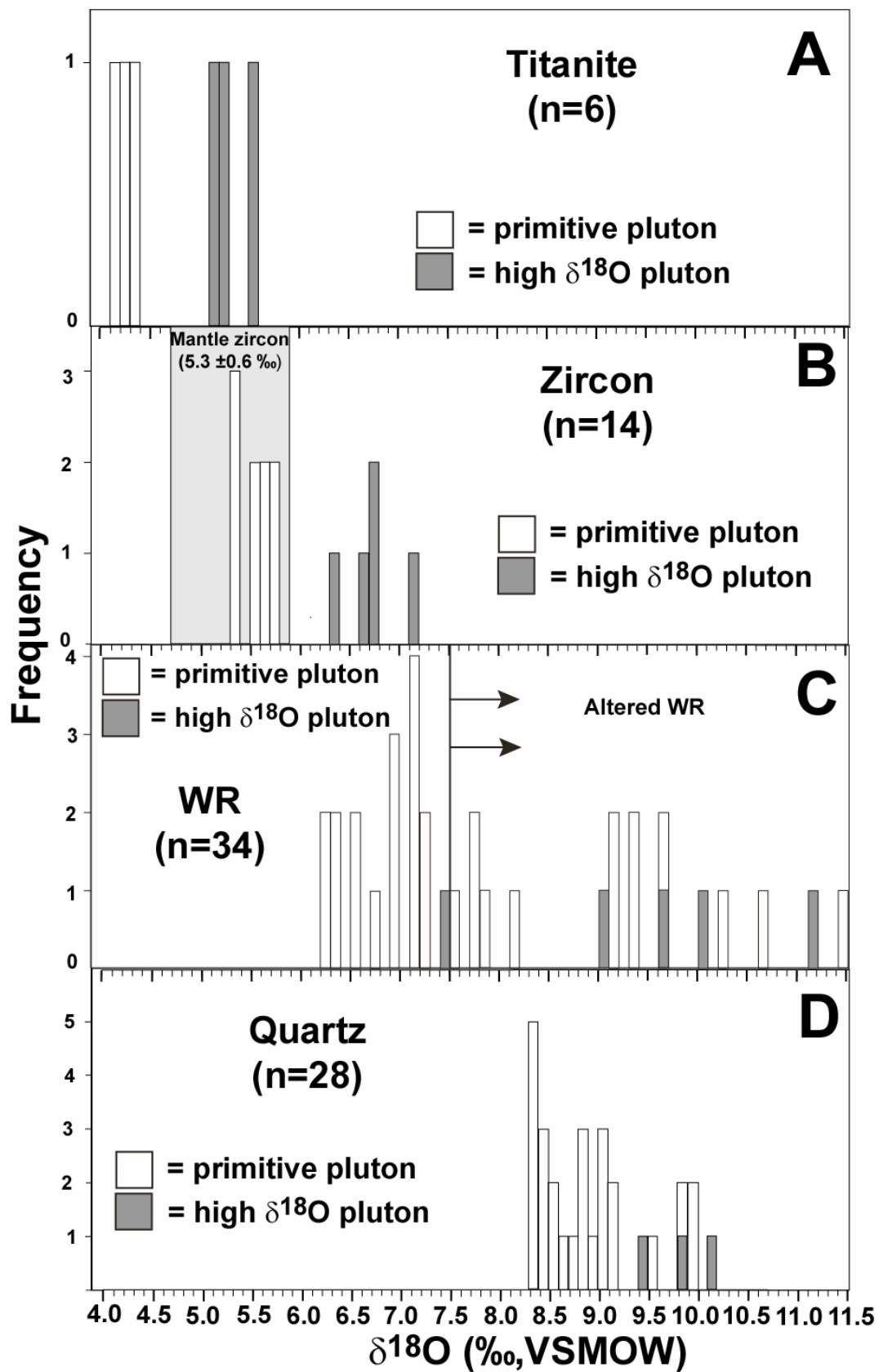


Figure 70

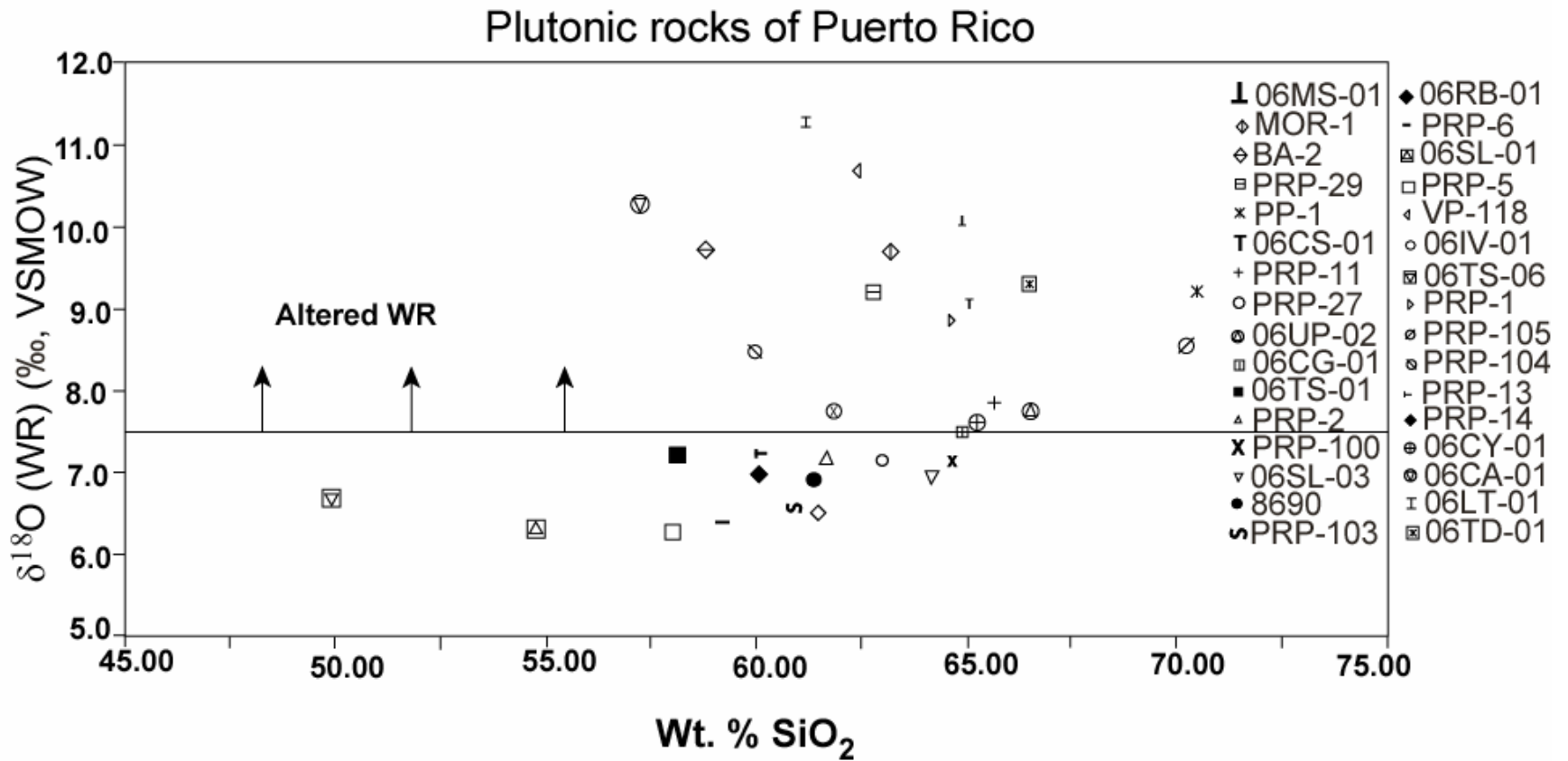


Figure 71

$\delta^{18}\text{O}$ WR vs. wt.% SiO_2 of xenoliths and host rock

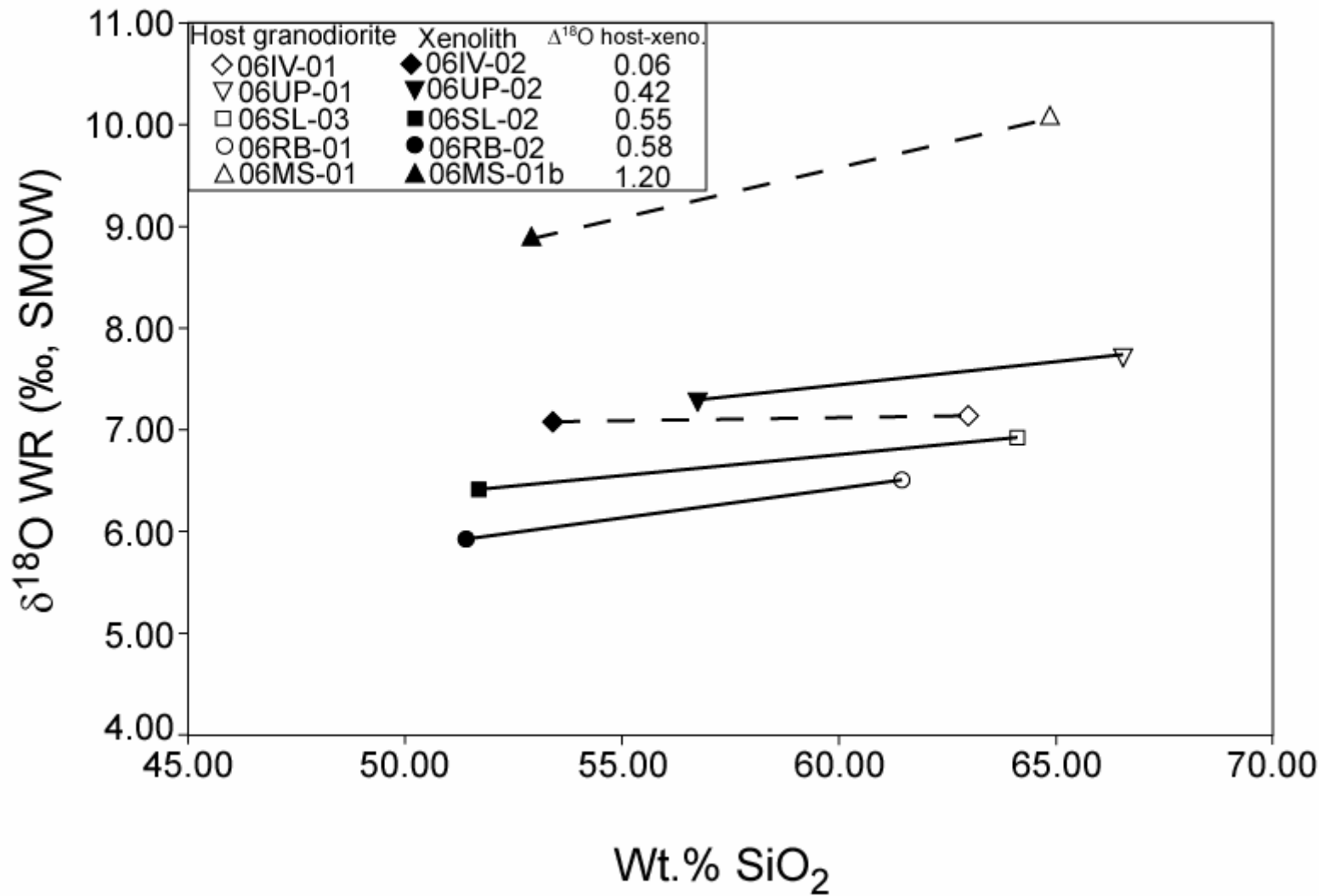


Figure 72

Calculated vs. measured $\delta^{18}\text{O}$ (WR-Zrc)

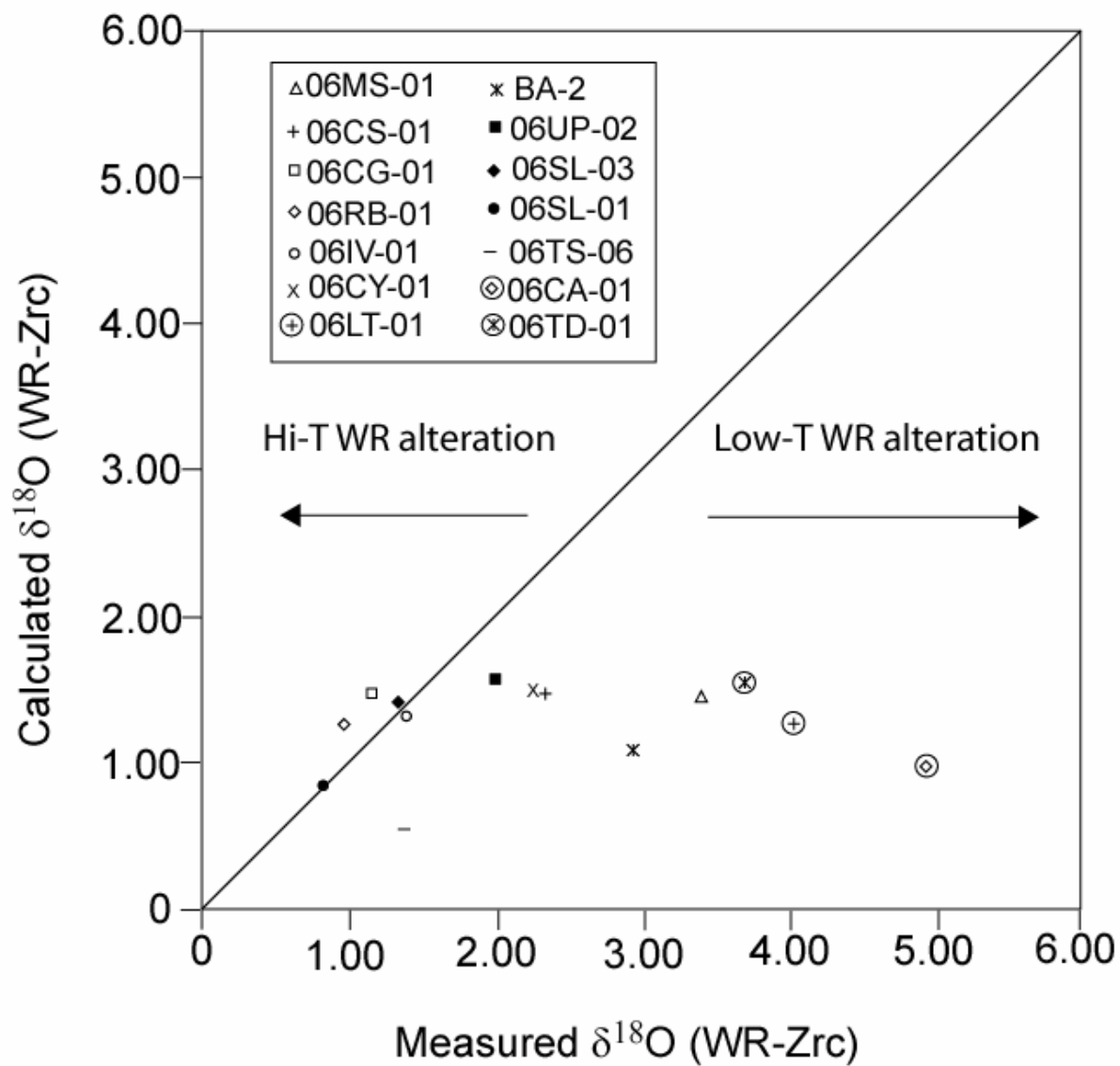


Figure 73

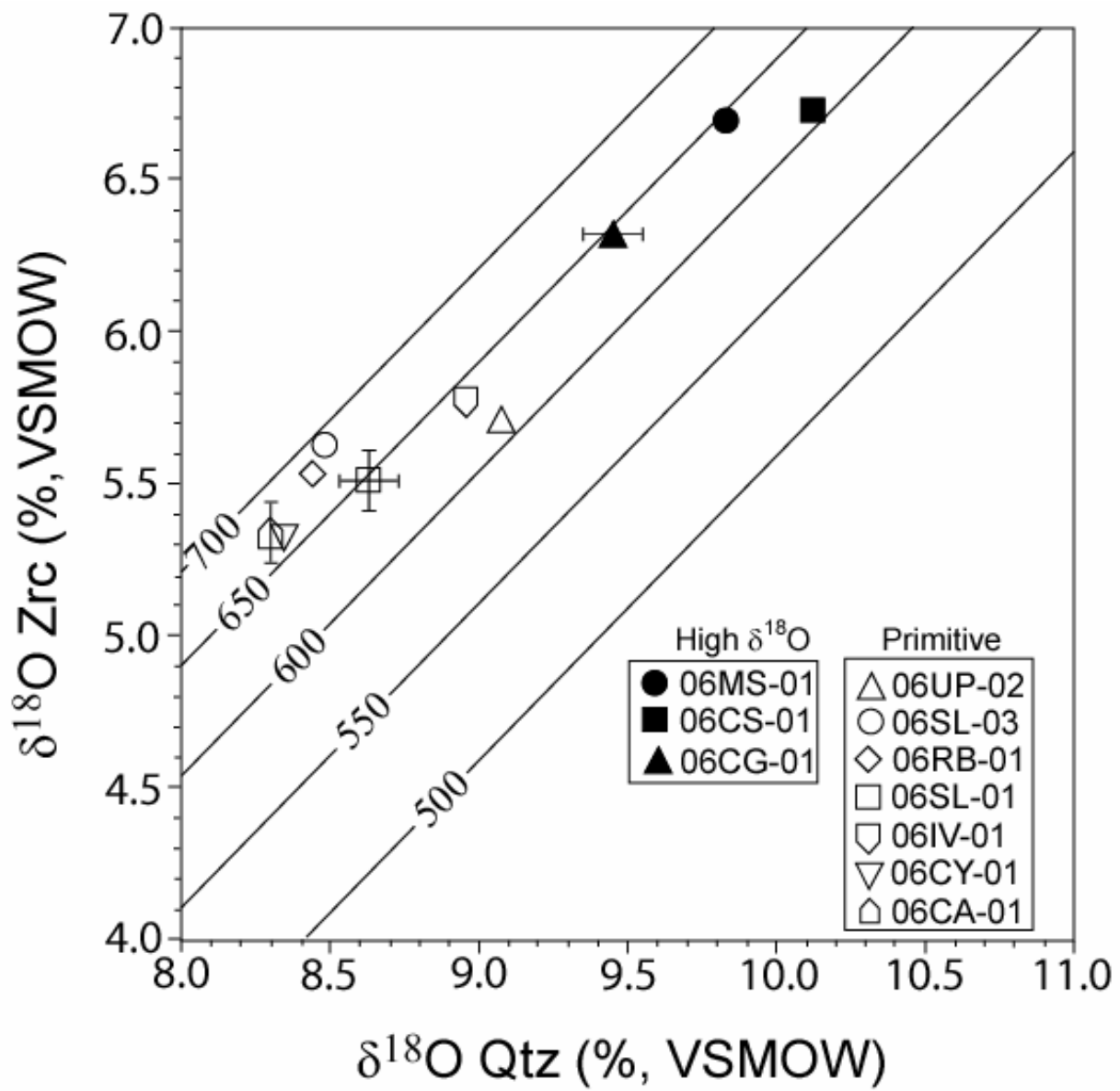


Figure 74

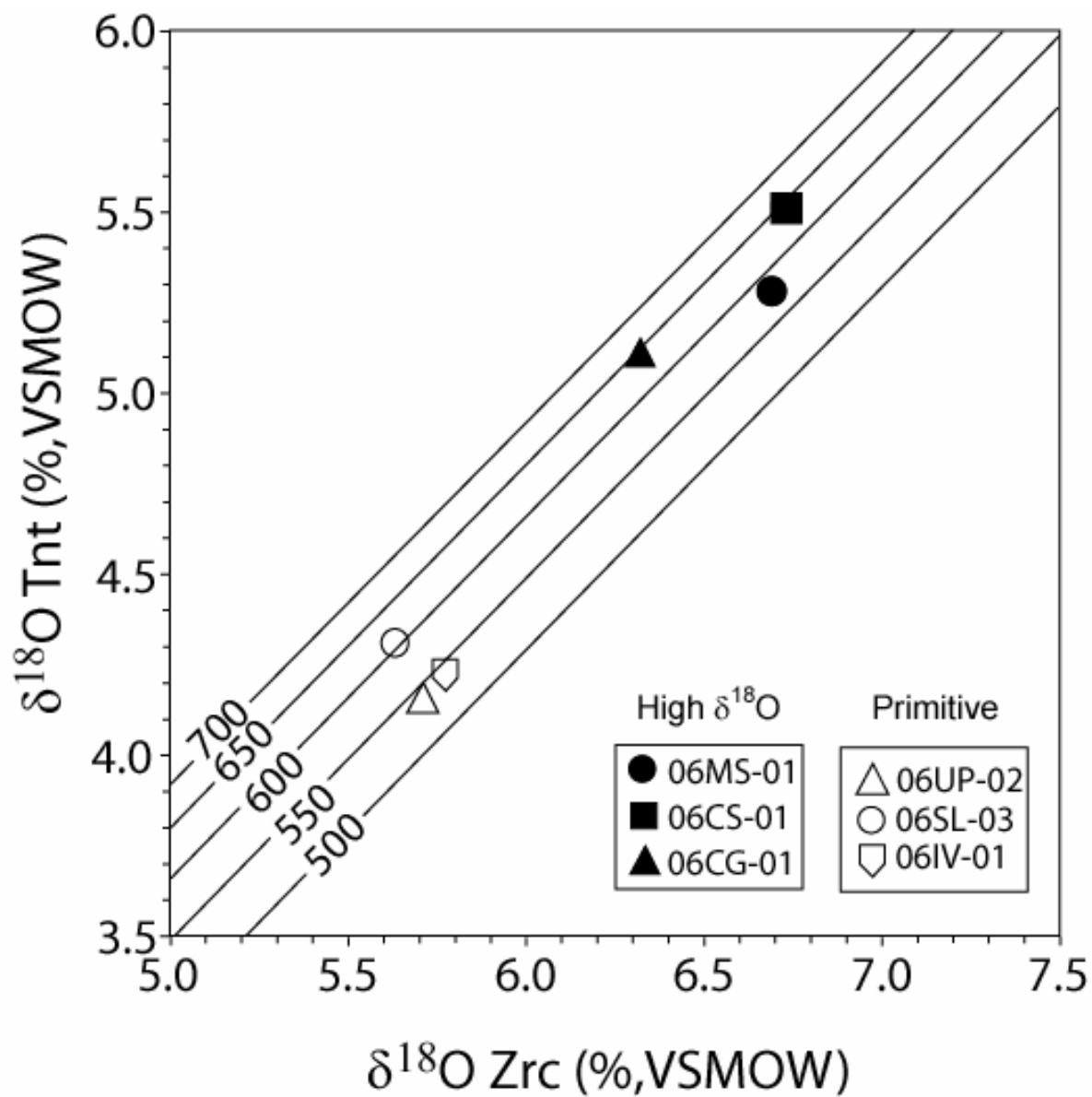


Figure 75

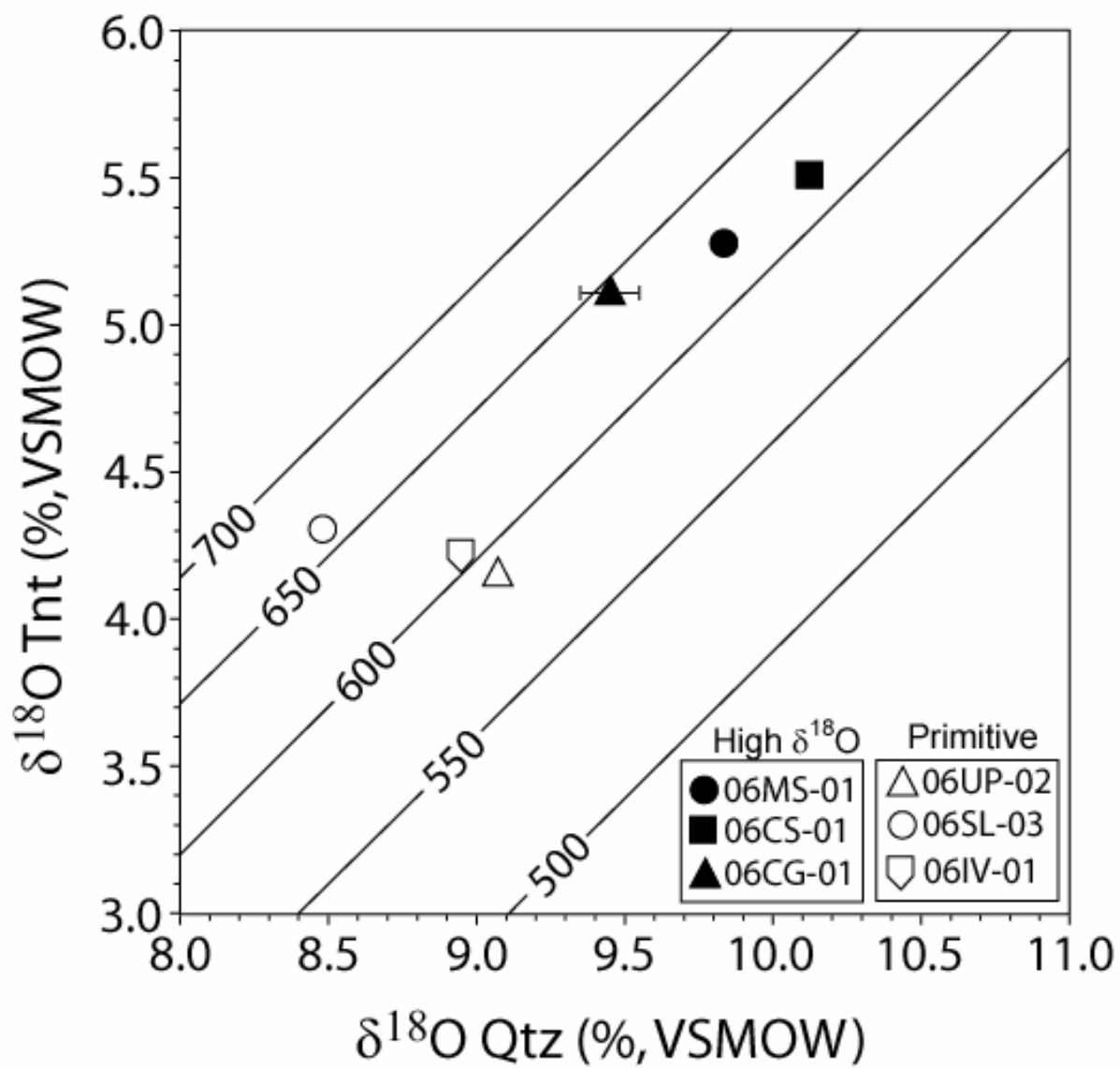


Figure 76

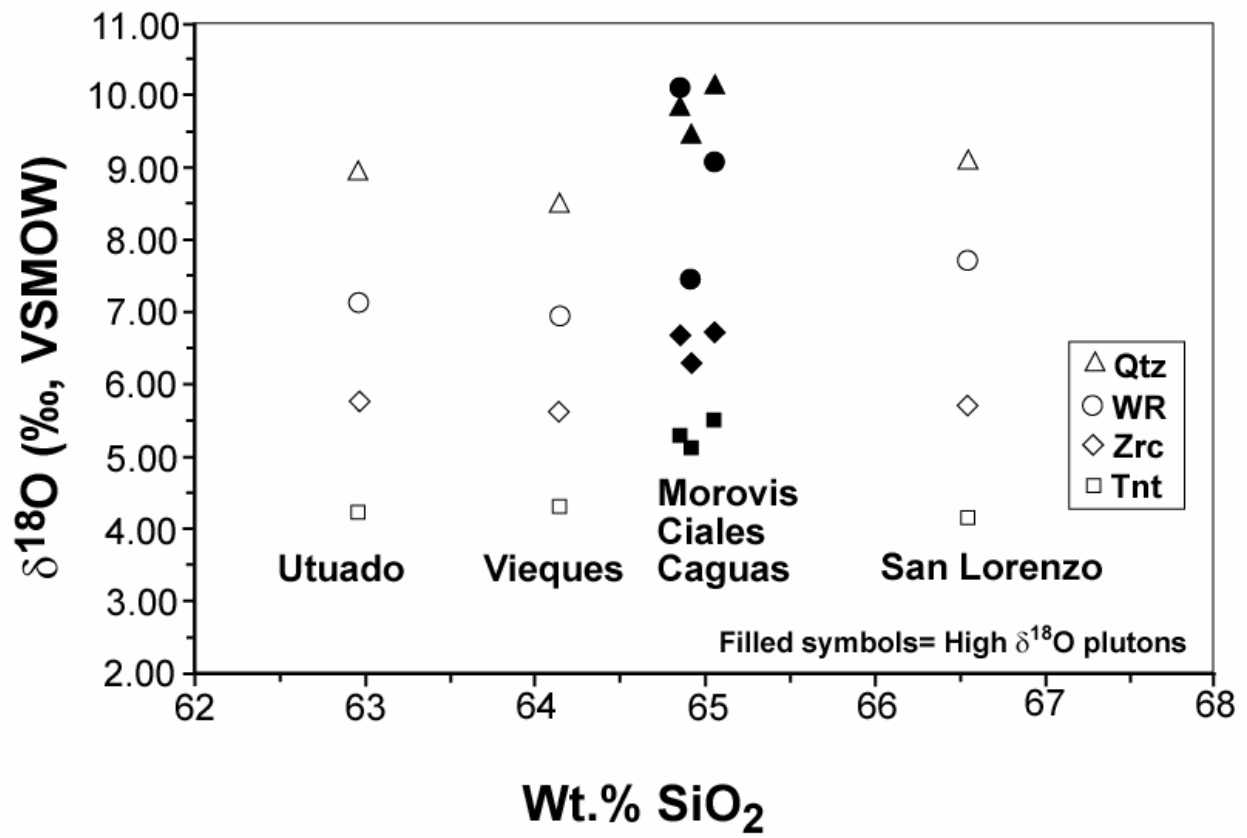


Figure 77

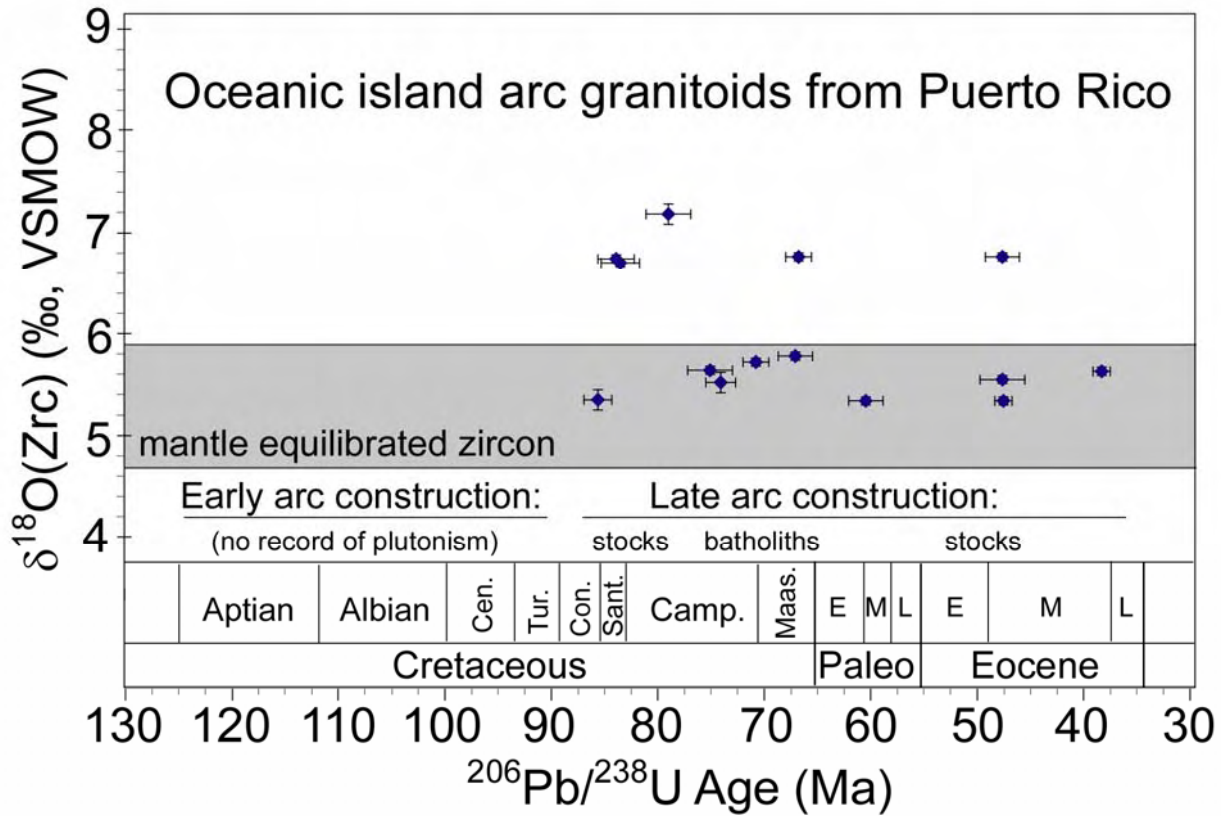


Figure 78

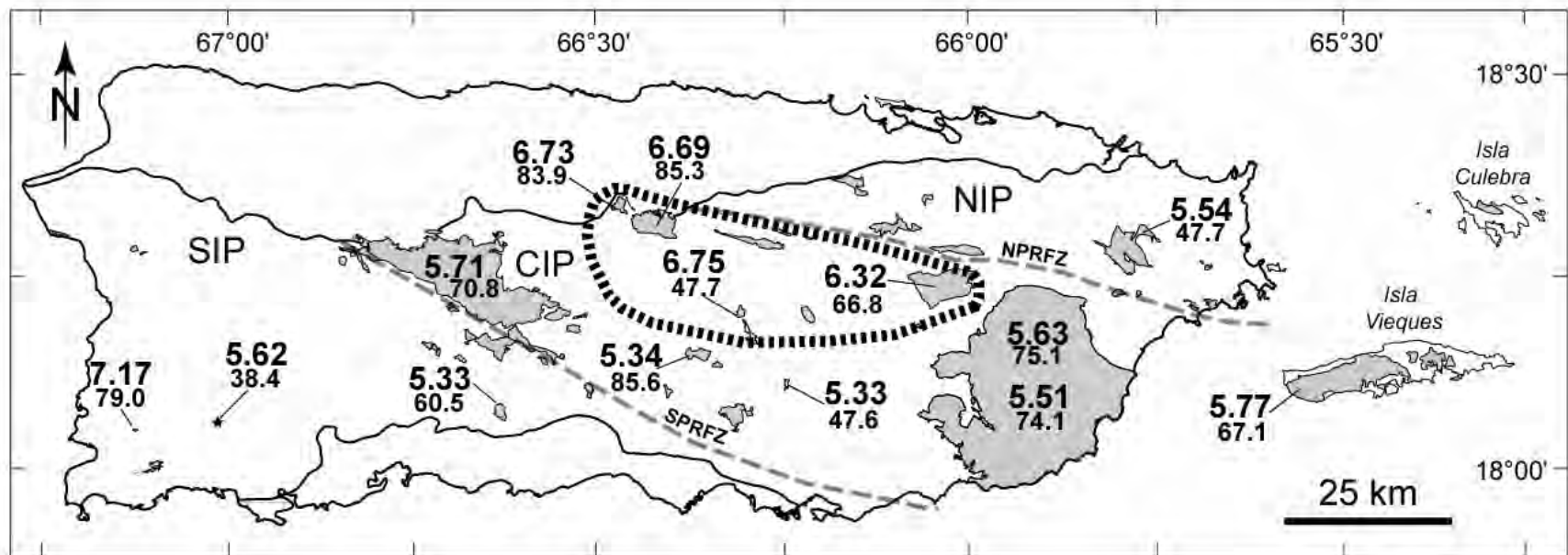


Figure 79

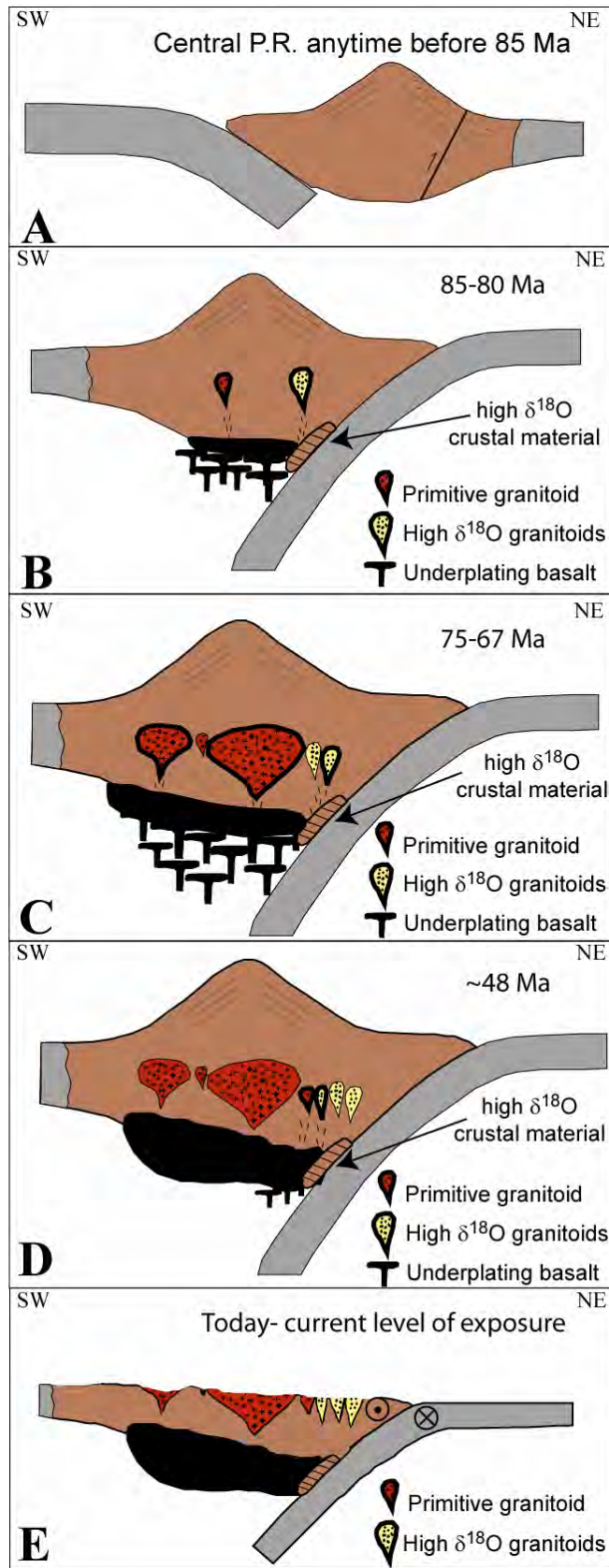


Figure 80